Mathematical Analysis of non-Newtonian Fluid Flows Over a Stretchable Surfaces

By

Muhammad Naveed Khan

Department of Mathematics

Quaid-i-Azam University
Islamabad, Pakistan

2021

Mathematical Analysis of non-Newtonian Fluid Flows Over a Stretchable Surfaces

By

Muhammad Naveed Khan

Supervised By

Prof. Dr. Sohail Nadem

Department of Mathematics
Quaid-i-Azam University
Islamabad, Pakistan

2021

Mathematical Analysis of non-Newtonian Fluid Flows Over a Stretchable Surfaces

By

Muhammad Naveed Khan

A DISSERTATION SUBMITTED IN THE PARTIAL FULFILLMENT OF THE REQUIREMENT
FOR THE DEGREE OF

DOCTOR OF PHILOSOPHY

IN

MATHEMATICS

Supervised by

Prof. Dr. Sohail Nadem

Department of Mathematics
Quaid-i-Azam University
Islamabad, Pakistan

2021

Author's Declaration

I, **Muhammad Naveed Khan,** hereby state that my PhD thesis titled **Mathematical Analysis of non-Newtonian Fluid Flows Over a Stretchable Surfaces** is my own work and has not been submitted previously by me for taking any degree from the Quaid-I-Azam University Islamabad, Pakistan or anywhere else in the country/world.

At any time if my statement is found to be incorrect even after my graduate the university has the right to withdraw my PhD degree.

Name of Student: **Muhammad Naveed Khan**

Date: **23-Aguest-2021**

Plagiarism Undertaking

I solemnly declare that research work presented in the thesis titled "**Mathematical Analysis of non-Newtonian Fluid Flows Over a Stretchable Surfaces**" is solely my research work with no significant contribution from any other person. Small contribution/help wherever taken has been duly acknowledged and that complete thesis has been written by me.

I understand the zero-tolerance policy of the HEC and **Quaid-i-Azam University** towards plagiarism. Therefore, I as an Author of the above titled thesis declare that no portion of my thesis has been plagiarized and any material used as reference is properly referred/cited.

I undertake that if I am found guilty of any formal plagiarism in the above titled thesis even afterward of PhD degree, the University reserves the rights to withdraw/revoke my PhD degree and that HEC and the University has the right to publish my name on the HEC/University Website on which names of students are placed who submitted plagiarized thesis.

Student/Author Signature

Name: **Muhammad Naveed Khan**

Mathematical Analysis of non-Newtonian Fluid Flows Over a Stretchable Surfaces

By

Muhammad Naveed Khan

CERTIFICATE

A THESIS SUBMITTED IN THE PARTIAL FULFILLMENT OF THE REQUIREMENTS FOR THE DEGREE OF THE

DOCTOR OF PHILOSOPHY IN MATHEMATICS

We accept this thesis as conforming to the required standard

1. ______________________
Prof. Dr. Sohail Nadeem
(Chairman)

2. ______________________
Prof. Dr. Sohail Nadeem
(Supervisor)

3. ______________________
Dr. Rahmat Ellahi
(External Examiner)

Department of Mathematics, International Islamic University, H-10, Islamabad.

4. ______________________
Dr. Noreen Sher Akbar
(External Examiner)

Department of Basic Humanities CE&ME, (NUST) Peshawar Road Rawalpindi

Department of Mathematics
Quaid-I-Azam University
Islamabad, Pakistan
2021

Certificate of Approval

This is to certify that the research work presented in this thesis entitled **Mathematical Analysis of non-Newtonian Fluid Flows Over a Stretchable Surfaces** was conducted by **Mr. Muhammad Naveed Khan** under the kind supervision of **Prof. Dr. Sohail Nadeem**. No part of this thesis has been submitted anywhere else for any other degree. This thesis is submitted to the Department of Mathematics, Quaid-i-Azam University, Islamabad in partial fulfillment of the requirements for the degree of Doctor of Philosophy in field of Mathematics from Department of Mathematics, Quaid-i-Azam University Islamabad, Pakistan.

Student Name: **Muhammad Naveed Khan** Signature:________

External committee:

a) **External Examiner 1**: Signature:________
Name: **Dr. Rahmat Ellahi**
Designation: Associate Professor
Department of Mathematics, International Islamic University, H-10, Islamabad

b) **External Examiner 2**: Signature:________
Name**: Dr. Noreen Sher Akbar**
Designation: Associate Professor
Department of Basic Humanities CE&ME, (NUST) Peshawar Road Rawalpindi

c) **Internal Examiner** Signature:________
Name: **Prof. Dr. Sohail Nadeem**
Designation: Professor
Office Address: Department of Mathematics, QAU Islamabad.

Supervisor Name: Signature:________
Prof. Dr. Sohail Nadeem

Name of Dean/ HOD Signature:________

Prof. Dr. Sohail Nadeem

ACKNOWLEDGEMENT

In the name of Allah, the most Beneficent and the most Merciful Lord, the creator, and all praises for "Allah Almighty", who has given me the chance, courage, and ability to complete this thesis. I am nothing without my Allah, but I can handle everything with his blessing. Also, I cannot forget the sources of humanity, idea personality of all creation for whom Allah has created the whole universe, who is forever a torch bearer of guidance for humanity, Hazrat Muhammad **(S.A.W.W).**

First and foremost, I would like to express my gratitude to my worthy supervisor **Prof. Dr. Sohail Nadeem** for his valuable suggestions and mentoring that helped me to accomplish this highly important research. His knowledge, accessibility and availability have been a critical motivational in driving this research. It would never have been possible for me to take this work to completion without his incredible support and encouragement. I am ever indebted and grateful to him.

I would like to thank my beloved mother, brother Rahim, and sister Labia Kanwal, whose love, prayers guidance are with me to follow my dream. I am very thankful to my family for their support and encouragement. I highly praise the cooperative behavior of my brothers who sacrifices for my education and betterment.

I have been lucky enough to have good friends in my academic and social life and cannot forget their role in my education and university life. It is a matter of great delight and pleasure for me to mention my truly wonderful friends and colleagues **Especially Shafiqa Ahmed, Dr. Nadeem Abbas, Dr. Aamir Hameed, Dr. Dr. Noor Muhammad, Dr. Mair Khan, Naeem Ullah, Salman Akhter, M. Salman Khan, M. Hafeez, Zahoor Iqbal, Awais Ahmed, Adil Sadique, and Aamir Abbas Khan.**

I gratefully acknowledgment the Department of Mathematics, Quaid-I-Azam University Islamabad for providing such wonderful facilities that made my work possible.

In the end I would like to thank to all my research fellows and those people who directly and indirectly helped me during my research work.

Dr. Muhammad Naveed Khan

DEDICATED TO

MY BELOVED Mother,

BROTHER, SISTER

AND

MY FATHER (Late)

Abstract

Flow behavior of several complex fluids is characterized by viscosity dependency on the rate of deformation. The viscosity dependency is the basic criteria of the non-Newtonian fluids rather than Newtonian fluids. The non-Newtonian (rate type) fluids with elastic and viscous forces exhibits the phenomena, which are known as relaxation and creep. The flow of viscoelastic materials in the nature has the application in polymers process, paints manufacturing, chemical and biological liquid production. The researchers developed several constitutive models to predict the rheological properties of non-Newtonian fluids model. The non-Newtonian fluid models under discussion in this study are consisting of Maxwell, Burger's, Oldroyd-B, and Casson fluid models. These models deliberate the relaxation and retardation aspect of fluids consequently. The main contribution of this thesis is to present the mathematical formulation of steady and unsteady, 2D and 3D, incompressible boundary layer flow of non-Newtonian fluid models with microorganisms over a stretchable surface. Further, the heat energy and mass transport in non-Newtonian fluid with various effects are examined in this thesis. The modelled partial differential equations of the flow problem are transformed into system of coupled ordinary differential equations by using similarity transformation. The whole computational work is carried out with the help of well-known numerical approaches built-in MATLAB solver (Bvp4c) and Richardson extrapolation (Bvp traprich) built-in MAPLE. A meaningful physical interpretation in the form of computational analysis is observed to characterize the behavior of velocity, temperature, concentration, and microorganism density of non-Newtonian fluid. It is interesting to observe that increment in the stress relaxation phenomenon, the fluid velocity declines, while fluid velocity is improved in the case of retardation phenomenon. Further, it is noted that higher trend of thermal and mass relaxation time (which are the results of Cattaneo-Christov theory), decreases the energy and mass transport in the fluid over a stretching surface. The comparison tables are presented for the validation of results.

Table of Contents

Chapter 01

Introduction to fundamentals of the fluid Mechanics

1.1. Introduction

Non-Newtonian fluid is one whose behavior deviates from that of Newtonian fluid (Newtonian is one, which relationship between shear stress and shear strain is linear with constant of proportionality normally called viscosity). The viscosity of non-Newtonian fluids depends upon share rate. The non–Newtonian fluids which used in the daily life are included the toothpaste, paper pulp, ketchup, yogurt, ice, certain oils, drilling muds, shampoos, paints, blood, starch, honey and many more. Moreover, all the chemical products, food stuffs, biological products are considered as a non–Newtonian fluids. Three main categories of non-Newtonian fluids are differential type, integral type, and rate type model. In the general flow conditions, the rate type fluid models exhibit the viscoelastic flow behavior. The viscoelastic fluids are those fluids which exhibit the viscous as well as elastic effect. These fluids are very important due to well-known applications such as, polymers processing, steel fiber coating, rubber, glasses, chemical equipment processing, metals, etc. In literature, the miner consideration has been acknowledged to the rate type (viscoelastic) fluid. The non–Newtonian fluid flow mechanism is analyzed by highly nonlinear coupled equations, in which closed form solutions are not possible. The non–Newtonian fluid models cannot be described by the Newtonian constitutive relation. Therefore, researchers have established several constitutive models to predict the various rheological properties of non-Newtonian fluid model, such as Maxwell, Burger's, Oldroyd–B, and Casson fluid. The Maxwell fluid model is the rate type model which described only the relaxation time, while the Oldroyd–B and Burgers fluid models have measurable both relaxation and retardation time. The Casson fluid model is one of the differential type model, which exhibits the yield stress. The starting studies about the rate type (Maxwell and Burgers) fluid model was given by Maxwell [1] and Burgers [2]. The Casson fluid model was initially reported by Casson [3] to predict the flow behavior of oil suspension. Eldabe et al. [4] conducted the theoretical analysis of heat transfer of Casson fluid flow between two rotating cylinders. The Oldroyd-B fluid via constantly accelerating plate for one dimensional flow was carried out by Vieru et al. [5]. Fetecau et al. [6] established the Fourier transforms to study the unsteady flow of Oldroyd-B fluid over a constantly accelerating plate. Zheng et al. [7] deliberated analytically the generalized Maxwell fluid by mean of constantly and oscillatory accelerating plate. Nadeem et al. [8] discussed the features of MHD flow of Casson fluid induced by an exponentially stretching / shrinking sheet. Numerical investigation of Oldroyd-B fluid flow with transverse magnetic field through an exponentially stretching surface was evaluated by Nadeem et al. [9]. Ramesh and Gireesha [10] considered convective boundary conditions to study the boundary layer flow of a Maxwell nanofluid across a stretching sheet. Mukopadhyay [11] analyzed the Casson fluid flow with diffusion of chemically reactive species through a stretching surface. Ramzan et al. [12] computed the 3D flow of Oldroyd-B fluid with the effect of Newtonian heating on a stretching sheet. Khan et al. [13] evaluated the MHD stagnation point flow of Burgers fluid through a rotating disk along uniform suction / injection. Khan and Khan [14] used a stretching sheet, to explore the boundary layer flow of Burgers fluid along the heat generation or absorption. Sandeep and Sulochana [15] reported the flow analysis of Maxwell, Jeffrey, and Oldroyd-B nanofluids past a stretching sheet with the effects of thermal radiation, magnetic field, and non-uniform heat source / sink. Ramesh et al. [16] proposed the three-dimensional Maxwell fluid flow across a stretching sheet along thermal radiation and suspended nanoparticles. Khan et al. [17] inspected the MHD stagnation point flow of a Casson fluid with homogeneous–heterogeneous reaction by a stretching surface. Safdar et al. [18] scrutinized the transient rotational flow of a generalized Burgers fluid across an infinite circular pipe. Waqas et al. [19] deliberated the mixed convective Burgers fluid flow with variable thermal conductivity across a moving surface. Farooq et al. [20] inspected the MHD Maxwell fluid flow along nanomaterials induced by an exponentially stretching sheet. Ahmed et al. [21] observed the Maxwell fluid flow by using Buongiorno's nanofluid model and stagnation point effect through a porous rotating disk. Tiwana et al. [22] scrutinized the MHD convective flow of Oldroyd-B fluid with wall temperature and velocity through an infinite vertical plate. Irfan et al. [23] evaluated the Oldroyd-B fluid with chemical reactions by stretched cylinder. Theoretical investigation of mixed convective MHD flow of chemically reactive Burger's fluid with heat source through a stretching sheet was carried out by Nirmala and Kumari [24]. The influence of convective boundary condition in the Casson fluid flow across an exponentially stretching curved surface was evaluated by Kumar et al. [25]. Shankar et al. [26] inspected the MHD flow of Casson fluid using nonporous medium and Cattaneo-Christov theory through a stretching sheet.

The mechanism of transportation of heat and mass are very important in many physical circumstances. Heat transfer mechanism arises by the temperature difference from one system to another, while mass transfer mechanism take place by the net movement of particle / molecules from one place to another or due to mass gradient. Such phenomena have extensive applications in the engineering and industrials prospective. The heat transfer mechanism is used in the power engineering, chemical engineering, nuclear plants, refrigerators, and petroleum production. The mass transport is occurred in the evaporation of water, the diffusion of chemical impurity in the oceans and rivers, separation of chemical in refinement procedure, etc. Furthermore, the heat and mass transfer are used in food industries and control the pollution in the water. The conventional Fourier's [27] and Fick's [28] law was endorsed in the beginning to analysis the heat and mass transfer, respectively. Later on, the researchers realized that there are some drawbacks of these conventional laws, because they presented the parabolic types of equations. Therefore, the Cattaneo [29] modified these conventional laws with the addition of time derivative factor, after a while the Christov [30] also modified these laws with the replacement of time derivative with Oldroyd–B upper convective derivative. Han et al. [31] investigated a comparison between Fourier and Cattaneo-Christov heat flux model to the thermal analysis on the Maxwell fluid by the stretched boundary layer flow. Sandeep et al. [32] illustrated the convective transfer of heat and mass of non-Newtonian nanofluid through a permeable stretching sheet. Khan [33] examined the heat and mass transfer of a Careau nanofluid flow across a non-linear stretching sheet. The Maxwell nanomaterial fluid flow along Cattaneo-Christov heat flux model was inspected by Sui et al. [34]. Nadeem et al. [35] considered an exponentially stretching surface to investigate the flow and heat transfer of Maxwell fluid with thermal stratification and Cattaneo-Christov theory. Hsiao [36] analyzed the forced convection flow and transport of heat on a Maxwell fluid along the viscous dissipation. Zhang et al. [37] considered a stretching sheet to analyze the Oldyrod-B fluid with double diffusion theory. The heat and mass transfer of chemically reactive Maxwell fluid flow with slip conditions past a stretching sheet was inspected by Khan et al. [38]. Sajid et al. [39] evaluated the flow and transfer of heat on non–Newtonian fluid with non–linear thermal radiation through a stretchable surface. Khan et al. [40] investigated the heat transfer of non-linear mixed convective slip flow of Walter-B nanofluid with gyrotactic microorganism induced by a non–linear stretching surface.

In recent eras, many researchers have keenly to study the importance of nanofluids. The nanofluids are formed by the mixture of nanoparticles in the convectional fluids. The heat transfer rate has been improved with the addition of nanoparticles in the base fluid. Improvement in the heat transfer is very significant in these days, because world is facing lot of energy crises. To overcome these crises we need more heat, therefore scientists moved towards the study of nanofluids. Choi [41] first time presented the term of nanofluids. The application of convective boundary layer flow of a nanofluid was examined by Buongiorno [42]. The detailed experimental and theoretical examination of the thermo-physical properties of nanofluids is examined by Khanafer and Vafai [43]. Uddin et al. [44] considered the vertical smooth surface to discuss the free convective boundary flow of nanofluids influenced by Newtonian heating boundary condition and magnetic effect. Rahman et al. [45] studied the second order slip flow of a nanofluid by Buongiorno's model over an exponentially stretching / shrinking surface. Hayat et al. [46] discussed the rotating flow of Maxwell nanofluid towards an exponentially stretching sheet. Shah et al. [47] considered a nonlinear stretching surface to observe the radiative MHD flow of Casson nanofluid with activation energy. Some representative analysis in the direction of nanofluids is presented in the Refs. [48-50].

Magentohydrodymics fluid flow is also very important, because the procedure of purification of molten metals from non-metallic inclusion, the magnetic field is used. Moreover, manufacturing process and industrial application, such as metallurgical procedures and petroleum production also encounter Magentohydrodymics. The electrically conducting fluids are used in cancer treatment therapy, MRI, heat exchanger process, manufacture of power generator, copper thinning wire, and many others. The most important aspect of the magnetic field has to control the rate of cooling to attain the anticipated worth of industrial products. The motion of non–

Newtonian fluid influence of the magnetic field was first time premeditated by Sarpkaya [51]. Later on, the study related to MHD non–Newtonian fluid was presented by Djukic [52]. Dhanai et al. [53] addressed the multiple solutions of MHD flow and heat transfer of Sisko nanofluid with convective boundary conditions. The MHD flow of Jeffrey fluid with the influence of Hall's current on a non-uniform rectangular duct was examined by Ellahi et al. [54]. The effect of MHD stagnation point flow of a Casson nanofluid along slip velocity and thermal radiation through a non-linear stretching surface was deliberated by Besthapu et al. [55]. Ahmed et al. [56] analyzed the transport of heat and mass of transient MHD flow of Maxwell nanofluid through a stretching cylinder with nonlinear thermal radiation.

The boundary layer flow which produced by the stretching surfaces have widespread applications in the industrial and engineering field. These applications contained the hot rolling and glass blowing, artificial fibers spinning, paper production, production of sheeting materials, sewer pipes, continuous casting, drawing of plastic films, and many others. Additionally, to the manufacturing of molten polymers, they play a vital role in polymers industries. The stretching sheet velocity is linearly proportional to the distance from the origin, but it is not necessarily that the plastic sheet should be linear, it is some time nonlinear or exponential. Crane [57] discussed the fluid flow that produced by stretching sheet. The heat and mass transfer of viscous fluid flow influenced with the suction and blowing over a stretchable surface was carried out by Gupta and Gupta [58]. Chakrabarti and Gupta [59] studied the hydromagnetic flow and heat transfer of viscous fluid over a stretching sheet. Magyari and Keller [60] explored the heat and mass transfer of a boundary layer flow by an exponentially continuous stretching surface. Paullet and Weidman [61] evaluated the behavior fluid flow in the neighborhood of a stagnation point through a stretching surface. Wang [62] observed the viscous fluid flow by a stretching surface by the consequence of slip and suction. Rosca and Pop [63] revealed the unsteady flow of viscous fluid along the mass suction through a stretching/ shrinking curved surface. The heat transfer of unsteady boundary layer flow of a Maxwell fluid with convective conditions on the surface through a permeable shrinking surface was examined by Mondal et al. [64]. Ali et al. [65] analyzed MHD tangent hyperbolic nanofluid flow with activation energy across a faster / slower stretching wedge surface. The MHD flow of rotating Maxwell nanofluid with Cattaneo-Christov theory and activation energy over a stretching surface is presented by Ali et al. [66].

The phenomenon of stratification is occurred due to the variation of temperature and concentration or due to different densities of the fluid. The stratification effect plays an important role to controlling the temperature difference between oxygen and hydrogen in the water to prevents the water becomes anoxic by the action of biological processes, which is harmful for the various living species. The double stratification phenomenon occurs when the heat and mass transfer produce together. The stratification flows take place in the rivers, lakes, oceans, ground water reservoirs, etc. The efficiencies of energy can be improved due to the better stratification. Chen and Eichhorn [67] first time study the thermally stratified fluid over a vertical surface. Yoon and Warhaft [68] analyzed the progression of grid turbulence under the thermal stratification conditions. Angirasa and Srinivasan [69] examined numerically, the transport of heat and mass of natural convection flow towards a vertical sheet affected by buoyancy forces and thermally stratified medium. Moorthy and Senthilvadivu [70] premeditated the influence of thermal stratification with variable viscosity on the free convective flow of non-Newtonian power-law fluid over a vertical plate. Rosmila et al. [71] explored the MHD natural convective flow of viscous nanofluid with thermal stratification towards a linearly porous stretching surface. The boundary layer flow of nanofluid influenced by stratification across a vertical plate was carried out by Ibrahim and Makind [72]. The boundary layer flow and heat transfer of a ferromagnetic fluid along the thermal stratification condition on a stretching surface is investigated by Muhammad et al. [73]. Sandeep and Reddy [74] premeditated the Oldroyd-B fluid with double stratification across the melting surface. The Darcy-Forchheimer flow of a Maxwell nanofluid with double stratification across a stretching surface was carried out by Lakshmi et al. [75]. Tlili et al. [76] inspected the Maxwell nanofluid flow with double stratification over a stretching sheet.

The bio-convection is macroscopic phenomenon of convection, which occurred by the density gradient of collective up swimming motile microorganism. The microorganisms which are swimming to the upper surface of fluid, where the density of fluid lesser than to the base fluid. The microorganisms live in approximately every habitat from the poles of the equator, geysers, deep seas, deserts, and the rocks. The bio-convection plays a vital role in the area of geophysical and rehabilitation phenomena. The termed gyrotaxis microorganism is introduced first time by Kessler [77-78]. The procedure of upswing of motile microorganism was firstly studied by Kuznetsov [79-80]. Further, the combination of microorganisms with nanoparticles is deliberated by Geng and Kuznetsov [81-82]. Nadeem et al. [83] elaborated the forced bio-convection flow of micropolar nanofluid towards an exponentially stretching surface. Rashad and Nabwey [84] considered convective boundary conditions to discuss the mixed bio-convection flow of nanofluid through a circular cylinder. Khan et al. [85] investigated the nonlinear mixed convective slip flow of Walter-B nanofluid induced by a stretching surface with gyrotactic microorganism.

1.2. Basic Governing Equations

The basics governing equations of the thesis is presented in this section. The continuity equation is represented in the vector form as,

$$\frac{\partial \rho}{\partial t} + \boldsymbol{\nabla} \cdot (\rho \mathbf{V}) = 0. \tag{1.1}$$

Where $\mathbf{V}$ and ρ is the velocity and density of the fluid, respectively. For incompressible fluid, the equation (1.1) is stated as,

$$\boldsymbol{\nabla} \cdot \mathbf{V} = 0. \tag{1.2}$$

The law of conservation of momentum is stated as follows,

$$\rho a_i = -\boldsymbol{\nabla} p + \operatorname{div}\boldsymbol{S} + \rho \boldsymbol{B}. \tag{1.3}$$

$$\left(1 + \lambda_1 \frac{D}{Dt} + \lambda_2 \frac{D^2}{Dt^2}\right)\boldsymbol{S} = \mu\left(1 + \lambda_3 \frac{D}{Dt}\right) A_1. \tag{1.4}$$

Here, $\boldsymbol{a_i}$ is the acceleration, $\boldsymbol{B}$ is the body force, $\boldsymbol{S}$ is the extra stress tensor, p is the pressure, and $A_1 = \boldsymbol{\nabla}\mathbf{V} + (\boldsymbol{\nabla}\mathbf{V})^{\boldsymbol{t}}$ is the first Rivlin-Ericksen tensor, λ_1, λ_3 is relaxation and retardation of time, and λ_2 is material parameter. Moreover, the upper convective derivative $\frac{D}{Dt}$ is defined as,

$$\frac{D\boldsymbol{a_i}}{Dt} = \frac{\partial \rho}{\partial t} + u_r \boldsymbol{a}_{i,r} - \boldsymbol{a}_i u_{r,i}. \tag{1.5}$$

By using operator and solving (1.3) and (1.4), we get the equation of Burgers fluid model, whereas for $\lambda_2 = 0$, we get equation of Oldroyd–B fluid model and for $\lambda_2 = 0 = \lambda_3$, we get the equation of Maxwell fluid model.

The energy equation can be written in standard form,

$$\rho c_p \frac{\partial T}{\partial t} + \mathbf{V} \cdot \boldsymbol{\nabla} T = -\mathrm{div}\boldsymbol{q}. \tag{1.6}$$

Mathematically $\boldsymbol{q}$ is stated as,

$$\boldsymbol{q} + k\boldsymbol{\nabla} T = \pi_1 \left(\boldsymbol{q} \cdot \boldsymbol{\nabla}\mathbf{V} - \mathbf{V} \cdot \boldsymbol{\nabla}\boldsymbol{q} - \frac{\partial \boldsymbol{q}}{\partial t} - (\boldsymbol{\nabla} \cdot \mathbf{V})\boldsymbol{q} \right). \tag{1.7}$$

Here c_p, π_1, and $\boldsymbol{q}$ are the specific heat, thermal relaxation time, and energy flux, respectively. By using the equation (1.7) into (1.6), we get the energy equation for generalized Fourier law. When we take $\pi_1 = 0$ the conventional Fourier law is achieved.

The equation of mass concentration is stated in the general form as,

$$\frac{\partial C}{\partial t} + \mathbf{V} \cdot \boldsymbol{\nabla} C = -\mathrm{div}\boldsymbol{J}. \tag{1.8}$$

The Mathematical form of $\boldsymbol{J}$ is,

$$\boldsymbol{J} + D_B \boldsymbol{\nabla} C = \pi_2 \left(\boldsymbol{J} \cdot \boldsymbol{\nabla}\mathbf{V} - \mathbf{V} \cdot \boldsymbol{\nabla}\boldsymbol{J} - \frac{\partial \boldsymbol{J}}{\partial t} - (\boldsymbol{\nabla} \cdot \mathbf{V})\boldsymbol{J} \right). \tag{1.9}$$

Here $\boldsymbol{J}$, π_2, D_B, and C is the mass flux, concentration relaxation time, diffusion coefficient, and mass concentration, respectively. By using the equation (1.9) into (1.8), we get the boundary layer equations for generalized Fick law. When we take $\pi_2 = 0$ the conventional Fick law is obtained.

The microorganism equation is stated in the general form as,

$$\frac{\partial n}{\partial t} + \mathbf{V} \cdot \boldsymbol{\nabla} n + \frac{\tilde{b}}{\boldsymbol{\nabla} C} W_c (\boldsymbol{\nabla} n \cdot \boldsymbol{\nabla} C) = D_m \boldsymbol{\nabla} n. \tag{1.10}$$

Here n is motile microorganism density, W_c is cell swimming speed, $\tilde{b}$ is chemotaxis constant, and D_m is microorganism diffusion coefficient.

1.3. Novelty and Methodology

The current thesis mainly focuses on the behavior of flows, transport of heat and mass of the bio-convective non–Newtonian fluids through different stretchable surfaces, because lot of its industrials and engineering applications. To empower the literature, we added some work in the literature related to non–Newtonian fluids model. We mainly focus on the rate type fluid. The dual solutions of the Maxwell fluid and comparison between linear and exponential sheet is presented in the thesis. Furthermore, the Cattaneo-Christov theory is used to analyze the heat and mass transfer of a Maxwell fluid. The non–Newtonian fluids flow model equations are transformed into coupled nonlinear ordinary differential equations by using appropriate transformation. The obtained equations are highly nonlinear, it is tough task to compute the exact solutions of these ODEs. Therefore, the numerical solutions of nonlinear ODEs are obtained with the help of shooting / Bvp4c Matlab technique and BVP midrich Maple technique. The graphical and tabulated discussion of the physical parameters has been conducted for the better understanding and the achievement perspective.

1.4. Thesis Layout

Keeping the above discussion in mind, this thesis consists of nine chapters, which mentioning the diverse features of the non–Newtonian fluids in detailed, the chapter one is the introductory chapter. The other chapters of thesis are arranged as following manner:

Chapter two is examined the flow and heat transfer analysis of bio-convective Maxwell nanofluid with external magnetic field and viscous dissipation. The multiple slip boundary conditions are imposed on the boundary of the exponentially stretching sheet. The solution of flow model is computed with bvp4c Matlab technique. The numerical outcomes of this chapter are discussed with graphically and tabulated data. The contents of chapter are published in the **“Canadian Journal of Physics**.”

The chapter three presented the theoretical investigation of radiative Oldroyd–B nanofluid with microorganisms over an exponentially stretching surface. The thermal jump and concentration slip boundary condition are imposed on the boundary of the sheet. The mathematical model is solved numerically by adopting BVP midrich Maple technique. This chapter contents are published in the **“Journal of Surfaces and Interfaces.”**

Chapter four analyzed the 3D MHD boundary layer flow of Maxwell fluid with variable thermal conductivity and thermophoretic effect through a stretching sheet. The transportation of heat and mass is presented by the influence of Cattaneo–Christov theory. The stratification boundary conditions are implemented on the sheet. Numerical technique bvp4c is used to solved mathematical flow model. The chapter contents are published in the **“Part c: Journal of Mechanical Engineering Science.”**

In chapter five, it is investigated that the double stratified Darcy-Forehheimer steady flow of radiative Maxwell fluid over a vertical stretching surface. The transport of heat and mass are discussed with the effect of Cattaneo–Christov theory and activation energy. Moreover, the bio-convection phenomenon is also considered in the current chapter due to buoyancy forces. The present chapter contents are published in the **“Journal of the Taiwan Institute of Chemical Engineers.”**

Chapter six investigated the transportation of heat and mass of MHD bio-convective flow of Casson nanofluid with viscous dissipation through a linear stretching surface. The thermal radiation and thermophoretic effects are also considered in this chapter. The stratification boundary conditions are applied on the surface. The flow model is numerically solved by bvp4c Matlab technique.

Chapter seven demonstrated the transportation of heat and mass on a chemically reactive Burgers nanofluid with induced magnetic field through an exponentially stretching surface. The thermal jump and concentration slip boundary conditions are considered in the current chapter. The transferred flow model is numerically solved by BVP midrich Maple technique. The contents of the current chapter are published in the **“Proceedings of the Institution of Mechanical Engineers, Part E.”**

Chapter eight observed the comparative study between linear and exponential stretching sheet of a rotating Maxwell nanofluid flow with double stratification. The transport of heat and mass is observed with the variable thermal conductivity and thermophoretic effect. In this chapter a comparison has been done between linear and exponential stretching sheet to see the better outcomes between two. The chapter contents are published in the **“Journal of Surfaces and Interfaces.”**

Chapter nine is explored the theoretical analysis of heat and mass transport on a transient Maxwell nanofluid through a permeable shrinking surface along thermal radiation. Brownian motion and thermophoresis phenomenon are also considered in the mass transport analysis. The main aim of this chapter is to examine the dual solution and stability analysis of the investigation. The chapter contents are published in the **“Journal of Surfaces and Interfaces.”**

1.5. Nomenclature

u_w	Stretching surface velocity (m/s)	a, b, c	Stretching constants
u_e	Free stream velocity (m/s)	T_0, C_0, n_0	Dimensionless constants
t	Time coordinate	g	Gravitational acceleration (m^2/s)
u, v, w	Velocity component in (x, y, z)-directions (m/s)	D_T, D_B, D_m	Thermophoresis, Brownian, and Microorganism diffusion coefficient
s	Suction / injection parameter	$\boldsymbol{q}, \boldsymbol{J}$	Heat flux, and mass flux
K	Permeability of porous medium	q_r	Radiative heat flux
C, C_w, C_∞	Volume, wall, and ambient concentration	L, L_1, L_2, L_3	Velocity, thermal, concentration, and microorganism slip factor
T, T_w T_∞	Fluid, wall, and ambient Temperature (K)	$k(T)$, k, k_∞	Temperature dependent, fluid, and ambient thermal conductivity (W/mK)
T_r	Reference temperature	$\tilde{b}$	Chemotaxis constant (m)
W_c	Maximum cell swimming speed (m/s)	n, n_w, n_∞	Motile, wall, and ambient microorganism density
S, S_1, S_2, S_3	Velocity, thermal, concentration, microorganism slip parameter	Nu_x, Sh_x, Qn_x	Local Nusselt, Sherwood, and Microorganism numbers
Ec_1, Ec_2	Eckert number in (x, y)-directions	Nt, Nb	Thermophoresis and Brownian motion parameter
A	Unsteadiness parameter	Sc	Schmidt number
m	Exponential index	Sb	Bio-convection Schmidt number
Re_x	Local Reynolds number	Pe	Peclet number
Pr	Prandtl number	$f(\eta), g(\eta)$	Dimensionless variables for velocity
Ec	Eckert number	Ha^2	Hartmann number
$h(\eta)$	Dimensionless microorganism factor	$H_1(t)$	External magnetic field
$h_1(\eta)$	Dimensionless induced magnetic field factor	H_1, H_2	Induced magnetic field in (x, y)-directions

H_0	Induced magnetic field	B_0	Magnetic field
H_e	Induced magnetic field at edge	c_p	Specific heat capacity
V_w	Suction / injection velocity	k_1	Chemical reaction constant
C_b	Drag coefficient	V_T	Thermophoretic velocity
Q_0	Heat generation / absorption coefficient	N, M	Temperature and concentration exponent
Q	Heat generation / absorption parameter	$f_0(\eta), \theta_0(\eta), \phi_0(\eta),$	Steady state solution
q_m, j_m, z_w	Surface heat, mass, and microorganism fluxes	a_1, b_1, c_1, d_1	Stratification constants
E_a	Activation energy	E_1	Activation energy parameter
l	Reference length	Cf_x	Local skin friction coefficient
M	Magnetic field parameter	Fr	Forchheimer number
Nr	Buoyancy ratio parameter	Gr	Mixed convection parameter
Rb	Rayleigh number	Rd	Radiation parameter
x, y, z	Spatial Coordinates	h_w	Heat transport coefficient
PDEs	Partial differential equations	3D	Three dimensional
2D	Two dimensional	ODEs	Ordinary differential equations
Eqs.	Equations	MHD	Magnetohydrodynamics
$f''(0)$, $g''(0)$	Velocity gradients	$-\theta'(0)$, $-\phi'(0)$	Temperature and concentration gradient
Greek Symbols			
σ^*	Boltzmann constant	σ_1	Electrical conductivity (s/m)
κ^*	Mean absorption coefficient	μ_0	Magnetic permeability
α_0	Dimensional constant (1/s)	τ	Ratio of heat capacity to the base fluid
β_1	Deborah number	μ_e	Magnetic diffusivity
Ω	Angular velocity	α	Thermal diffusion coefficient

σ	Chemical reaction parameter	δ	Temperature difference parameter
Ψ	Concentration difference parameter	λ_r	Rotation parameter
θ_e	Temperature ratio parameter	β	Casson fluid parameter
Γ	Bio-convection difference parameter	ρ	Density of fluid
λ_2	Retradation of time	λ_1, λ_3	Relaxation time of fluid
ρ_p	Density of particle	ρ_m	Density of microorganism
ε	Thermal conductivity parameter	η	Similarity variable
μ	Dynamic viscosity	ν	Kinematic viscosity
τ_1	Thermophoretic parameter	Λ	Magnetic Prandtl number
λ_c	Critical value	$\tau_{wx,}\ \tau_{wy}$	Surface shear stresses
λ	Stretching / shrinking parameter	$\theta(\eta)$	Dimensionless temperature factor
ψ	Stream function	$\phi(\eta)$	Dimensionless concentration factor
β_2	Retradation parameter	β_3	Burger's fluid parameter
π_1, π_2	Thermal and concentration relaxation time	γ_1, γ_2	Volumetric thermal and concentration expansion
ϕ_1	Porosity of porous medium	γ_3	Avarge volume of microorganism
δ_1, δ_2	Thermal and concentration stratification parameter	δ_t, δ_c	Thermal and concentration relaxation time parameter
γ	Eigenvalues	Υ	Porosity parameter
γ^*	Biot number	δ_3	Microorganism stratification parameter

Chapter 02

Theoretical analysis of unsteady bio-convective Maxwell nanofluid through an exponentially stretching surface

In this chapter, the flow analysis of time dependent 2D Maxwell nanofluid with external magnetic field and viscous dissipation is examined. The flow induced by an exponentially stretching surface with the implementation of multiple slip boundary conditions. The bio-convection and chemical reaction effect also considered in this chapter. The modelled PDEs are transformed into nonlinear coupled ODEs with the utilization of appropriate similarity variables. The bvp4c Matlab technique is used to solve the coupled nonlinear ODEs. The graphical discussion on the velocity, thermal, concentration, and microorganism distribution against the physical parameters is presented. Moreover, the tabulated values for the skin friction, Nusselt number, Sherwood number, and microorganism number are manipulated and discussed.

2.1. Mathematical Modelling

Here we considered 2D, incompressible, unsteady, boundary layer flow of Maxwell nanofluid with bio-convection through an exponentially stretching surface. The multiple slip boundary conditions along with viscous dissipation and chemical reaction effect is also considered. The external magnetic field applied to the normal of the sheet. The flow along x-axis and y-axis normal to the direction of fluid flow. The flow pattern is illustrated in **Fig. (2.1).** The stretching velocity of the surface is $u_w = \frac{cExp(\frac{x}{l})}{1-\alpha_0 t}$. The temperature, nanoparticle concentration, and microorganism density are T, C, and n respectively. Further, the T_w, C_w, and n_w are the wall temperature, concentration, and microorganism density respectively, while ambient temperature, concentration, and microorganism density are stated by C_∞, T_∞, and n_∞ respectively. With the velocity field $\mathbf{V} = [u(x,y,t), v(x,y,t), 0]$ and using of above assumption, the governing equations are stated as,

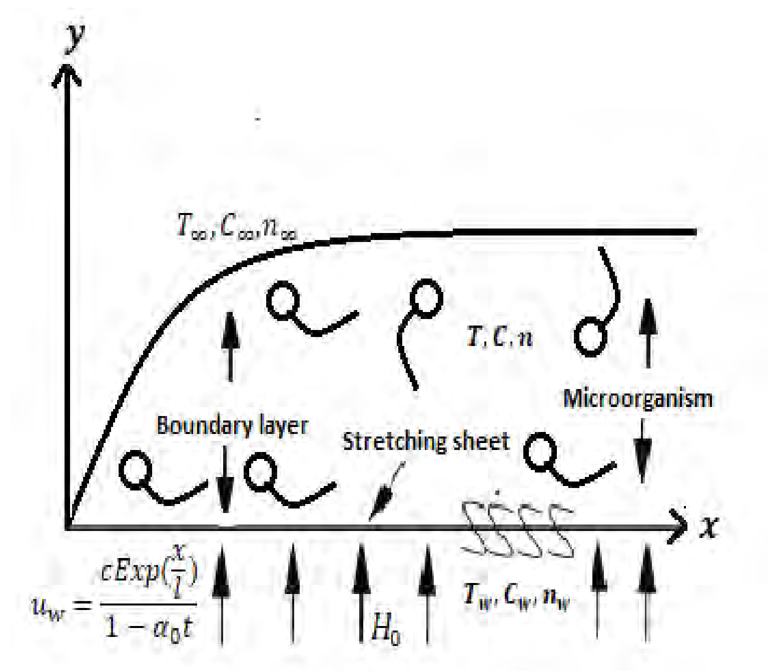

Fig. (2.1): Flow pattren of the problem.

$$\frac{\partial u}{\partial x} + \frac{\partial v}{\partial y} = 0, \tag{2.1}$$

$$\frac{\partial u}{\partial t} + u\frac{\partial u}{\partial x} + v\frac{\partial u}{\partial y} + \lambda_1 \begin{pmatrix} \dfrac{\partial^2 u}{\partial t^2} + u^2\dfrac{\partial^2 u}{\partial x^2} + v^2\dfrac{\partial^2 u}{\partial y^2} \\ +2u\left(\dfrac{\partial^2 u}{\partial x\,\partial t} + v\dfrac{\partial^2 u}{\partial x\,\partial y}\right) \\ +2v\dfrac{\partial^2 u}{\partial y\,\partial t} \end{pmatrix} = \nu\frac{\partial^2 u}{\partial y^2} - \frac{\sigma_1 \mu_0^2 H_1(t)^2}{\rho}\left(u + \lambda_1 v\frac{\partial u}{\partial y}\right), \tag{2.2}$$

$$\frac{\partial T}{\partial t} + u\frac{\partial T}{\partial x} + v\frac{\partial T}{\partial y} = \alpha\frac{\partial^2 T}{\partial y^2} + \tau\left(\frac{D_T}{T_\infty}\left(\frac{\partial T}{\partial y}\right)^2 + D_B\frac{\partial T}{\partial y}\frac{\partial C}{\partial y}\right) + \frac{\nu}{c_p}\left(\frac{\partial u}{\partial y}\right)^2, \tag{2.3}$$

$$\frac{\partial C}{\partial t}+u\frac{\partial C}{\partial x}+v\frac{\partial C}{\partial y}=D_B\frac{\partial^2 C}{\partial y^2}+\frac{D_T}{T_\infty}\frac{\partial^2 T}{\partial y^2}-k_1\left(C-C_\infty\right), \tag{2.4}$$

$$\frac{\partial n}{\partial t}+u\frac{\partial n}{\partial x}+v\frac{\partial n}{\partial y}+\frac{\tilde{b}W_c}{C_w-C_\infty}\left[\frac{\partial}{\partial y}\left(n\frac{\partial C}{\partial y}\right)\right]=D_m\frac{\partial^2 n}{\partial y^2}. \tag{2.5}$$

The related boundary conditions given are defined as,

$$u=u_w+L_1(t)\left(\frac{\partial u}{\partial y}\right), v=0, T=T_w+L_2(t)\left(\frac{\partial T}{\partial y}\right), C=C_w+L_3(t)\left(\frac{\partial C}{\partial y}\right),$$
$$n=n_w+L_4(t)\left(\frac{\partial n}{\partial y}\right), \text{ when } y\to 0. \tag{2.6}$$

$$u=0, T\to T_\infty, \mathrm{C}\to C_\infty, n\to n_\infty, \text{ when } y\to\infty. \tag{2.7}$$

The velocity components are u and v in the $x-$ and $y-$direction respectively. The variable external magnetic field is defined by $H_1(t)=\sqrt{\frac{H_0^2}{2l(1-\alpha_0 t)}}$. The wall temperature, wall concentration, and wall microorganisms are stated by $T_w=T_\infty+\frac{T_0 Exp(\frac{x}{2l})}{(1-\alpha_0 t)^2}$, $C_w=C_\infty+\frac{C_0 Exp(\frac{x}{2l})}{(1-\alpha_0 t)^2}$, and $n_w=n_\infty+\frac{n_0 Exp(\frac{x}{2l})}{(1-\alpha_0 t)^2}$ respectively. Here T_0, C_0, and n_0 all are constants.

The slip factor for velocity, temperature, concentration, and microorganism are expressed by $L_1(t)=(L_1)_0\sqrt{\frac{2l(1-\alpha_0 t)}{va}}$, $L_2(t)=(L_2)_0\sqrt{\frac{2l(1-\alpha_0 t)}{va}}$, $L_3(t)=(L_3)_0\sqrt{\frac{2l(1-\alpha_0 t)}{va}}$, and $L_4(t)=(L_4)_0\sqrt{\frac{2l(1-\alpha_0 t)}{va}}$ respectively. It is noted when $L_1=L_2=L_3=L_4=0$, then no slip conditions is recovered.

Similarity variables [86] are stated as,

$$\psi = \sqrt{\frac{2\nu l a}{(1-\alpha_0 t)}} f(\eta) Exp\left(\frac{x}{2l}\right), \eta = y\sqrt{\frac{a}{2\nu l(1-\alpha_0 t)}} Exp\left(\frac{x}{2l}\right),$$

$$T = T_\infty + \frac{T_0 Exp\left(\frac{x}{2l}\right)}{(1-\alpha_0 t)^2}\theta(\eta), C = C_\infty + \frac{C_0 Exp\left(\frac{x}{2l}\right)}{(1-\alpha_0 t)^2}\phi(\eta), n = n_\infty + \frac{n_0 Exp\left(\frac{x}{2l}\right)}{(1-\alpha_0 t)^2} h(\eta). \tag{2.8}$$

The components of velocity are stated as,

$$u = \frac{af'(\eta)Exp\left(\frac{x}{2l}\right)}{(1-\alpha_0 t)}, v = -\sqrt{\frac{\nu a}{2l(1-\alpha_0 t)}} Exp\left(\frac{x}{2l}\right)[f(\eta) + \eta f'(\eta)]. \tag{2.9}$$

Using Eqs. (2.8) and (2.9), Eq. (2.1) is satisfied automatically, while Eqs. (2.2-2.7) becomes,

$$f''' - \begin{pmatrix} A(2f' + \eta f'') \\ +2f'^2 + ff'' \end{pmatrix} - \beta_1 \begin{pmatrix} A^2\left(2f' + \frac{7\eta}{2}f'' + \frac{\eta^2}{4}f'''\right) - 6ff'f'' \\ +A(4f'^2 + 2\eta f'f'') + f^2 f''' - \eta f'^2 f'' \\ -A(3ff'' + \eta ff''') + 4f'^3 \\ +Ha^2(ff'' - f' + \eta f'f'') \end{pmatrix} = 0, \tag{2.10}$$

$$\theta'' + \Pr(f\theta' - f'\theta) - \Pr A(4\theta + \eta\theta') + \Pr(Nb\theta'\phi' + Nt\theta'^2) + \Pr Ecf''^2 = 0, \tag{2.11}$$

$$\phi'' + Sc(f\phi' - f'\phi) - ScA(4\phi + \eta\phi') + Sc\sigma\phi + \frac{Nt}{Nb}\theta'' = 0, \tag{2.12}$$

$$h'' + Sb(fh' - f'h) - SbA(4h + \eta h') - Pe\big((h + \Gamma)\phi'' + h'\phi'\big) = 0. \tag{2.13}$$

The concerned boundary conditions are,

$$f'(\eta) = \lambda + Sf''(\eta), f(\eta) = 0, \theta(\eta) = 1 + S_1\theta'(\eta),$$

$$\phi(\eta) = 1 + S_2\phi'(\eta),\ h(\eta) = 1 + S_3 h'(\eta) \text{ as } \eta \to 0. \tag{2.14}$$

$$f'(\eta) = 0, \theta(\eta) = 0, \phi(\eta) = 0, h(\eta) = 0 \text{ as } \eta \to \infty.$$

Here the prime represented the derivative with respect to η. The dimensional form of physical parameters are stated as,

$$A = \frac{l\alpha_0}{a}, \lambda = \frac{c}{a}, \beta_1 = \frac{\lambda_1 a}{2l(1-\alpha_0 t)}, Ha^2 = H_0\mu_0\sqrt{\frac{\sigma}{\rho a}},$$

$$Nb = \frac{\tau D_B \Delta C}{\nu}, Nt = \frac{\tau D_T \Delta T}{\nu T_\infty}, Sc = \frac{\nu}{D_B}, Sb = \frac{\nu}{D_m}, \mathrm{Pr} = \frac{\upsilon}{\alpha}, \tag{2.15}$$

$$Pe = \frac{\tilde{b} W_c D_m}{\nu^2}, \sigma = \frac{k_1 \Delta C}{a}, Ec = \frac{u_w^2}{c_p \Delta T}, S_i = (L_{\mathrm{i}})_0 \ (\mathrm{i} = 1, 2, 3),$$

2.1.1. Physical Quantities

Quantities of physical interest like as skin friction, Nusselt number, Sherwood number, and microorganism number are very significant from engineering point of view. These physical quantities are specified as,

$$C_{fx} = \frac{\tau_{wx}}{\rho u_w^2}, Nu_x = \frac{x q_m}{k(T_w - T_\infty)}, Sh_x = \frac{x j_m}{D_B(C_w - C_\infty)}, \ Q_{nx} = \frac{x z_w}{D_m n_w}. \tag{2.16}$$

In Eqs. (2.16), τ_{wx} is the shear stress, q_m is the heat flux, j_m is the mass flux, and z_w is the microorganism flux, which are defined as,

$$\tau_{wx} = \mu \frac{\partial}{\partial y}\left(u + \lambda_1 v \frac{\partial u}{\partial y}\right)\Big|_{y=0}, \ q_m = -k\frac{\partial T}{\partial y}\Big|_{y=0}, \ j_m = -D_B \frac{\partial C}{\partial y}\Big|_{y=0}, \ z_w = -D_m \frac{\partial n}{\partial y}\Big|_{y=0}. \tag{2.17}$$

These quantities are in dimensionless form,

$$Re_x^{1/2} C_{fx} = f''(0) - \beta_1 \begin{pmatrix} f'''(0)f(0) + \eta f'(0)f''(0) \\ +2f'(0)f''(0) + \eta f''^2(0) \end{pmatrix}, \tag{2.18}$$

$$\begin{pmatrix} Re_x^{-1/2} Nu_x = -\theta'(0), \\ Re_x^{-1/2} Sh_x = -\phi'(0), \\ Re_x^{-1/2} Q_{nx} = -h'0). \end{pmatrix}. \tag{2.19}$$

The local Reynolds number is $Re_x = \frac{lu_w}{\nu}$.

2.1.2. Numerical Description

The numerical solutions of Eqs. (2.10–2.13) with Eq. (2.14) is developed by means of bvp4c Matlab technique. To employ bvp4c technique first we transferred the Eqs. (2.10–2.14) into system of first order ODEs. The convergence criteria were taken as 10^{-6} [87].

$$\begin{pmatrix} f = y(1), f' = y(2), f'' = y(3), \theta = y(4), \theta' = y(5), \\ \phi = y(6), \phi' = y(7), h = y(8), h' = y(9), \end{pmatrix}, \tag{2.20}$$

$$yy_1 = \left(\frac{1}{1 - \beta_1 A^2 \frac{\eta^2}{4} + \beta_1 A \eta y(1) - \beta_1 y(1)^2} \right) \begin{pmatrix} 2y(2)^2 - y(1)y(3) + A(2y(2) + \eta y(3)) \\ +\beta_1 A^2 (2y(2) + \frac{7\eta}{4} y(3)) \\ +\beta_1 A (2y(2)^2 + 2\eta y(2)y(3) - 3y(1)y(3)) \\ +\beta_1 (4y(2)^3 - \eta y(2)^2 y(3) - 6y(1)y(2)y(3)) \\ +Ha^2 \{y(2) - \beta_1 (y(1)y(3) + \eta y(2)y(3))\} \end{pmatrix}, \tag{2.21}$$

$$yy_2 = \Pr \begin{pmatrix} y(2)y(4) - y(1)y(5) + A\{4y(4) + \eta y(5)\} \\ -Nby(5)y(7) - Nty(5)^2 - Ecy(3)^2 \end{pmatrix}, \tag{2.22}$$

$$yy_3 = Sc(y(2)y(6) - y(1)y(7) + A\{4y(6) + \eta y(7)\} + \sigma y(6)) - \frac{Nt}{Nb} yy_2, \tag{2.23}$$

$$yy_4 = Sb \begin{pmatrix} y(2)y(8) - y(1)y(9) \\ +A\{4y(8) + \eta y(9)\} \end{pmatrix} + Pe(y(7)y(9) + (y(8) + \Gamma)yy_3). \tag{2.24}$$

The associated boundary conditions in the first order are,

$$\begin{pmatrix} y_0(1) = 0, y_0(2) = \lambda + Sy_0(3), y_0(4) = 1 + S_1 y_0(5), \\ y_0(6) = 1 + S_2 y_0(7), y_0(8) = 1 + S_3 y_0(9). \end{pmatrix}, \tag{2.25}$$

$$y_{\inf}(2) = y_{\inf}(4) = y_{\inf}(6) = y_{\inf}(8) = 0. \tag{2.26}$$

2.2. Results and Discussion

The current chapter mainly focuses on the flow and heat transfer of Maxwell nanofluid with the influence of multiple slip boundary conditions and external magnetic field. Numerical solution of ODEs are obtained with the usage of bvp4c Matlab technique. The computed results are discussed and observed by graphically and tabulated data. The values of physical parameters are fixed by $A = 0.3,\ \lambda = 0.5,\ \Pr = 6.0,\ Ec = 0.2,\ \sigma = \beta_1 = Nb = Nt = Ha^2 = 0.1,\ Sc = 2.0,$ $Sb = 1.0,\ Pe = 1.0, S = S_1 = S_2 = S_3 = 0.5$.

Table (2.1) is the comparison table of Pr against the Nusselt number, Sherwood number, and microorganism number, it shows good similarity with previous published results. It is noted that higher values of Pr diminishes the microorganism transfer rate, but heat and mass transfer rate is boosted. **Table (2.2)** represents the variation in the skin friction, heat, mass, and microorganism transfer rate for the several values of physical parameters. It is noticed from the tabulated data that the stronger estimation of the stretching ratio parameter declines the heat transfer rate, but improves the skin friction, mass transfer rate, and microorganism transfer rate. The all physical quantities showing diminishes effect for the higher values of β_1, but opposite trend is noted for the several values of A. Further, it is observed that heat dissipation potential falls due to enlargement of Ec, therefore Nusselt number decays, while mass and microorganism transfer rate improves. The enhancement is noted in the microorganism transfer rate for growing estimation of Sb.

The impact of λ (stretching ratio parameter) on the velocity profile is depicted in **Fig. (2.2).** It is noticed that stronger values of λ improves the velocity of fluid as well as momentum boundary layer thickness. **Fig. (2.3)** discloses the variation in the velocity profile for the various estimation of A (unsteadiness parameter). It is visualized that fluid velocity and related boundary layer thickness decays for the greater values of A. The variation of velocity graph for higher estimation of β_1 (Deborah number) is found in **Fig. (2.4).** It is examined that, growing values of β_1 diminishes the fluid velocity and thickness of boundary layer. Physically, it is illustrated that due to higher values β_1, the fluid behaves like a solid, therefore the fluid resistance improved as a result the velocity of fluid declines. The diversity in Ha^2 (Hartmann number) against the velocity profile is pictured in **Fig. (2.5).** It is exhibited from the plot that stronger estimation of Ha^2 declines the velocity of fluid. Physically, Ha^2 is the ratio between electromagnetic to viscous forces, therefore for the stronger Ha^2 the electromagnetic force is improved, which declines the velocity field. The influence of S (velocity slip parameter) on the velocity sketch is found in the **Fig. (2.6).** It is scrutinized that the fluid velocity reduces for the growing values S. **Fig. (2.7)** is sketched to examine the temperature variation against the S_1 (thermal slip parameter). It is observed that the related boundary layer thickness and temperature become stronger for the higher estimation of S_1. **Fig. (2.8)** reveals the variation in the temperature against the several values of A. It is noted that temperature of fluid reduces for the greater values of A. The tendency of Eckert number to improve the temperature and boundary layer thickness, as enlarging the values of Ec **(**see in the **Fig. (2.9)).** Physically, Ec is the ratio between kinetic energy and enthalpy. As increasing the Ec the kinetic energy of the system enhances, which improves the temperature. Moreover, the frictional heating energy stored in the nanofluid therefore the enhancement in the temperature is occurred. **Fig. (2.10)** describes the influence of Pr (Prandtl number) against the $\theta(\eta)$. It is seen that the temperature and related boundary layer thickness decreases for the stronger Pr. Physically, Pr control the heat transfer rate during the cooling process in the industries. Therefore, stronger values of Pr declines the temperature of the fluid. **Fig. (2.11)** is depicted the effects of Sc (Schmidt number) against the $\phi(\eta)$. The devaluation is occurred in the $\phi(\eta)$ distribution for the rising values of Sc. The variation in $\theta(\eta)$ and $\phi(\eta)$ sketch for stronger estimation of Nb (Brownian motion parameter) is shown in **Fig. (2.12)** and **Fig. (2.13)**. It is portrayed that by the enlargement of Nb, the mass diffusivity is mounting, which leads to improves the temperature, while reverse trend is seen for the concentration sketch. From physical point of view, the disorderness is occurred by the stronger values of Nb, as a result the heat transfer rate increases, which produce more temperature in the system. The influence of Nt (thermophoresis parameter) on $\theta(\eta)$ and $\phi(\eta)$ plot is shown in **Fig. (2.14)** and **(2.15).** It is designated from the sketch that due to temperature gradient the thermophoresis force induced on nanoparticles, as a result the fast flow away from the surface. Hence, more fluid is heated away from the sheet, which leads to increment in the temperature as well as nanoparticle concentration. Physically, one can say that the increment is occurred in thermophoretic force due to the increment Nt. The variation in the $\phi(\eta)$ plot against the several values of S_2 (concentration slip parameter) and A (unsteadiness parameter) is plotted in **Fig. (2.16)** and **Fig. (2.17)**. It is examined that reduction is occurred in the $\phi(\eta)$ plot and associated boundary layer becomes thin due to the increment in the values S_2 and A. **Fig. (2.18)** and **Fig. (2.19)** depicts the diversion in the microorganism density plot for distinct values of Pe (Peclet number) and Sb (bio-convection Schmidt number). It is sketched that higher estimation of Pe and Sb declines the $h(\eta)$ plot for both parameters. Physically, it is noted that Pe has direct relation with W_c and $\tilde{b}$ and inverse relation with microorganism diffusivity, by the increment of Pe, the diffusivity of microorganism reduces, as a result the reduction is occurred in the microorganism density profile. Moreover, by the enhancement of Sb, the microorganism diffusivity decays, as a result density of microorganism also declines. **Fig. (2.20)** and **Fig. (2.21)** represents the lowering behavior against the $h(\eta)$ plot due to the increment of A (unsteadiness parameter) and S_3.

Table (2.1): Numerical results of $Re_x^{-1/2}Nu_x$, $Re_x^{-1/2}Sh_x$, and $Re_x^{-1/2}Qn_x$ for various values of Pr.

	$Re_x^{-1/2}Nu_x$		$Re_x^{-1/2}Sh_x$		$Re_x^{-1/2}Qn_x$	
Pr	Ref. [88]	Current	Ref. [88]	Current	Ref. [88]	Current
0.5	0.34689119	0.3468912	1.61983352	1.619336	0.31941987	0.3194199
1.0	0.57428288	0.5742829	1.80285833	1.802859	0.14721928	0.1472193
3.0	1.15942580	1.1594260	2.33075212	2.330753	−0.31099156	−0.310092
5.0	1.56331503	1.5633150	2.71619820	2.716199	−0.64301399	−0.643014

Table (2.2): Table of $Re_x^{1/2}C_{fx}$, $Re_x^{-1/2}Nu_x$, $Re_x^{-1/2}Sh_x$, $Re_x^{-1/2}Qn_x$ for several parameters.

λ	β_1	A	Ec	Sb	$Re_x^{1/2}C_{fx}$	$Re_x^{-1/2}Nu_x$	$Re_x^{-1/2}Sh_x$	$Re_x^{-1/2}Qn_x$
0.5	0.1	0.9	0.4	1.0	0.39933	1.104	1.0474	1.3127
0.7	-	-	-	1.0	0.56412	1.103	1.0598	1.3196
0.9	-	-	-	-	0.73046	1.097	1.0730	1.3264
0.5	0.0	-	0.4	-	0.40745	1.105	1.0480	1.3132
-	0.1	-	-	-	0.39683	1.104	1.0474	1.3127
-	0.2	-	-	-	0.38570	1.103	1.0470	1.3124
-	0.1	0.3	-	-	0.31940	0.8708	0.8094	1.1538
-	-	0.6	0.4	1.0	0.36212	1.013	0.9554	1.2537

0.5	-	0.9	-	-	0.39683	1.104	1.0475	1.3128
-	-	0.9	0.2	-	-	1.109	1.0456	1.3121
-	0.1	-	0.4	-	-	1.104	1.0475	1.3128
-	-	-	0.6	1.0	-	1.099	1.0494	1.3134
-	-	-	-	1.0	-	-	-	1.3128
-	0.1	-	-	2.0	-	-	-	1.3830
0.5	-	0.9	-	3.0	-	-	-	1.4299

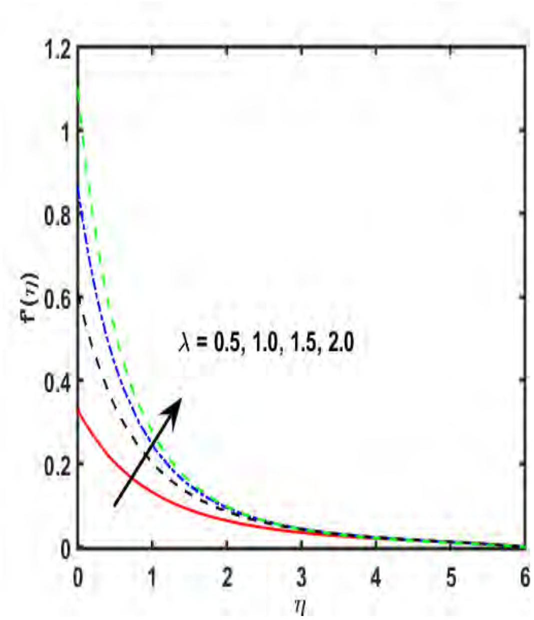

Fig. (2.2): Effect of λ on $f'(\eta)$.

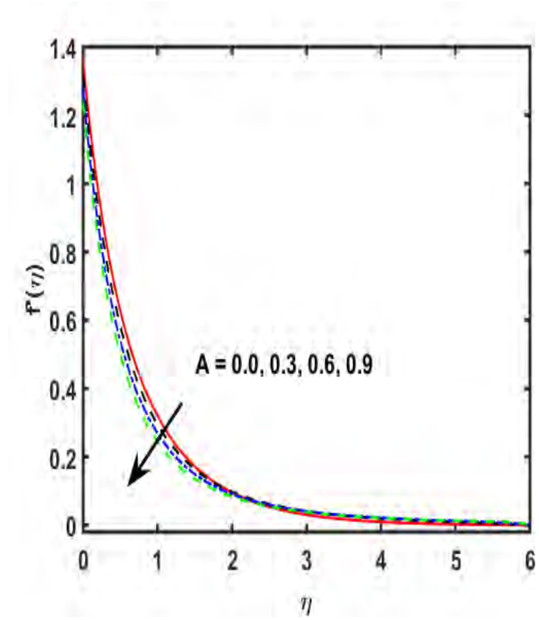

Fig. (2.3): Effect of A on $f'(\eta)$.

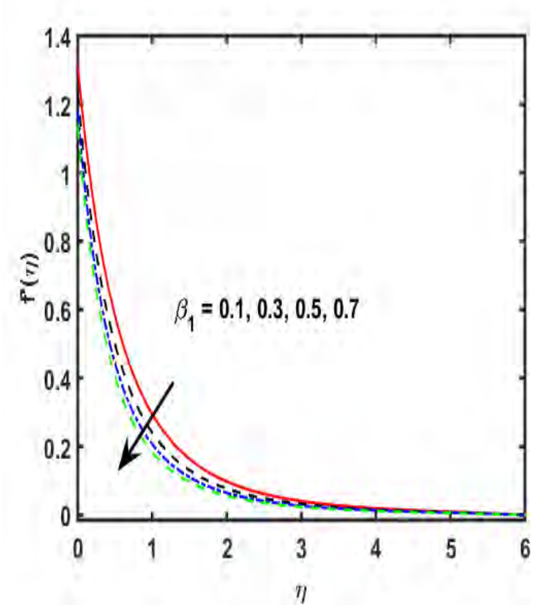

Fig. (2.4): Effect of β_1 on $f'(\eta)$.

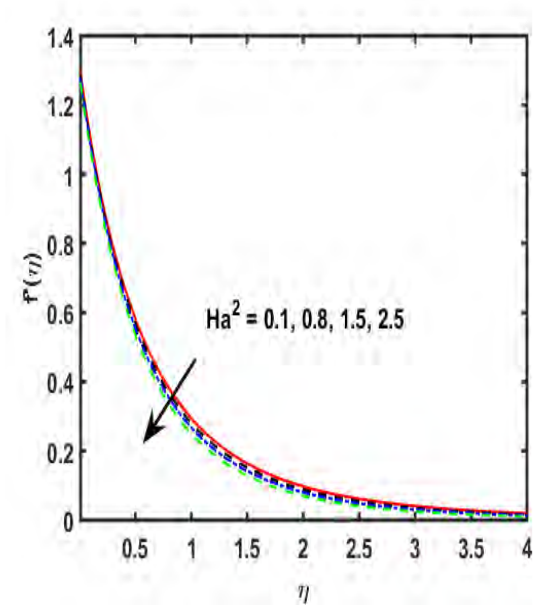

Fig. (2.5): Effect of Ha^2 on $f'(\eta)$.

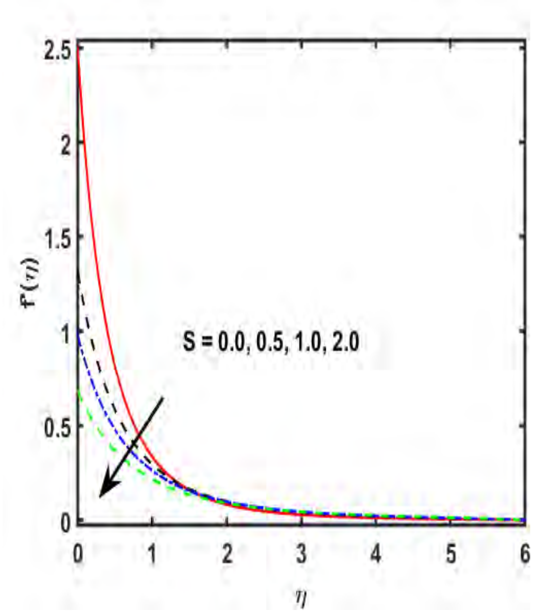

Fig. (2.6): Effect of S on $f'(\eta)$.

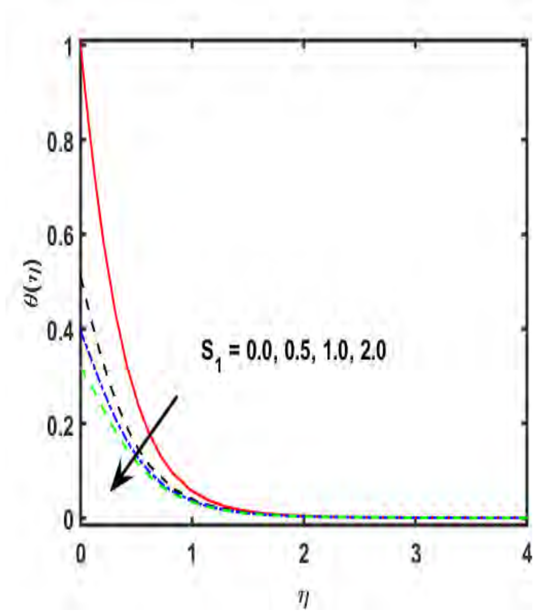

Fig. (2.7): Effect of S_1 on $\theta(\eta)$.

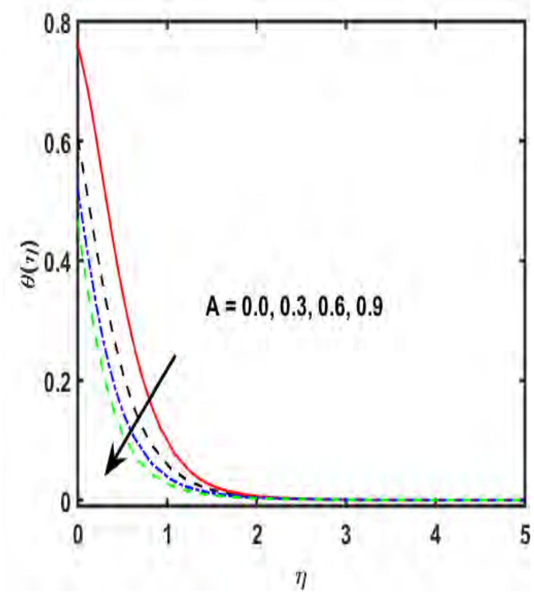

Fig. (2.8): Effect of A on $\theta(\eta)$.

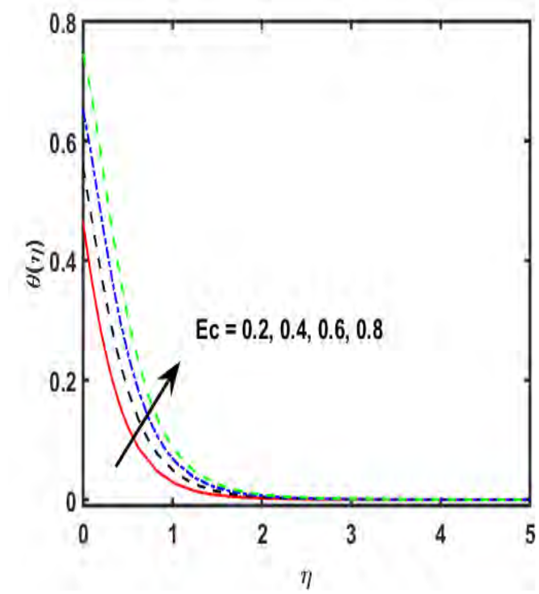

Fig. (2.9): Effect of Ec on $\theta(\eta)$.

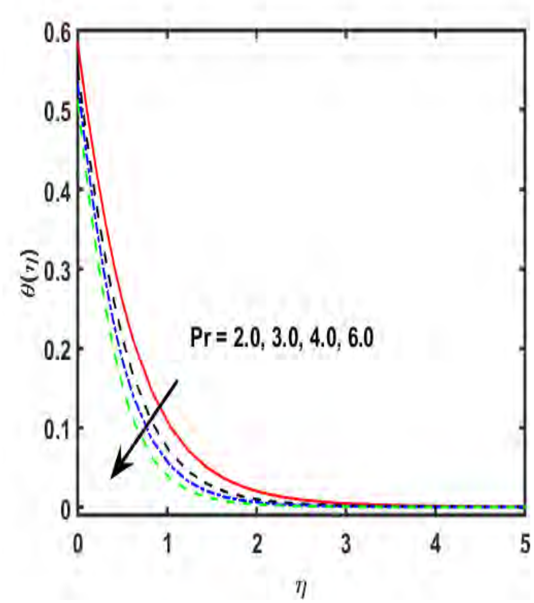

Fig. (2.10): Effect of Pr on $\theta(\eta)$.

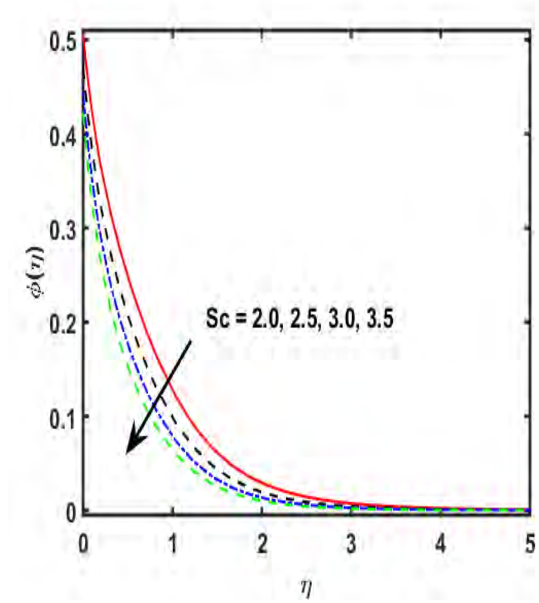

Fig. (2.11): Effect of Sc on $\phi(\eta)$.

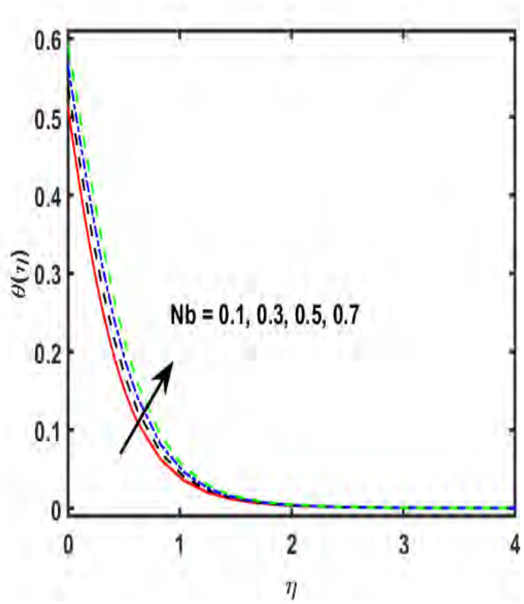

Fig. (2.12): Effect of Nb on $\theta(\eta)$.

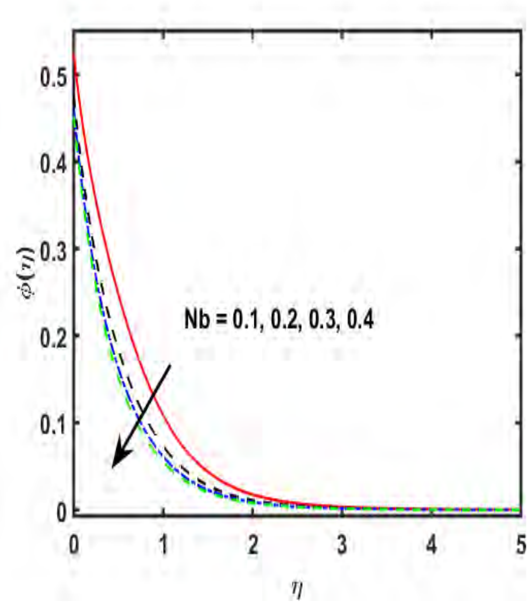

Fig. (2.13): Effect of Nb on $\phi(\eta)$.

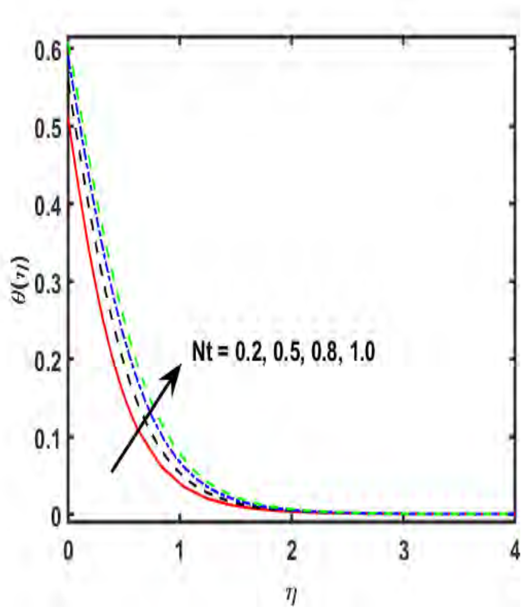

Fig. (2.14): Effect of Nt on $\theta(\eta)$.

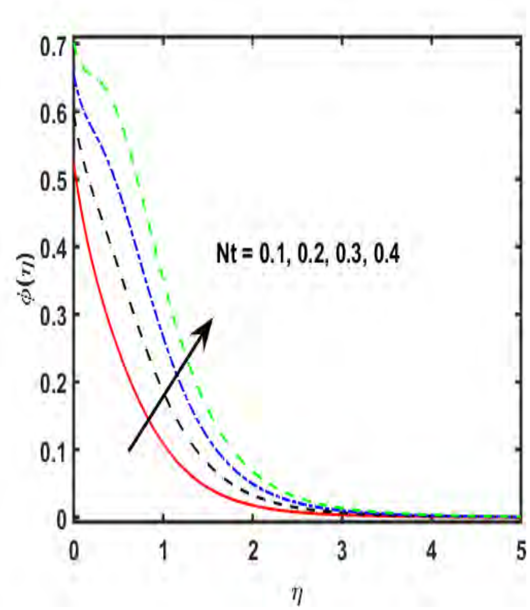

Fig. (2.15): Effect of Nt on $\phi(\eta)$.

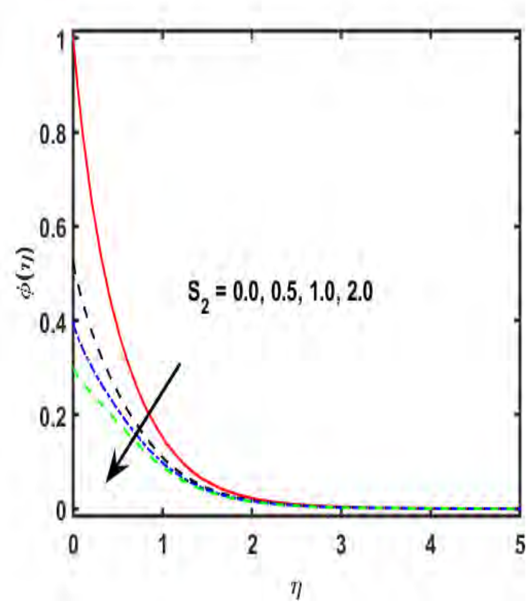

Fig. (2.16): Effect of S_2 on $\phi(\eta)$.

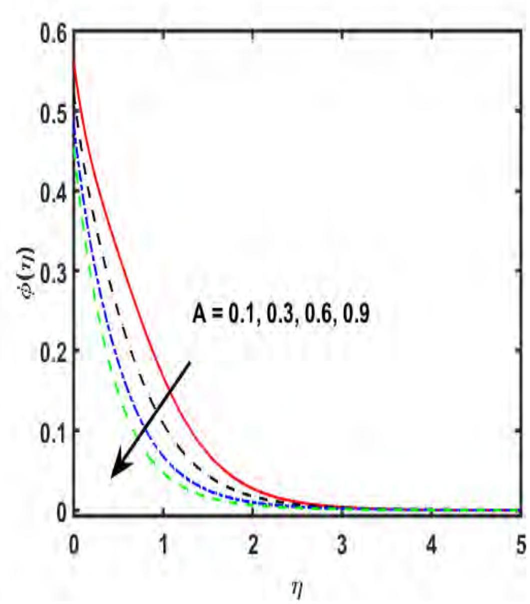

Fig. (2.17): Effect of A on $\phi(\eta)$.

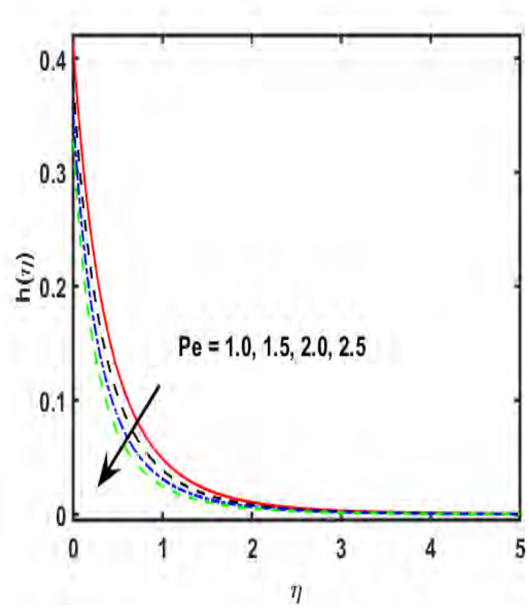

Fig. (2.18): Effect of Pe on $h(\eta)$.

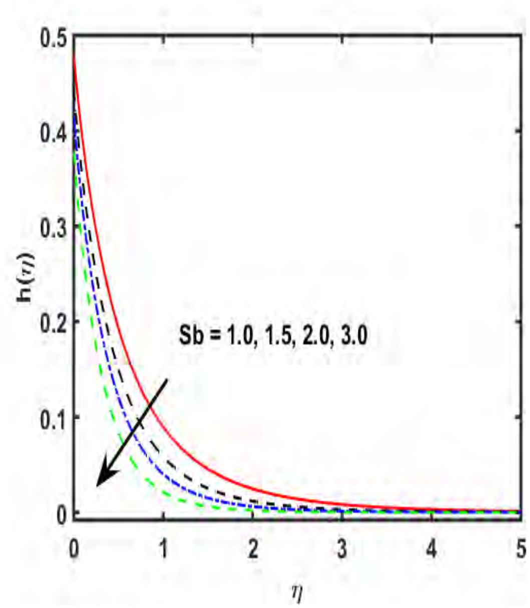

Fig. (2.19): Effect of Sb on $h(\eta)$.

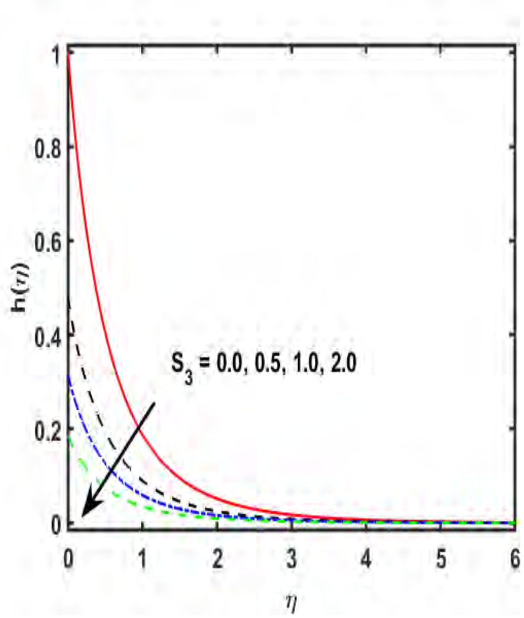

Fig. (2.20): Effect of S_3 on $h(\eta)$.

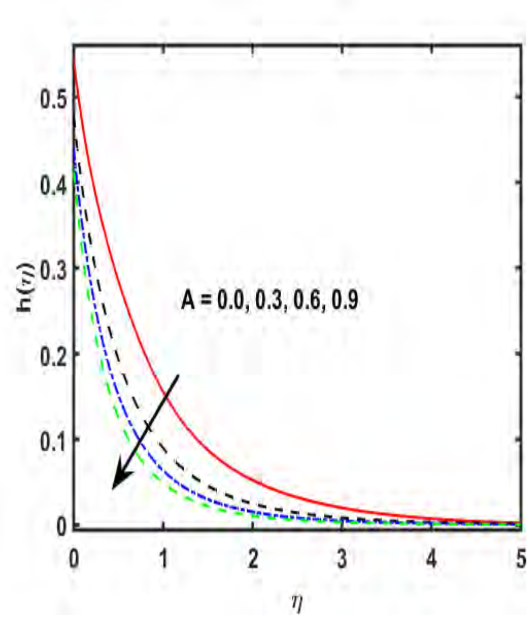

Fig. (2.21): Effect of A on $h(\eta)$.

2.3. Conclusion

The numerical computations of unsteady 2D MHD boundary layer flow of bio-convective Maxwell nanofluid with multiple slip boundary conditions through an exponentially stretching surface is examined. The key deductions of current chapter are,

- The boundary layer thickness and fluid velocity improve for larger values of λ.
- The fluid behaves like a solid for the stronger estimation of β_1. Hence, the velocity declines.
- The boundary layer thickness and velocity of fluid decays for Hartmann number.
- The $\theta(\eta)$ sketch enhances by stronger Ec, because K.E of the system increases by Ec.
- The concentration sketch leads to decaying for larger estimation of Sc and Nb.
- The enhancement of Sb and Pe diminishes the microorganism density distribution.
- The heat, mass, and microorganism transfer rate improve for stronger β_1.
- The non-Newtonian fluid model reduces to Newtonian by taking $\beta_1 = 0$.

Chapter 03

Theoretical analysis of Oldroyd-B nanofluid with microorganism and thermal radiation across an exponentially stretching surface

This chapter describes the transient two-dimensional radiative Oldroyd-B nanofluid flow over an exponentially stretchable permeable surface which is convectively heated. In the fluid regime microorganisms have been added in order to improve the stability of the nanofluid. Additionally, the heat and mass transport is examined with the influence of heat generation and chemical reaction. The mathematical model is into ODEs by incorporating self-similar transformations, which is solved numerically by using BVP midrich Maple technique. The outcome of the physical parameters is presented by the help of graphs and tabulated data. It is depicted that greater values of Deborah number minimizes the fluid velocity, whereas for retardation parameter its behavior increases. Further, higher values of relaxation parameter correspond to maximum heat and mass transfer rate, while it gives lower values against retardation parameter.

3.1. Mathematical Formulations

In this chapter, we evaluated an unsteady, two-dimensional, radiative Oldroyd-B nanofluid with chemical reaction and heat generation. The multiple slip conditions are imposed on the boundary of exponentially stretching sheet. The physical depiction of the paper is shown in **Fig. (3.1).** In the figure the stretching velocity is $u_w = \frac{cExp\left(\frac{x}{l}\right)}{1-\alpha_0 t}$. The temperature, concentration, and microorganism density are denoted by T, C, and n respectively. Further, T, C, and n are expressed at the wall by T_w, C_w, n_w and away from the wall by T_∞, C_∞, n_∞ respectively. By utilizing above mentioned consideration and approximation the governing equations are,

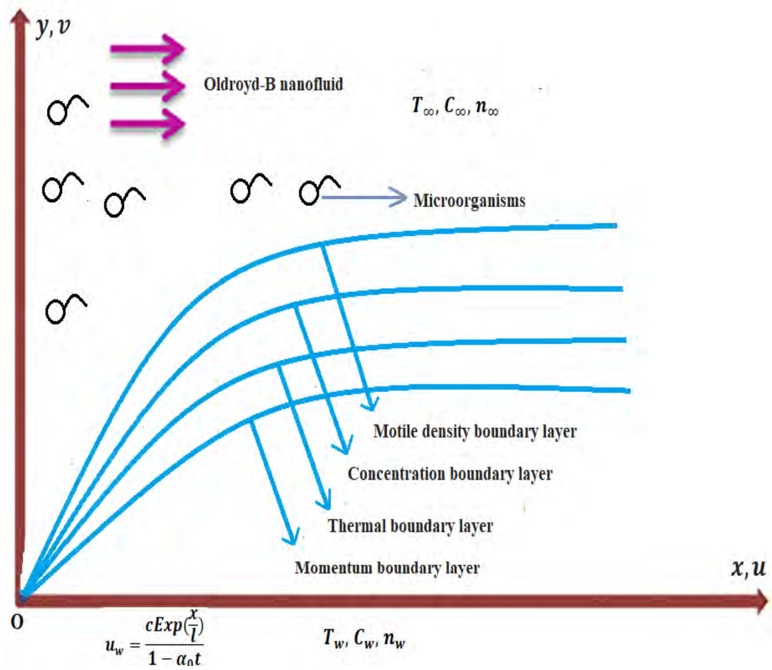

Fig. (3.1): Physics of the chapter.

$$\frac{\partial u}{\partial x}+\frac{\partial v}{\partial y}=0, \tag{3.1}$$

$$\frac{\partial u}{\partial t}+u\frac{\partial u}{\partial x}+v\frac{\partial u}{\partial y}+\lambda_1\begin{pmatrix}\frac{\partial^2 u}{\partial t^2}+2u\frac{\partial^2 u}{\partial x\,\partial t}+2uv\frac{\partial^2 u}{\partial x\,\partial y}\\ +u^2\frac{\partial^2 u}{\partial x^2}+v^2\frac{\partial^2 u}{\partial y^2}+2v\frac{\partial^2 u}{\partial y\,\partial t}\end{pmatrix}=\nu\frac{\partial^2 u}{\partial y^2}+\nu\lambda_2\begin{pmatrix}\frac{\partial^3 u}{\partial y^3}+\frac{\partial^3 u}{\partial t\,\partial y^2}+u\frac{\partial^3 u}{\partial x\,\partial y^2}\\ -\frac{\partial u}{\partial y}\frac{\partial^2 v}{\partial y^2}-\frac{\partial u}{\partial x}\frac{\partial^2 u}{\partial y^2}\end{pmatrix}, \tag{3.2}$$

$$\frac{\partial T}{\partial t}+u\frac{\partial T}{\partial x}+v\frac{\partial T}{\partial y}=\alpha\frac{\partial^2 T}{\partial y^2}+\tau\left(\frac{D_T}{T_\infty}\left(\frac{\partial T}{\partial y}\right)^2+D_B\frac{\partial T}{\partial y}\frac{\partial C}{\partial y}\right)+\frac{Q_0}{\rho c_p}(T-T_\infty)-\frac{1}{\rho c_p}\frac{\partial q_r}{\partial y}, \tag{3.3}$$

$$\frac{\partial C}{\partial t}+u\frac{\partial C}{\partial x}+v\frac{\partial C}{\partial y}=D_B\frac{\partial^2 C}{\partial y^2}-\frac{D_T}{T_\infty}\frac{\partial^2 T}{\partial y^2}+k_1(C_\infty-C), \tag{3.4}$$

$$\frac{\partial n}{\partial t}+u\frac{\partial n}{\partial x}+v\frac{\partial n}{\partial y}+\frac{\tilde{b}W_c}{C_w-C_\infty}\left[\frac{\partial}{\partial y}\left(n\frac{\partial C}{\partial y}\right)\right]=D_m\frac{\partial^2 n}{\partial y^2}. \tag{3.5}$$

Employing Rosseland approximation [89] the radiative heat flux is defined as,

$$q_r = -\frac{4\sigma^*}{3k^*}\frac{\partial T^4}{\partial y} \tag{3.6}$$

Now we expand T^4 about T_∞ by Taylor series, we get the expression as,

Using above equations (3.6) and (3.7) in equation (3.3), we get

$$T^4 = 4T^3T_\infty - 3T_\infty^4 \tag{3.7}$$

$$\frac{\partial T}{\partial t} + u\frac{\partial T}{\partial x} + v\frac{\partial T}{\partial y} = \left(\alpha + \frac{16\sigma^*}{3k^*\rho c_p}\right)\frac{\partial^2 T}{\partial y^2} + \tau\left(\frac{D_T}{T_\infty}\left(\frac{\partial T}{\partial y}\right)^2 + D_B\frac{\partial T}{\partial y}\frac{\partial C}{\partial y}\right) + \frac{Q_0}{\rho c_p}\left(T - T_\infty\right), \tag{3.8}$$

The related boundary conditions [90] are defined as,

$$\begin{gathered} u = u_w,\ v = V_w,\ T = T_w + L_2(t)\left(\frac{\partial T}{\partial y}\right), C = C_w + L_3(t)\left(\frac{\partial C}{\partial y}\right), n = n_w, \text{ when } y \to 0. \\ u = 0,\ T \to T_\infty, \text{C} \to C_\infty, n \to n_\infty, \text{ when } y \to \infty. \end{gathered} \tag{3.9}$$

In above equations the velocity component in $x-$ and $y-$directions are u and v respectively. The λ_1 and λ_2 represents the relaxation and retardation time of the fluid respectively. Moreover, V_w denotes the heat source / sink.

The wall temperature, wall concentration, and wall microorganism density are defined as, $T_w = T_\infty + \frac{T_0 Exp(\frac{x}{2l})}{(1-\alpha_0 t)^2}$, $C_w = C_\infty + \frac{C_0 Exp(\frac{x}{2l})}{(1-\alpha_0 t)^2}$, and $n_w = n_\infty + \frac{n_0 Exp(\frac{x}{2l})}{(1-\alpha_0 t)^2}$ respectively. Here b, T_0, C_0, and n_0 all are constants. The $L_2(t) = (L_2)_0\sqrt{(1-\alpha_0 t)}$, and $L_3(t) = (L_3)_0\sqrt{(1-\alpha_0 t)}$, are the variable thermal slip and concentration slip factors and $(L_1)_0$ and $(L_2)_0$ are initial thermal and concentration slip respectively.

The similarity variables [91] are stated as,

$$\eta = y\sqrt{\frac{a}{2\nu l(1-\alpha_0 t)}}Exp(\frac{x}{2l}),\ T = T_\infty + \frac{T_0 Exp(\frac{x}{2l})}{(1-\alpha_0 t)^2}\theta(\eta),\ C = C_\infty + \frac{C_0 Exp(\frac{x}{2l})}{(1-\alpha_0 t)^2}\phi(\eta),$$

$$n = n_\infty + \frac{n_0 Exp\left(\frac{x}{2l}\right)}{(1-\alpha_0 t)^2}h(\eta),\ u = \frac{af'(\eta)Exp\left(\frac{x}{l}\right)}{(1-\alpha_0 t)},\ v = -\sqrt{\frac{\nu a}{2l(1-\alpha_0 t)}}Exp\left(\frac{x}{2l}\right)[f(\eta)+\eta f'(\eta)]. \quad (3.10)$$

Using Eq. (3.10), Eq. (3.1) satisfied automatically, while other equations. take the form,

$$f''' - \begin{pmatrix} A(2f'+\eta f'') \\ +2f'^2 + ff'' \end{pmatrix} - \beta_1 \begin{pmatrix} A^2\left(2f' + \frac{7\eta}{4}f'' + \frac{\eta^2}{4}f'''\right) \\ +A(4f'^2 + 2\eta f'f'') + 4f'^3 \\ -A(3ff'' + \eta ff''') \\ -\eta f'^2 f'' - 6ff'f'' + f^2 f''' \end{pmatrix} + \beta_2 \begin{pmatrix} 3f''^2 + 2f'f''' \\ -ff'''' \\ +A(4f''' + \eta f'''') \end{pmatrix} = 0, \quad (3.11)$$

$$(1+\frac{4}{3}Rd)\theta'' + \Pr\left(f\theta' - f'\theta - A\left(2\theta + \frac{\eta}{2}\theta'\right) + Nb\theta'\phi' + Nt\theta'^2 + Q\theta\right) = 0, \quad (3.12)$$

$$\phi'' + Sc(f\phi' - f'\phi) - ScA(4\phi + \eta\phi') + Sc\sigma\phi + \frac{Nt}{Nb}\theta'' = 0, \quad (3.13)$$

$$h'' + Sb(fh' - f'h) - SbA(4h + \eta h') - Pe((h+\Gamma)\phi'' + h'\phi') = 0. \quad (3.14)$$

The disturbed boundary conditions are,

$$f(\eta) = s,\ f'(\eta) = \lambda,\ \theta(\eta) = 1 + S_1\theta'(\eta),\ \phi(\eta) = 1 + S_2\phi'(\eta),\ h(\eta) = 1 \text{ as } \eta \to 0.$$
$$f'(\eta) = 0,\ \theta(\eta) = \phi(\eta) = h(\eta) = 0 \text{ as } \eta \to \infty. \quad (3.15)$$

The parameter s is the heat source / sink parameter. Further, S_1 and S_2 are signify the thermal slip and concentration slip parameter, respectively. Further, we take $\lambda_1 = \lambda_0(1-\alpha_0 t)$, $\lambda_2 = \lambda_0^*(1-\alpha_0 t)$, $k_1 = \frac{k_0}{(1-\alpha_0 t)}$, and $Q_0 = \frac{Q_1}{(1-\alpha_0 t)}$. The parameters are in dimensionless form,

$$A=\frac{l\alpha_0}{a},\lambda=\frac{c}{a},\beta_1=\frac{\lambda_0 a}{2l},\ Rd=\frac{4T_\infty^3\sigma^*}{3k^*k},\ \beta_2=\frac{\lambda_0^* a}{2l},$$

$$Nb=\frac{\tau D_B\Delta C}{\nu},Nt=\frac{\tau D_T\Delta T}{\nu T_\infty},Sc=\frac{\nu}{D_B},Sb=\frac{\nu}{D_m},\Pr=\frac{\upsilon}{\alpha},\tag{3.16}$$

$$Pe=\frac{\tilde{b}W_c D_m}{\nu^2},\sigma=\frac{k_0\Delta C}{a},S_1=(L_2)_0\sqrt{\frac{a}{2l\nu}},S_2=(L_3)_0\sqrt{\frac{a}{2l\nu}},Q=\frac{Q_1}{\rho c_p a}.$$

3.1.1. Physical Quantities

The quantities of physical interest like Nusselt number, Sherwood number, and microorganism number are very vital to engineering perspective. These quantities are characterized as,

$$C_{fx}=\frac{\tau_{xy}\big|_{y=0}}{\rho {u_w}^2},\qquad Nu_x=\frac{xq_m}{k(T_w-T_\infty)},\qquad Sh_x=\frac{xj_m}{D_B(C_w-C_\infty)},Q_{nx}=\frac{xz_w}{D_m n_w}.\tag{3.17}$$

In above equation k is thermal conductivity. The heat flux (q_m), mass flux (j_m), and microorganism flux (z_w), which are defined as,

$$\tau_{xy}=\lambda_1\left(\begin{matrix}\frac{\partial^2 u}{\partial t^2}+u^2\frac{\partial^2 u}{\partial x^2}+v^2\frac{\partial^2 u}{\partial y^2}\\+2u\frac{\partial^2 u}{\partial x\,\partial t}+2v\frac{\partial u}{\partial y\,\partial t}+2uv\frac{\partial^2 u}{\partial x\,\partial y}\end{matrix}\right)-\nu\lambda_2\left.\left(\begin{matrix}\frac{\partial^3 u}{\partial t\,\partial y^2}+u\frac{\partial^3 u}{\partial x\,\partial y^2}+\frac{\partial^3 u}{\partial y^3}\\-\frac{\partial u}{\partial x}\frac{\partial^2 u}{\partial y^2}-\frac{\partial u}{\partial y}\frac{\partial^2 v}{\partial y^2}\end{matrix}\right)\right|_{y=0}\tag{3.18}$$

$$q_m=\left|\left(k\frac{\partial T}{\partial y}-\frac{4\sigma^*}{3k^*}\frac{\partial T^4}{\partial y}\right)\right|_{y=0},j_m=-D_B\left|\frac{\partial C}{\partial y}\right|_{y=0},\ z_w=-D_m\left|\frac{\partial n}{\partial y}\right|_{y=0}.\tag{3.19}$$

The dimensionless form of physical quantities are defined as,

$$\left(\begin{matrix}Re_x^{\frac{1}{2}}Cf_x=\frac{\beta_1}{\lambda^2}\left(\frac{\left(f'(0)+2A\right)^2 f'(0)}{A}-3f(0)f''(0)(1+f'(0))\right)\\ Re_x^{-\frac{1}{2}}Nu_x=-\left(1+\frac{4}{3}Rd\right)\theta'(0),\\ Re_x^{-\frac{1}{2}}Sh_x=-\phi'(0),\\ Re_x^{-1/2}Q_{nx}=-h'0)\end{matrix}\right).\tag{3.20}$$

3.2. Results and Discussion

In this section, we evaluated an unsteady two-dimensional radiative Oldroyd-B nanofluid towards an exponentially stretching surface with boundary slip effect. The influence of emerging parameters, such as relaxation parameter (β_1), retardation parameter (β_2), heat generation parameter (Q), unsteadiness parameter (A), radiation parameter (Rd), thermophoresis parameter (Nt), Brownian motion parameter (Nb), chemical reaction parameter (σ), bio-convection Schmidt number (Sb), thermal slip parameter (S_1), and concentration slip parameter (S_2). on the velocity profile, temperature distribution, and concentration distribution is presented. Further, tabulated data is determined for the Nusselt, Sherwood, and microorganism number. The values of controlling parameters are specified as $\beta_1 = \beta_2 = 1.0$, $A = 0.1$, $Q = 0.2$, $\lambda = 1.0$, $\Pr = 2.0$, $Nb = 0.3$, $Rd = 0.2$, $\sigma = Nt = 0.1$, $Sc = 2.0$, $Pe = Sb = 2.0$, $S_1 = S_2 = 0.5$. A comparison of limiting case of our results and previously published articles is made in **Table 3.1.** It shown from the tabulated data that $-f''(0)$ have good agreement with the earlier published results. It is exposed that higher estimation of s declines the velocity gradient. The influence of the various emerging parameters β_1, β_2, A, Sb, and Pe on the Nusselt, Sherwood, and microorganism number are shown in **table (3.2).** It is examined that as escalating the values of β_1, β_2, and A, the heat, mass, and microorganism transfer rate declines for β_1, while it exhibits opposite trend for β_2 and A. The effect of microorganism transfer rate for numerous values of Sb and Pe also revealed in the **table (3.2).** It is noted in **table 3.2** that microorganism transfer rate enhances for higher values of Sb and Pe.

Table 3.1: Comparison of $-\boldsymbol{f}''(\mathbf{0})$ against $\boldsymbol{s}$, when $\boldsymbol{\beta_1} = \boldsymbol{\beta_2} = \boldsymbol{Nb} = \boldsymbol{Nt} = \mathbf{Q} = \mathbf{0}, \boldsymbol{S_1} \to \infty$.

$\boldsymbol{s}$	Sandeep and Sulochana [92]	Afify et al. [93]	Present
0.0	0.6776564	0.677648	0.677656
0.5	0.8736448	0.873643	0.873644
0.75	0.9844402	0.984439	0.984440

Table 3.2: The variation in $\boldsymbol{Nu_x}$, $\boldsymbol{Sh_x}$, and $\boldsymbol{Qn_x}$ against various parameter.

$\boldsymbol{\beta_1}$	β_2	A	Sb	Pe	Nu_x	Sh_x	Qn_x
0.0	0.5	0.1	2.0	2.0	0.60912	0.58576	2.56758
0.5	-				0.60068	0.57499	2.50536
1.0	-		2.0		0.59408	0.56654	2.45831
0.5	0.2			2.0	0.57279	0.54028	2.31593
	0.5	0.1			0.58423	0.55417	2.39082
0.5	1.0		2.0		0.59408	0.56654	2.45831
	0.5	0.0		2.0	0.57072	0.54349	2.10486
		0.1			0.59369	0.56658	2.45655
0.5		0.2			0.61251	0.58536	2.80931
	0.5		1.5				2.22982
0.5			2.0	2.0			2.45655
		0.1	2.5				2.66067
	0.5		2.0	1.5			2.24279
0.5		0.1		2.0			2.45655
	0.5		2.0	2.5			2.67479

The impact Pr, Nb and Nt on the Nusselt number is graphically found in **Fig. 3.2 (a-b).** From **Fig. 3.2 (a** and **b),** it is seen that the heat transport rate decays as growing the Nb and Nt, while reverse trend is noticed for higher values of Pr. **Fig. 3.3** exhibits the mass transfer rate for various Sc against σ. It is cleared form the figure that as enhancing the values of Sc the Sh_x curve rises. This is because as increase the Schmidt number implies the reduction in mass diffusion, which reducing the concentration distribution, therefore the concentration rate at the surface is increased. The microorganism transfer rate for various values of Sb and Pe is demonstrated in **Fig. 3.4**. From the figure it is seen that microorganism transfer rate enhances for both Sb and Pe. The effect of different values of β_1 and β_2 on the velocity field is illustrated in the **Fig. 3.5 (a** and **b)**. It is demonstrated that plot of $f'(\eta)$ declines as uplifting the values of β_1, but opposite behavior is noticed for higher values of β_2. Physically, by the increment of β_1 leads to the stronger viscous forces which resist the fluid motion and hence velocity of the fluid shrinkages. In addition, it is presented that for higher values of β_2, the viscous forces reduce therefore velocity of fluid enlarges. Moreover, when $\beta_1 = \beta_2 = 0$ the viscous fluid is obtained. **Fig. 3.6 (a-d)** shows the diversity in the thermal distribution against the various values of β_1, β_2, Nb and Nt. It is signified that $\theta(\eta)$ plots maximize for β_1, because the viscous forces are dominates as boosting the β_1, which is reported in **Figs. 3.6 (a)**. Hence the production of heat cause to enhances the temperature and concentration. The **Fig. 3.6 (b)** possess the diminishing behavior for $\theta(\eta)$ against the various values of β_2. Additionally, we see that for greater values of β_2 the elasticity increases, thereby the temperature declines. The impact of radiation parameter and heat generation / absorption parameter on thermal distribution is considered in **Fig. 3.7(a-b)**. It is portrayed in **Fig. 3.7(a)** that due to higher radiation effect the temperature boundary layer thickness increase, consequently the enhancement in temperature of the nanofluid is occurred, which is reported in **Fig. 3.7(a)**. Physically, for the larger values of Rd the surface flux enhances which is responsible for the augmentation of temperature. The influence of heat generation effect are illustrated in **Fig. 3.7(b).** It is observed that temperature of higher generation effect is maximum. Further, in the occurrence of heat generation the temperature of fluid and thermal boundary layer always raises. The influences β_1, β_2, A and Nb on concentration distribution are considered in **Fig. 3.8(a-b).** An opposite behavior of $\phi(\eta)$ can be observed against relaxation and retardation time parameter. Concentration sketch has increasing nature for higher β_1, whereas it depicts decreasing trend against maximum values of β_2, which is shown in **Fig. 3.8(a** and **b)**. **Fig. 3.9(a-b)** shows the behavior of $\phi(\eta)$ against various Sc and σ. It is observed that for larger values of Sc the concentration plot tends to reduce. This is because of the direct relation of Sc to diffusion rate and its addition reduces the mass concentration. This explanation is established in **Fig. 3.9(a**). The chemical reaction influences on mass concentration are depicted in **Fig. 3.9(b**). It is revealed that the $\phi(\eta)$ is an increasing function for σ. In **Fig. 3.10 (a** and **b)** the graphs of $\boldsymbol{h(\eta)}$ against different values of relaxation and retardation time, an opposite behavior is obtained. Which can be clarified from figures that by escalating the values of β_1 the microorganism density intensifies, whereas its density reduces for various values of β_2. The decreasing behavior in $\boldsymbol{h(\eta)}$ curve is noticed for various values of and Pe and Sb in **Fig. 3.10(c** and **d)**. It is illustrated that enhancement in Pe leads to decays the microorganism diffusivity, hence density of microorganism reduces in the nanofluid. Further, it is noticed that due to higher Sb the rapid reduction in the $\boldsymbol{h(\eta)}$ occurs, because Sb opposed the fluid motion.

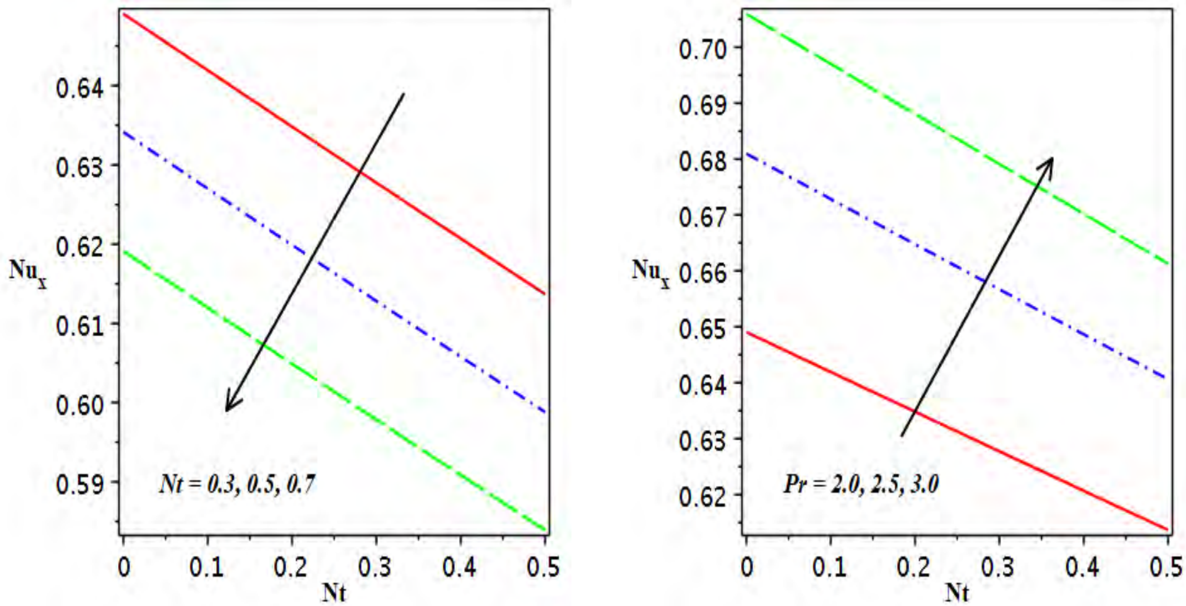

(a) (b)

Figs. 3.2 (a and b): Heat transfer rate for various values of Nb and Pr against Nt.

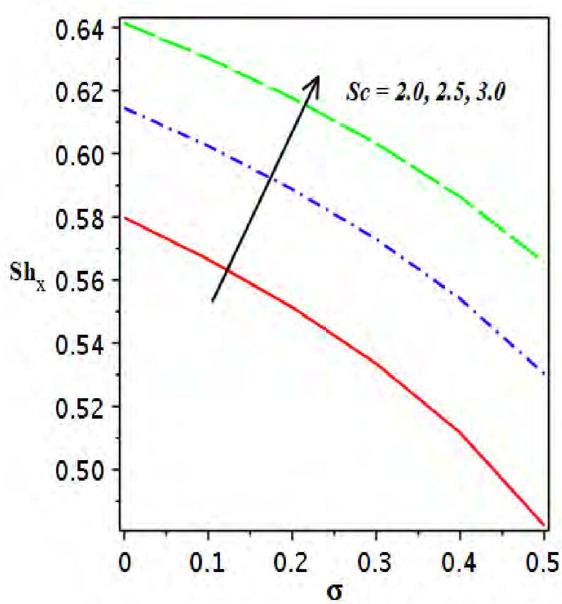

Fig. 3.3: The plot mass transfer rate various value of Sc against σ.

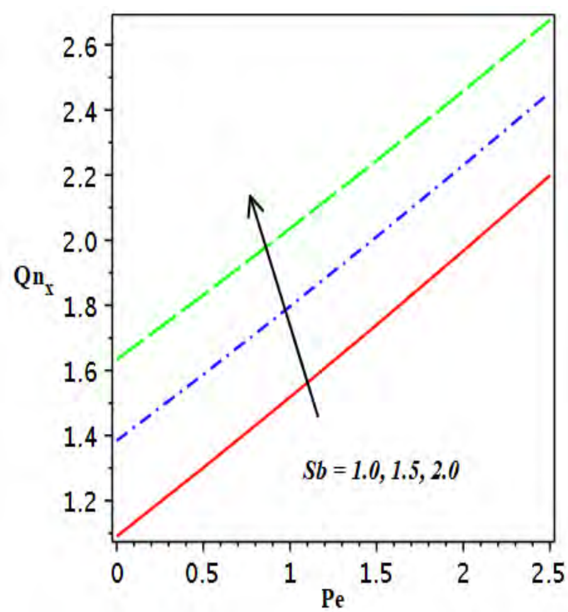

Fig. 3.4: The plot of microorganism transfer rate various value of Sb against Pe.

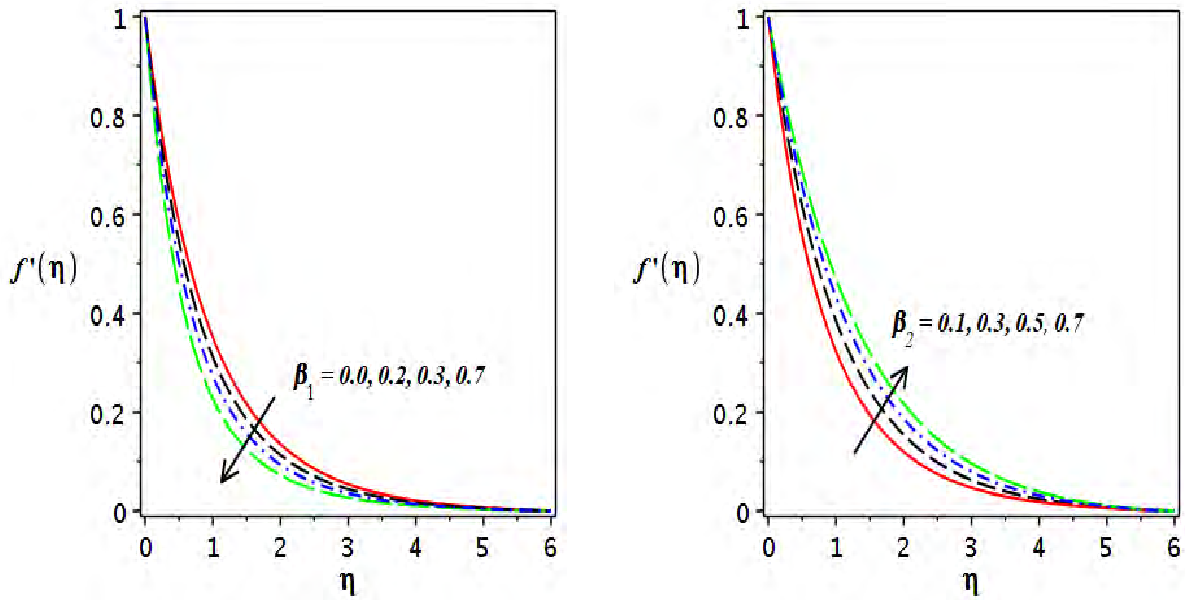

(a) (b)

Fig. 3.5: Plot of $f'(\eta)$.against various values of (a) β_1 and (b) β_2.

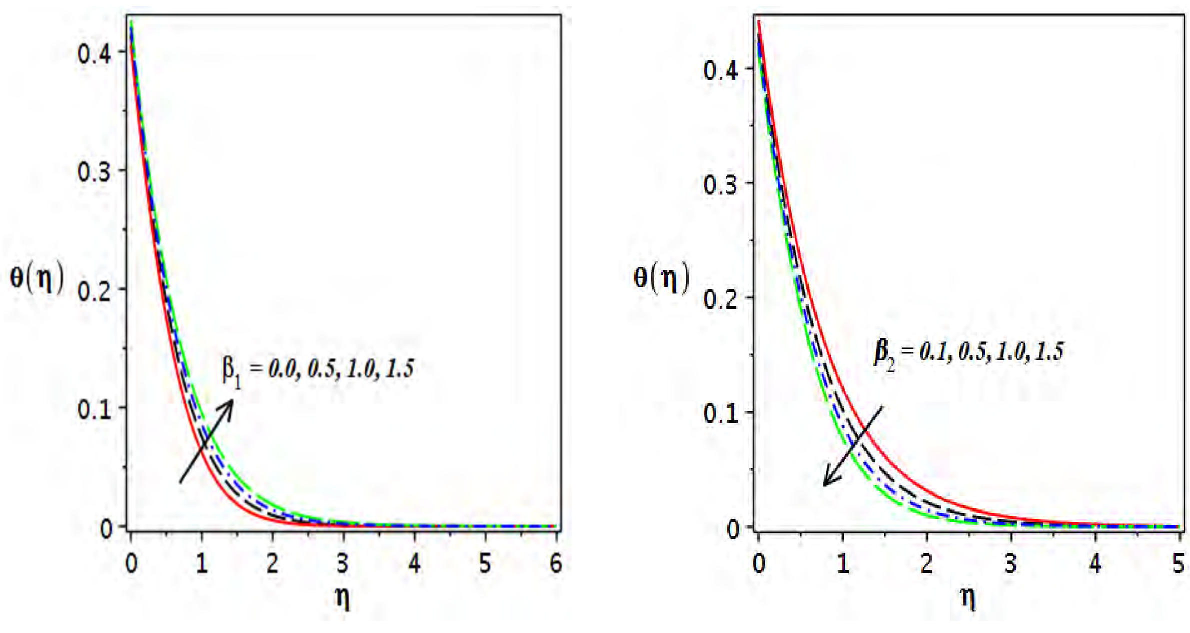

(a) (b)

Fig. 3.6: Impact of (a) $\beta_1$and (b) β_2, on $\theta(\eta)$.

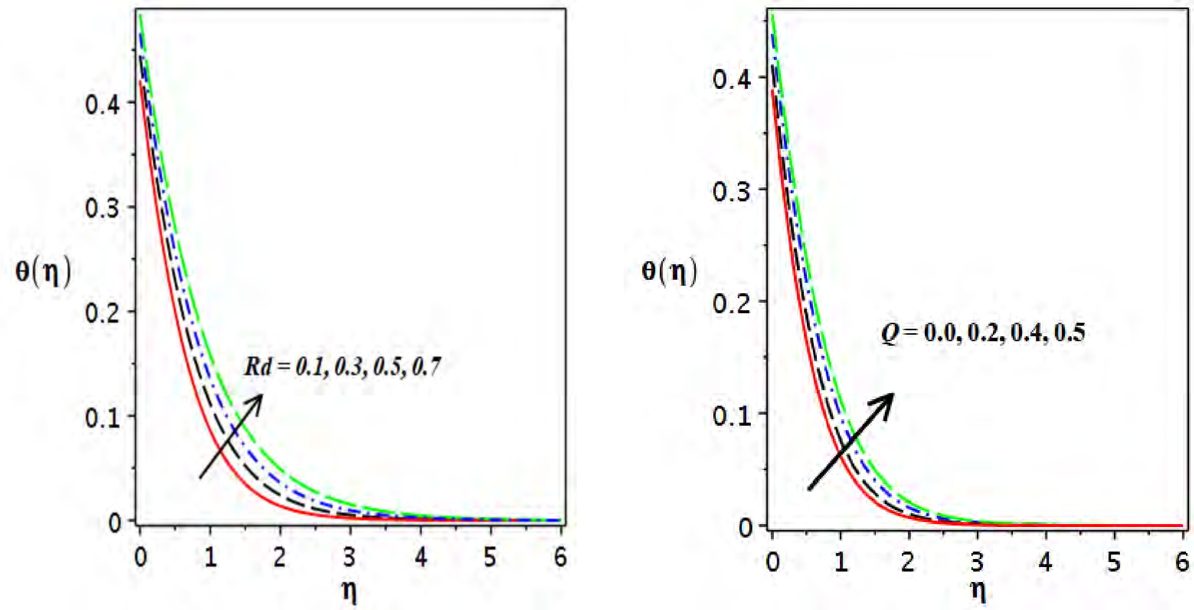

(a) (b)

Fig. 3.7: Impact of (a) Rd and (b) Q on $\theta(\eta)$.

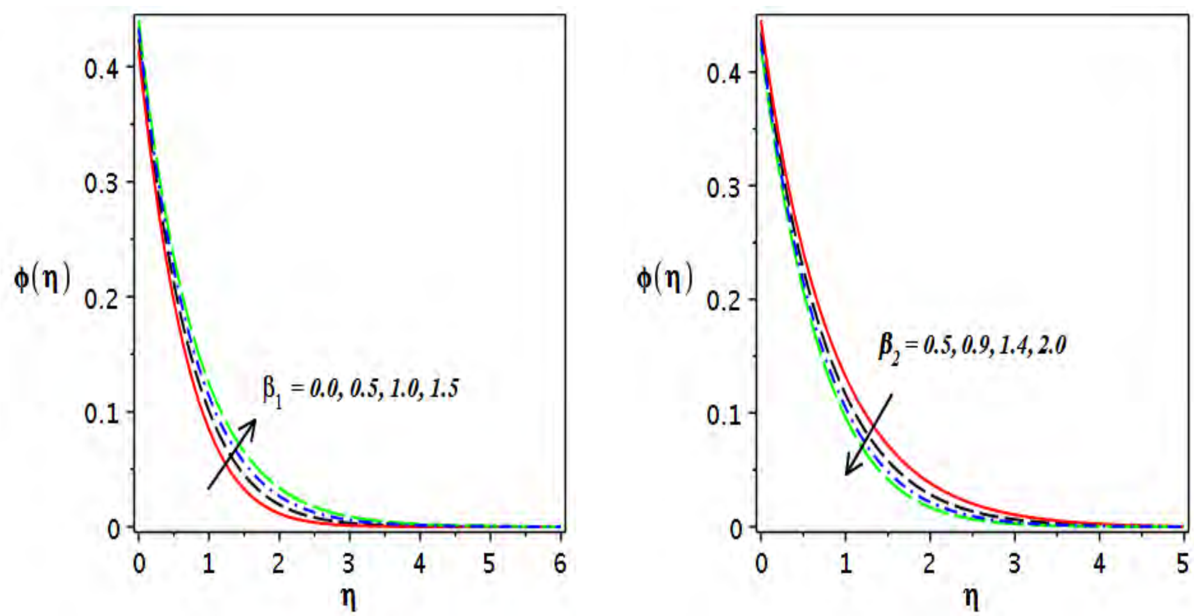

(a) (b)

Fig. 3.8: Variations in conceteration plot due to disticnt (a) β_1 and (b) β_2.

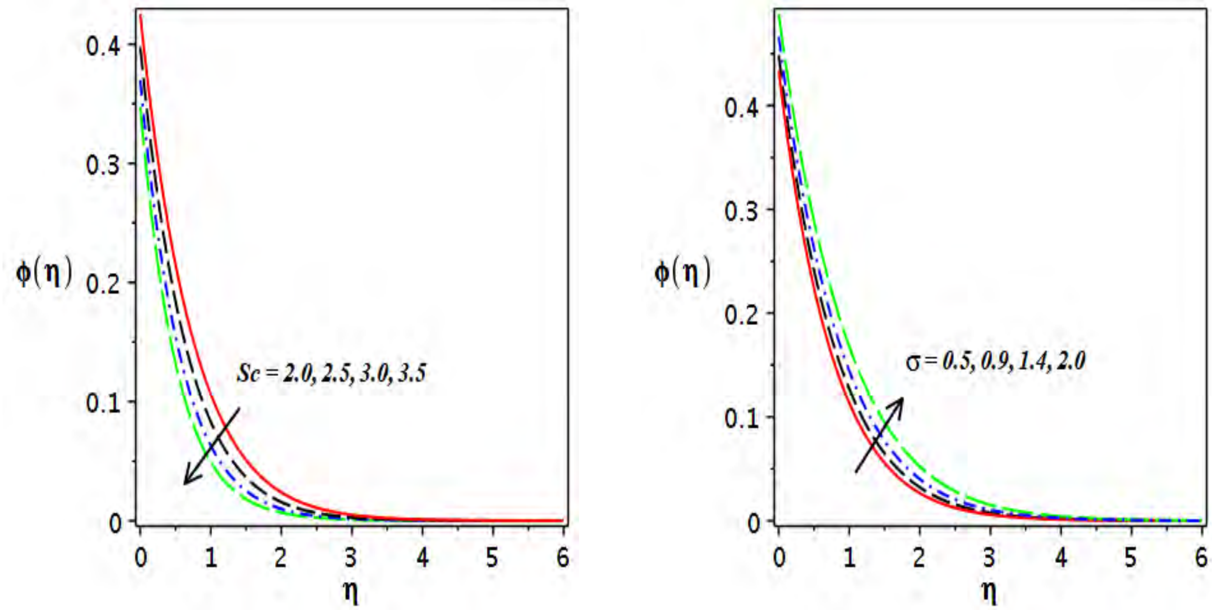

(a) (b)

Fig. 3.9: Concentration distribution for several values of (a) Sc and (b) σ.

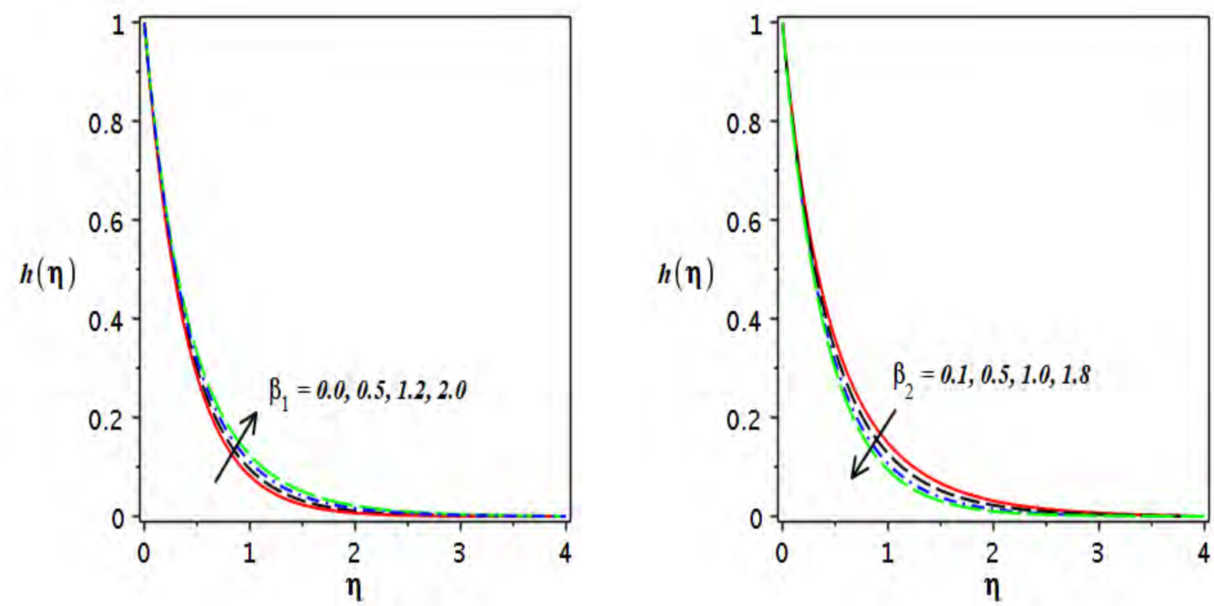

(a) (b)

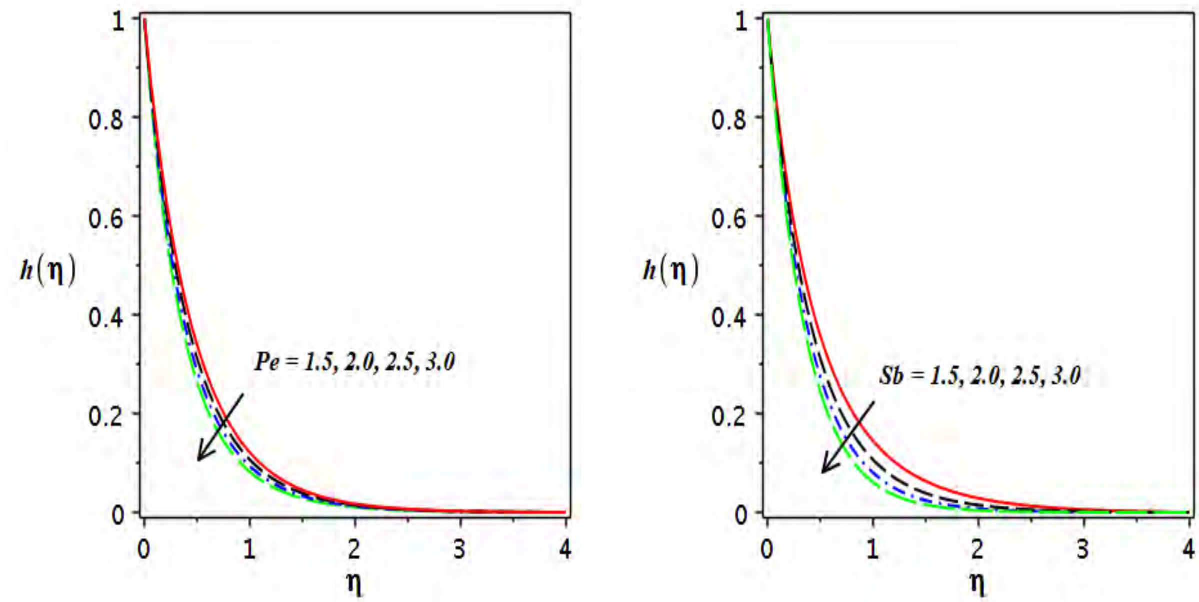

(c) (d)

Fig. 3.10: Impact of (a) β_1 (b) β_2, (c) Pe, and (d) Sb on microorganism density plot.

3.3. Concluding Remarks

The numerical investigation of two-dimensional radiative Oldroyd-B nanofluid through an exponentially stretching surface influence by the heat generation and chemical reaction is presented. Some useful results are mentioned as,

- The velocity profile showing opposite trend for β_1 and β_2. It is implying that the $f'(\eta)$ depressed for β_1, but improved for β_2.
- Surface flux increases due to rising the value of Rd, which causes an increment in the temperature.
- Lager values of Sb.and Pe decays the $h(\eta)$ curve due to decaying microorganism diffusivity.
- The higher values Nt shows increasing effect for both $\theta(\eta)$ and $\phi(\eta)$ plots.

Chapter 04

Mathematical analysis of thermal and solutal transport in a Maxwell fluid

The objective of this chapter is to perform the analysis on energy transport mechanism in the flow of a Maxwell fluid over a stretchable sheet under the influence of magnetic field and double stratification. The conductivity of fluid is assumed as variable and transport phenomenon of thermal and solutal energy is studied in the view of Cattaneo-Christov theory and thermophoretic effect. The under-consideration flow is modelled in the form of PDEs and converted into a set of coupled ODEs by using suitable transformation. The coupled ODEs are numerically solved by implementing the bvp4c Matlab technique. The results of velocity profile, temperature distribution, and concentration distribution are discussed against the emerging parameters. It is observed that fluid velocity decreases for larger values of Deborah number, Further, it is noticed that both thermal and concentration stratification parameters diminish the heat and mass transfer rate.

4.1. Mathematical Modelling

Here, we examined the laminar, steady, and 3D incompressible flow of Maxwell fluid flow generated by a stretching surface subjected to stratification conditions and normally applied magnetic field B_0. The transport of mass and heat is examined by employing thermophoretic effect and Cattaneo-Christov theory. Additionally, heat source and chemical reactions are also considered here. The flow pattern is revealed in **Fig. 4.1**. The stretching velocities in the $x-$ and $y-$direction are assumed by $u_w = ax$ and $v_w = by$ respectively. The fluid velocity field of the problem is $\mathbf{V} = \left(u(x,y,z), v(x,y,z), w(x,y,z)\right)$. The governing boundary layer equations of flow, energy, and mass transport are follows as [94],

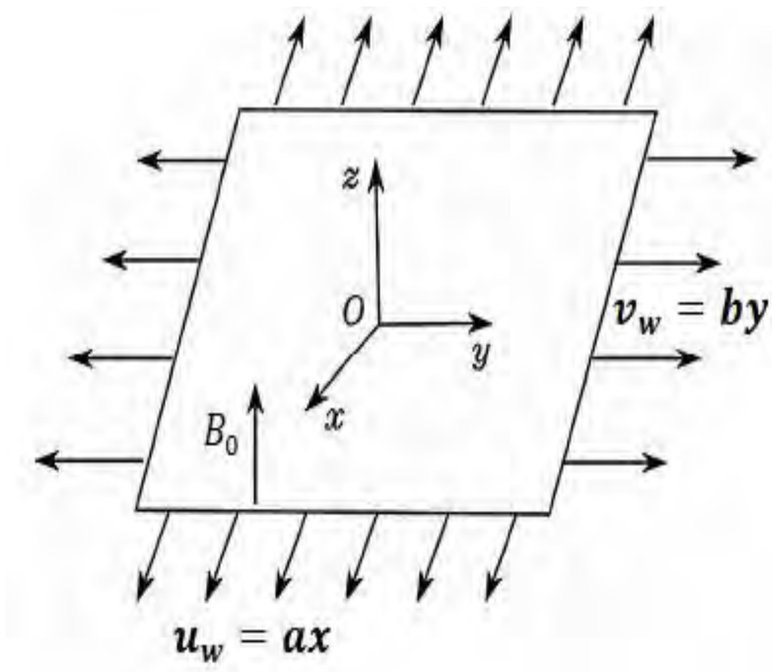

Fig. 4.1: flow diagram of the chapter.

$$\frac{\partial u}{\partial x} + \frac{\partial v}{\partial y} + \frac{\partial w}{\partial z} = 0, \tag{4.1}$$

$$u\frac{\partial u}{\partial x} + v\frac{\partial u}{\partial y} + w\frac{\partial u}{\partial z} + \lambda_1 \begin{pmatrix} u^2 \dfrac{\partial^2 u}{\partial x^2} + 2w\left(v\dfrac{\partial^2 u}{\partial y \partial z} + u\dfrac{\partial^2 u}{\partial x \partial z} \right) \\ + v^2 \dfrac{\partial^2 u}{\partial y^2} + 2uv\dfrac{\partial^2 u}{\partial x \partial y} + w^2 \dfrac{\partial^2 u}{\partial z^2} \end{pmatrix} = \nu \frac{\partial^2 u}{\partial z^2} - \frac{\sigma_1 B_0^2}{\rho}\left(\lambda_1 w \frac{\partial u}{\partial z} + u \right), \tag{4.2}$$

$$u\frac{\partial v}{\partial x} + v\frac{\partial v}{\partial y} + w\frac{\partial v}{\partial z} + \lambda_1 \begin{pmatrix} u^2 \dfrac{\partial^2 v}{\partial x^2} + 2w\left(v\dfrac{\partial^2 v}{\partial y \partial z} + u\dfrac{\partial^2 v}{\partial x \partial z} \right) \\ + v^2 \dfrac{\partial^2 v}{\partial y^2} + 2uv\dfrac{\partial^2 v}{\partial x \partial y} + w^2 \dfrac{\partial^2 v}{\partial z^2} \end{pmatrix} = \nu \frac{\partial^2 v}{\partial z^2} - \frac{\sigma_1 B_0^2}{\rho}\left(\lambda_1 w \frac{\partial v}{\partial z} + v \right), \tag{4.3}$$

$$u\frac{\partial T}{\partial x}+v\frac{\partial T}{\partial y}+w\frac{\partial T}{\partial z}+\pi_1\Theta_E-\frac{Q_0}{\rho c_p}(T-T_\infty)=\frac{1}{\rho c_p}\frac{\partial}{\partial z}\left(k\left(T\right)\frac{\partial T}{\partial z}\right), \tag{4.4}$$

$$u\frac{\partial C}{\partial x}+v\frac{\partial C}{\partial y}+w\frac{\partial C}{\partial z}+\pi_2\Phi_C+k_1(C-C_\infty)=D_B\frac{\partial^2 C}{\partial z^2}-\frac{\partial}{\partial z}\left(V_T(C-C_\infty)\right). \tag{4.5}$$

Here,

$$\Theta_E=\begin{pmatrix} u^2\frac{\partial^2 T}{\partial x^2} & +\left(\frac{\partial u}{\partial x}\frac{\partial T}{\partial x}+\frac{\partial w}{\partial x}\frac{\partial T}{\partial z}+\frac{\partial v}{\partial x}\frac{\partial T}{\partial y}\right)u+2uv\frac{\partial^2 T}{\partial x\partial y}+v^2\frac{\partial^2 T}{\partial y^2}+2vw\frac{\partial^2 T}{\partial y\partial z}+w^2\frac{\partial^2 T}{\partial z^2} \\ +\left(\frac{\partial u}{\partial y}\frac{\partial T}{\partial x}+\frac{\partial w}{\partial y}\frac{\partial T}{\partial z}+\frac{\partial v}{\partial y}\frac{\partial T}{\partial y}\right)v & +\left(\frac{\partial u}{\partial z}\frac{\partial T}{\partial x}+\frac{\partial w}{\partial z}\frac{\partial T}{\partial z}+\frac{\partial v}{\partial z}\frac{\partial T}{\partial y}\right)w+2uw\frac{\partial^2 T}{\partial x\partial z} \end{pmatrix}, \tag{4.6}$$

$$\Phi_C=\begin{pmatrix} u^2\frac{\partial^2 C}{\partial x^2} & +\left(\frac{\partial u}{\partial x}\frac{\partial C}{\partial x}+\frac{\partial w}{\partial x}\frac{\partial C}{\partial z}+\frac{\partial v}{\partial x}\frac{\partial C}{\partial y}\right)u+2uv\frac{\partial^2 C}{\partial x\partial y}+v^2\frac{\partial^2 C}{\partial y^2}+2vw\frac{\partial^2 C}{\partial y\partial z}+w^2\frac{\partial^2 C}{\partial z^2} \\ +\left(\frac{\partial u}{\partial y}\frac{\partial C}{\partial x}+\frac{\partial w}{\partial y}\frac{\partial C}{\partial z}+\frac{\partial v}{\partial y}\frac{\partial C}{\partial y}\right)v & +\left(\frac{\partial u}{\partial z}\frac{\partial C}{\partial x}+\frac{\partial w}{\partial z}\frac{\partial C}{\partial z}+\frac{\partial v}{\partial z}\frac{\partial C}{\partial y}\right)w+2uw\frac{\partial^2 C}{\partial x\partial z} \end{pmatrix}. \tag{4.7}$$

$$k\left(T\right)=k_\infty\left(1+\varepsilon\left(\frac{T-T_\infty}{T_w-T_0}\right)\right),\ V_T=-\nu\frac{k_t}{T_r}\frac{\partial T}{\partial z} \tag{4.8}$$

The concerned surface and free boundary conditions are defined as:

$$u=u_w=ax,\ v=v_w=by,\ w=0,\ T=T_w=a_1x+T_0,\ C=C_w=b_1x+C_0,\ \text{When }\ z=0,, \tag{4.9}$$

$$u\to 0,\ v\to 0,\ T\to T_\infty=c_1x+T_0,\ C\to C_\infty=d_1x+C_0.\ \text{When }\ z\to\infty. \tag{4.10}$$

In the above Eqs. symbols $B_0, \pi_1, \pi_2, \rho,\ V_T, \sigma_1,$ and $k\left(T\right)$ are symbolized the magnetic field, thermal relaxation time, concentration relaxation time, fluid density, thermophoretic velocity, electrical conductivity of fluid, and variable thermal conductivity, respectively. Moreover, νk_t is the thermophoretic coefficient and $a_1, b_1, c_1,$ and d_1 represents the constants.

4.1.1. Similarity Transformation

The appropriate similarity variables are defined as,

$$\begin{aligned}&\eta = z\sqrt{\left(\frac{a}{\nu}\right)},\, u = axf\,'(\eta),\, v = ayg\,'(\eta), w = -\sqrt{(\nu a)}\left(f(\eta)+g(\eta)\right),\\&T = \left(T_w - T_0\right)\theta(\eta) + T_\infty,\, C = \left(C_w - C_0\right)\phi(\eta) + C_\infty.\end{aligned} \tag{4.11}$$

Using above transformations, the Eqs. (4.2-4.5) with Eqs. (4.9-4.10) take the form,

$$\left(1-\beta_1\left(f+g\right)^2\right)f''' + \left(f+g\right)f'' - M^2 f' - f'^2 + 2\beta_1\left(f+g\right)f'f'' + M^2\left(\beta_1\left(f+g\right)f''\right) = 0, \tag{4.12}$$

$$\left(1-\beta_1\left(f+g\right)^2\right)g''' + \left(f+g\right)g'' - M^2 g' - g'^2 + 2\beta_1\left(f+g\right)g''g' + M^2\left(\beta\left(f+g\right)g''\right) = 0, \tag{4.13}$$

$$\begin{aligned}&\left(\left(1+\varepsilon\theta\right) - \Pr\delta_t\left(f+g\right)^2\right)\theta'' + \Pr\left(\delta_t\left(f+g\right)\left(f'+g'\right) + \left(f+g\right)\right)\theta' + \Pr Q\theta + \varepsilon\theta'^2\\&-\Pr\delta_t\left(\left(\delta_1+\theta\right)\left(f'^2 - \left(f+g\right)f''\right) - 2\left(f+g\right)f'\theta'\right) - \Pr\left(\theta+\delta_1\right)f' = 0,\end{aligned} \tag{4.14}$$

$$\begin{aligned}&\left(1-\delta_c Sc\left(f+g\right)^2\right)\phi'' + Sc\left(\delta_c\left(f+g\right)\left(f'+g'\right) + \left(f+g\right)\right)\phi' - Sc\tau_1\left(\phi'\theta' - \left(\phi+\Psi\right)\theta''\right)\\&-Sc\delta_c\left(\left(\delta_2+\phi\right)\left(f'^2 - \left(f+g\right)f''\right) - 2\left(f+g\right)f'\phi'\right) - Sc\left(\phi+\delta_2\right)f' + Sc\sigma\phi = 0.\end{aligned} \tag{4.15}$$

The concerned boundary conditions are,

$$\begin{aligned}&f'(0)=1,\; f(0)=0,\; g'(0)=\lambda,\; g(0)=0,\; \theta(0)=1-\delta_1,\; \phi(0)=1-\delta_2,\\&f'(\eta)=0,\; g'(\eta)=0,\; \theta(\eta)=0=\phi(\eta),\; at\;\; \eta\to\infty.\end{aligned} \tag{4.16}$$

The emerging parameters are symbolized as β_1, M, δ_t, δ_2, and τ_1, which denotes the relaxation time parameter, magnetic field parameter, thermal relaxation parameter, concentration stratification parameter, and thermophoretic parameter, respectively. The mathematically form of concerned parameters are,

$$\Pr = \frac{\nu}{\alpha},\ \tau_1 = \frac{-k_t\left(T_w - T_\infty\right)}{T_r},\ Q = \frac{Q_0}{a\rho c_p},\ \beta_1 = a\lambda_1,\ Sc = \frac{\nu}{D_B},\ \delta_1 = \frac{c_1}{a_1},$$
$$\lambda = \frac{b}{a},\ \delta_2 = \frac{d_1}{b_1},\ \sigma = \frac{k_1}{a},\ M = \sqrt{\frac{\sigma B_0^2}{a\rho}},\ \delta_t = \pi_1 a,\ \delta_c = \pi_2 a. \tag{4.17}$$

4.2. Results and Discussion

The ordinary differential Eqs. (4.12–4.15) with boundary conditions (4.16) are numerically tackled by the utilization of bvp4c Matlab technique. The obtained results are examined graphically across velocity field, thermal distribution, and concentration distribution for various physical parameters. The validation results are proved in **table 4.1** by the comparison of previously published results of Mukhopadhyay [95] and Khan et al. [96]. **Table 4.2** displays the numerical outcomes of the velocity gradient for several estimation of the magnetic parameter. It is noticed that the higher trend in magnetic parameter enhance the velocity gradient significantly.

Table 4.1: Comparison of $f''(0)$ with previously available data, when $\delta_1 = \delta_2 = 0 = \lambda = \delta_t = \delta_c$.

β_1	Mukhopadhyay [95]	Khan et al. [96]	Current results
0.0	0.9999963	1.00000	1.00048
0.2	1.051949	1.05189	1.052150
0.4	1.101851	1.10190	1.102042
0.6	1.150162	1.15014	1.150221
0.8	1.196693	1.19671	1.196720

Table 4.2: The velocity gradient for several values of M , as $\lambda = 0.5$ and $\beta_1 = 0.2$ **.**

M	$f''(0)$	$g''(0)$
0.00	1.224761	0.519116
0.20	1.242440	0.530168
0.30	1.294221	0.561457
0.60	1.382370	0.609008
0.80	1.491211	0.672113
1.00	1.627810	0.744985

Figs. 4.2 and **4.3** demonstrates the impact of a Deborah number β_1 against the velocity field $\left(f'(\eta) \text{ and } g'(\eta) \right)$. It is examined that the sketch of velocity is declining along x-axis and y-axis for the larger values of β_1. Actually, β_1 determine the difference between fluids and solids. For larger values of β_1 material behave like a solid whereas for smaller values of β_1 it behaves like a fluid. Furthermore, non-zero value of β_1 exhibits the elastic effect which restricts the flow and therefore boundary layer become thinner. The influence of magnetic parameter on velocity field is illustrated in **Figs. 4.4 and 4.5**. The fluid velocity reduces by the larger values of M . Physically, the magnetic parameter produced the Lorentz force due to which the retarding force is occurred in the fluid motion. Hence, due to greater values of M the velocity profile declines. The effect of λ (stretching parameter) against the $f'(\eta)$ and $g'(\eta)$ can be noted in **Figs. 4.6 and 4.7**. Stronger values of λ means the greater stretching rate in $y-$direction relative to the $x-$direction. Thus, the fluid velocity in $y-$direction is increased, although velocity in $x-$direction decreases. The variation in $\theta(\eta)$ plot for several values of ε is described in **Fig. 4.8.** It is noticed that $\theta(\eta)$ plot is increased as raising ε . Physically, due to stronger values of ε the more heat is transmitted from sheet to fluid and consequently enhancement occurs in the

temperature distribution. The behavior of τ_1 is discussed in **Figs. 4.9**. **Fig. 4.9** suggests that the $\phi(\eta)$ sketch is an increasing function for thermophoretic parameter by enlarging the values of τ_1. The characteristics of M on thermal and solutal plots $\theta(\eta)$ and $\phi(\eta)$ are depicted in **Figs. 4.10 and 4.11**. The $\theta(\eta)$ and $\phi(\eta)$ plots are boosted for larger values of M. Physically, fluid friction improves by lager values of M, as a result the thermal and concentration distribution boosts. **Figs. 4.12 and 4.13** proved that thermal and concentration relaxation time parameters δ_t and δ_c significantly decline the $\theta(\eta)$ and $\phi(\eta)$ plots, respectively. It is noted that, the case of classical Fourier's law and Fick's law is obtained when ($\delta_t = 0 = \delta_c$) and Cattaneo-Christov heat conduction model and generalized Fick's law is obtained when ($\delta_t, \delta_c > 0$). The δ_1 shows declining effect on the $\theta(\eta)$ plot, which is shown in **Fig. 4.14**. Physically, due to stratification effect, the effective temperature of fluid between sheets and away from the sheet is declined, which correspond to thinner thermal boundary layer and weaker temperature. The variation in the $\phi(\eta)$ plot for several values of δ_2 is designated in the **Figs. 4.15**. It is observed that the concentration plot ($\phi(\eta)$) diminishes by the growing values of δ_2. This is the fact, that the fluid has lower concentration near the plate as compared to ambient medium. Moreover, due to enhancement of δ_2 the volumetric fraction between surface and reference nanoparticles is examined to decaying.

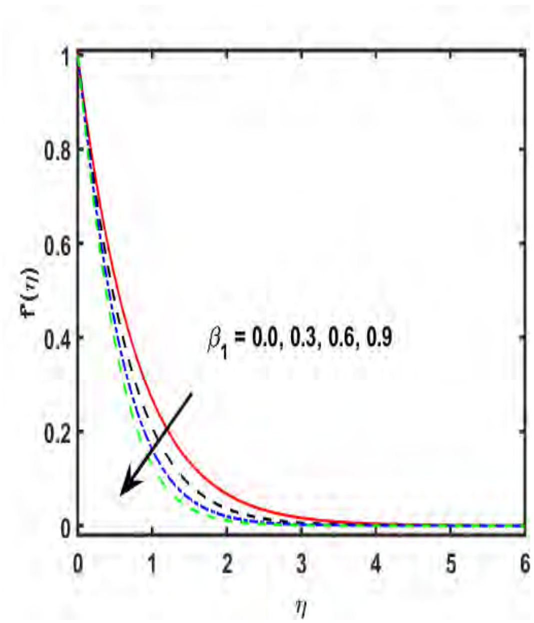

Fig. 4.2: Result of β_1 against $f'(\eta)$.

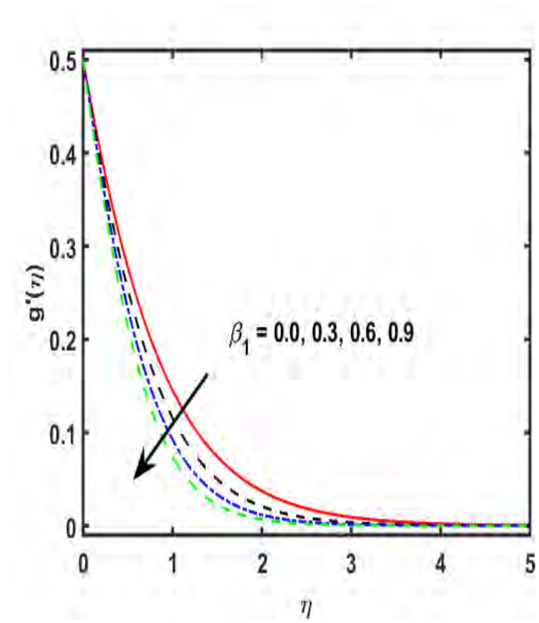

Fig. 4.3: Result of β_1 against $g'(\eta)$.

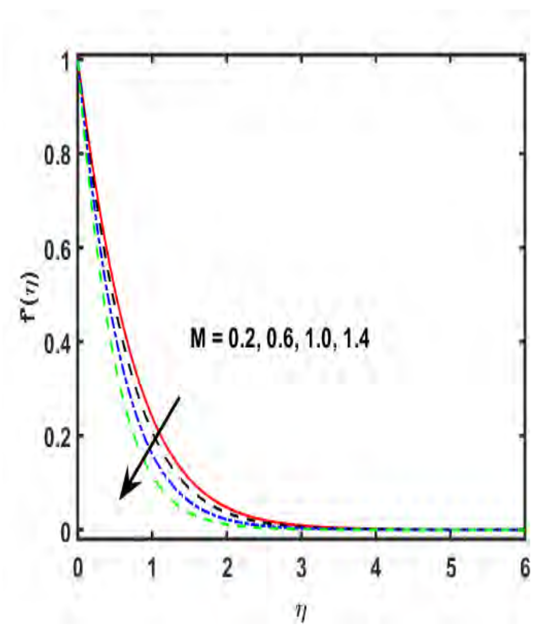

Fig. 4.4: Result of M against $f'(\eta)$.

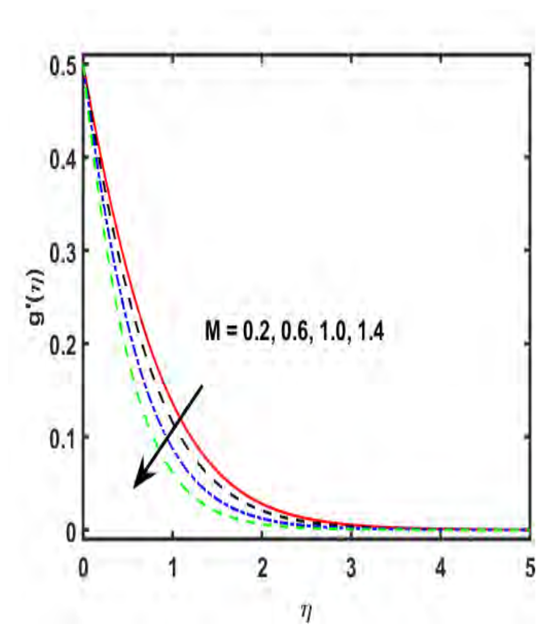

Fig. 4.5: Result of M against $g'(\eta)$.

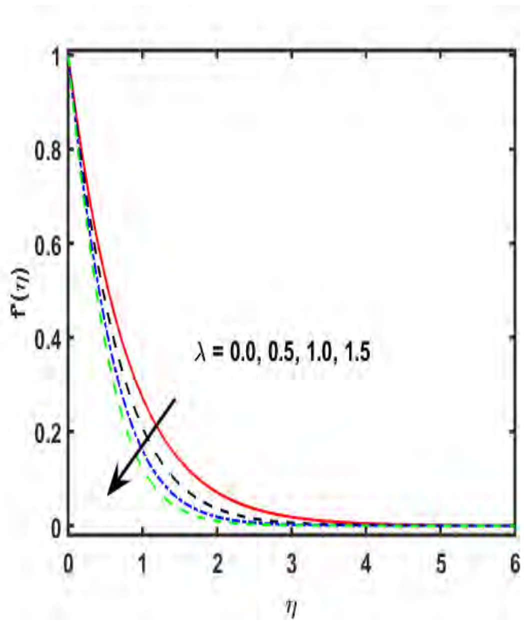

Fig. 4.6: Result of λ against $f'(\eta)$.

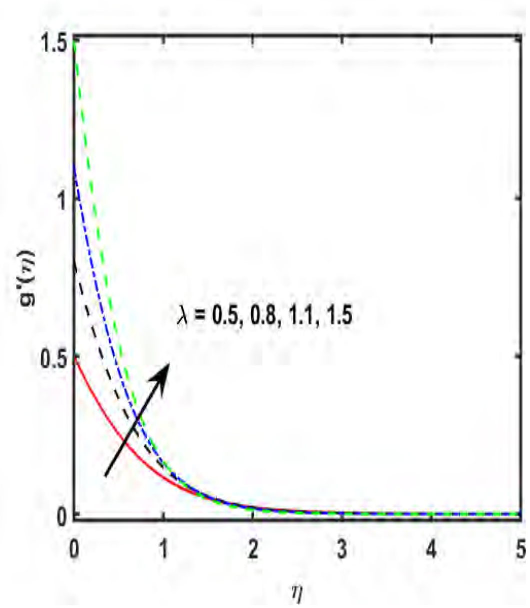

Fig. 4.7: Result of λ against $g'(\eta)$.

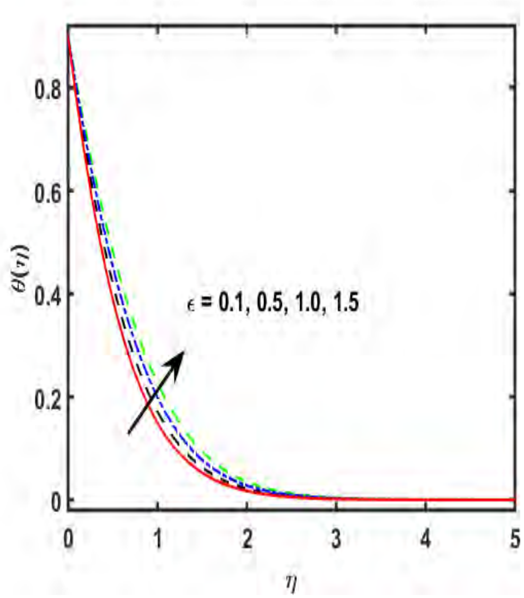

Fig. 4.8: Result of ε against $\theta(\eta)$.

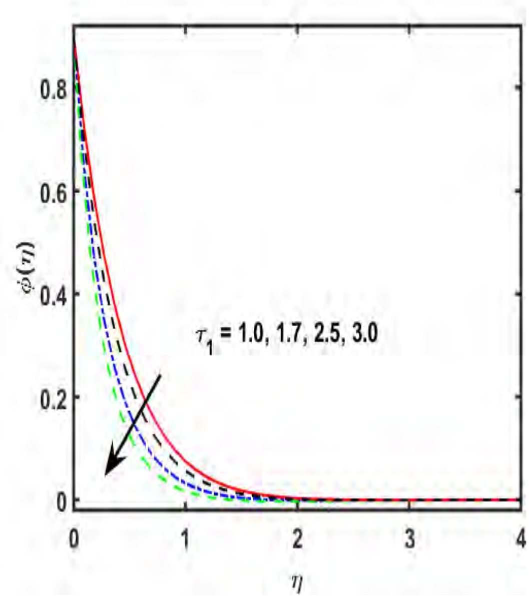

Fig. 4.9: Result of τ_1 against $\phi(\eta)$.

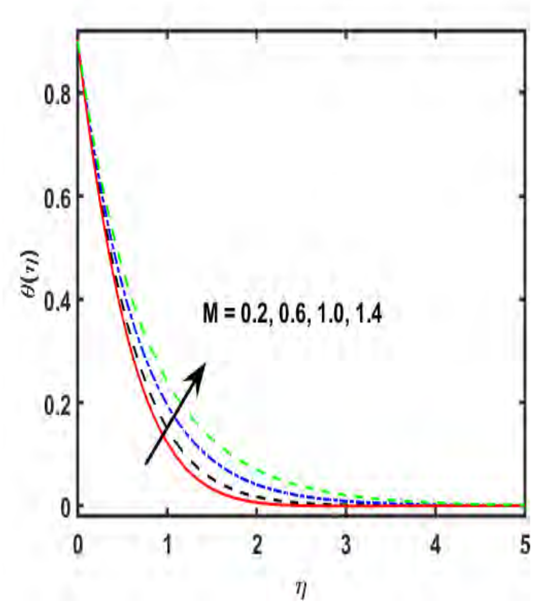

Fig. 4.10: Result of M against $\theta(\eta)$.

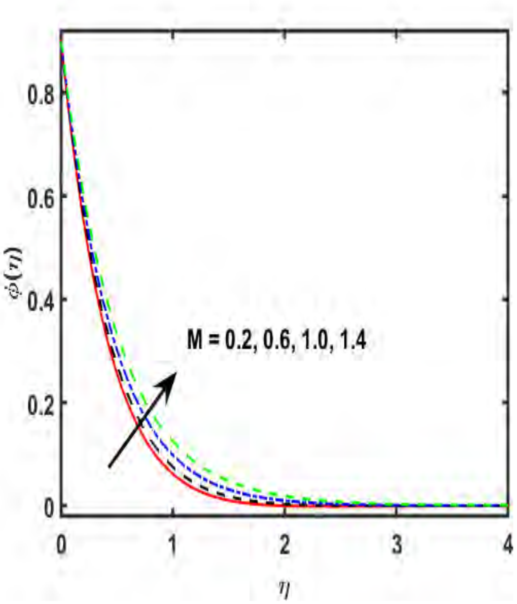

Fig. 4.11: Result of M against $\phi(\eta)$.

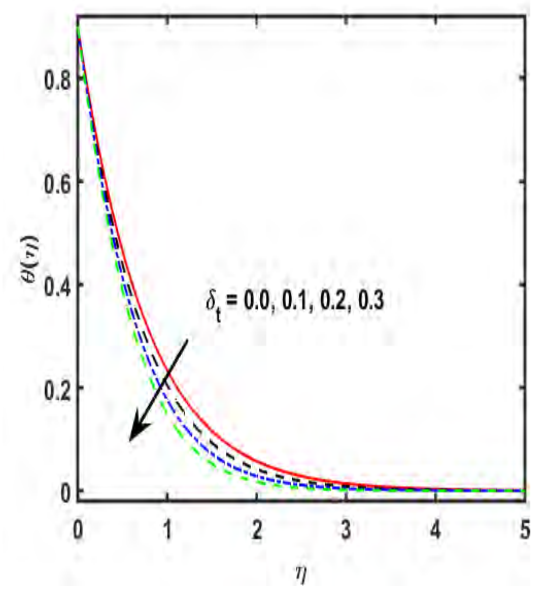

Fig. 4.12: Result of δ_t against $\theta(\eta)$.

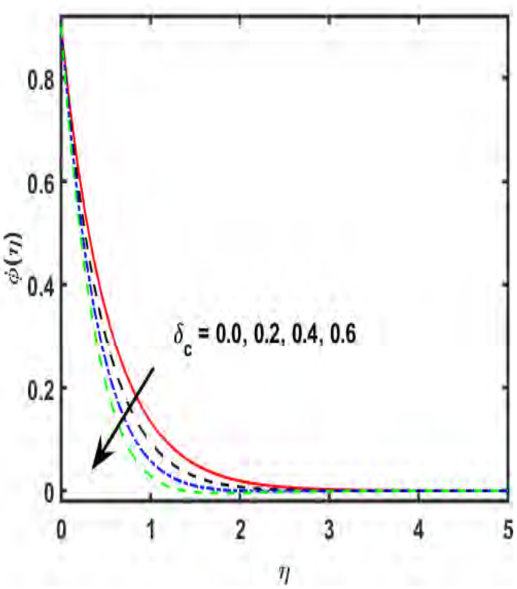

Fig. 4.13: Result of δ_c against $\phi(\eta)$.

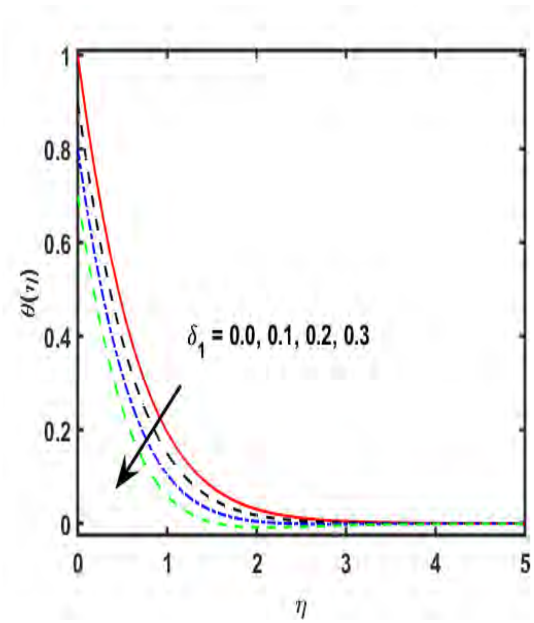

Fig. 4.14: Result of δ_1 against $\theta(\eta)$.

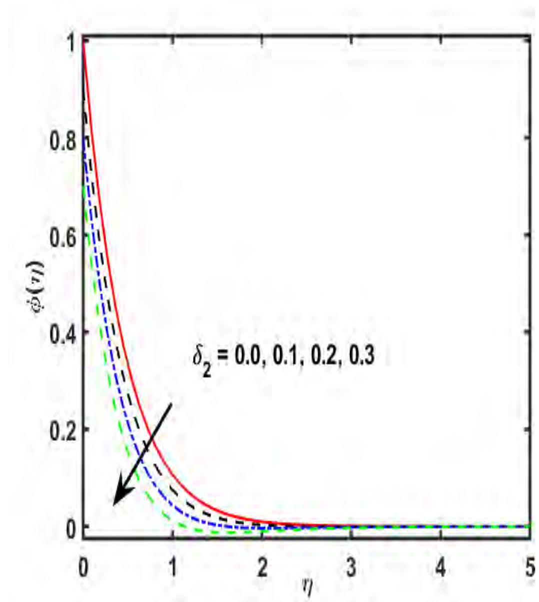

Fig. 4.15: Result of δ_2 against $\phi(\eta)$.

4.3. Final Observations

The mathematical model of Maxwell viscoelastic fluid flow and energy transport with Cattaneo-Christov theory and thermophoretic effect is developed here. The heat source and chemical reaction are also incorporeted in heat and solutal transportation. Numerical technique bvp4c Matlab is utilized for the solution of non-linear differential equations. The main result of the study is illustrated as follows:

- The flow field components $f'(\eta)$ and $g'(\eta)$ is a reducing function for M and β_1.
- The plot of $\theta(\eta)$ and $\phi(\eta)$ improves as rising the values of M and ε.
- For higher values of both δ_t and δ_1 shows the diminishing trend on the temperature plot.
- The higher values of δ_2 and δ_c declines the concentration distribution.
- The velocity gradient $f''(0)$ and $g''(0)$ increases for the higher estimation of M.

Chapter 05

Consequences of Darcy-Forchheimer medium and Cattaneo-Christov model on a three-dimensional Maxwell fluid flow

In this chapter, the mathematical model is established to discuss the double stratified Darcy–Forehheimer steady flow of radiative Maxwell fluid across a vertical stretching surface. Investigation of solutal and thermal energy are carried out in the occurrence of activation energy effect and Cattaneo–Christov theory. Moreover, the gyrotactic microorganism is used to study bio-convection influenced by buoyancy forces. The modelled equations are converted into nonlinear ODEs with suitable transformation. The solutions of non-linear equations are numerically manipulated by bvp4c Matlab technique. The impact of different evolving parameters is discussed through graphs. It is viewed that for greater values of Forehheimer number (Fr) and porosity parameter (Υ) the momentum boundary layer becomes thicker, hence the velocity profile decline. It is noted from the tabulated date that for different values of β_1 and Fr the microorganism number shows decreasing behavior.

5.1. Modelling of the Problem

In the present chapter we evaluated an steady, three-dimensional, radiative Maxwell fluid containing heat generation / absorption, activation energy, and gyrotactic microorganisms. The analysis of energy and concentration are developed with the effect of Cattaneo-Christov theory and double stratification. The physical presentation is illustrated in **Fig. (5.1).** Let the stretching velocities in x −direction and y −direction are $u_w = ax$ and $v_w = by$ respectively. The T_w, C_w, and n_w are represented the temperature, concentration, and microorganism density of the sheet.

Additionally, away from the sheet temperature, concentration, and the microorganism are represented by T_∞, C_∞, n_∞ respectively. According to above assumption the equations of mass, momentum, temperature, concentration, microorganism are follows as [97],

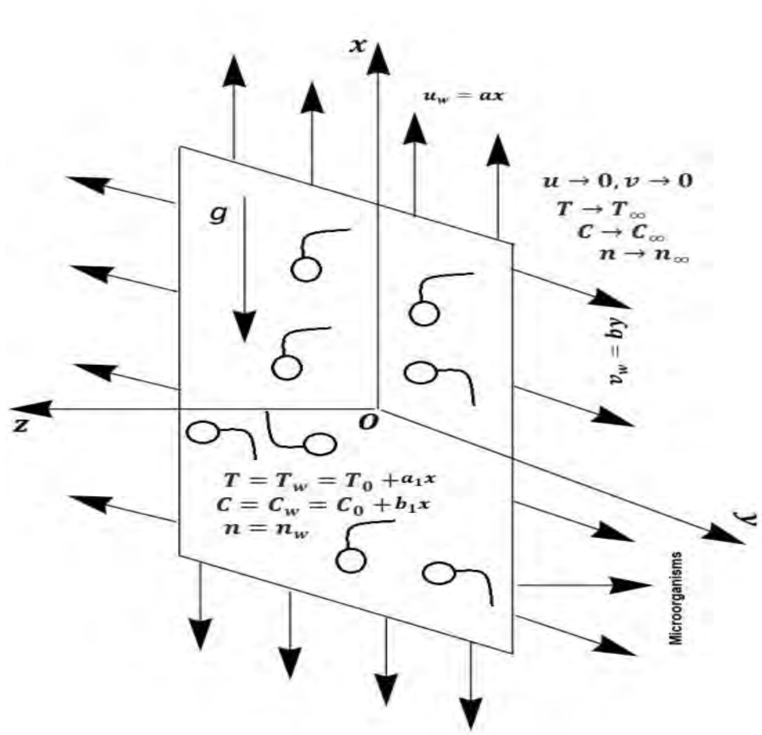

Fig. (5.1): Geometrical presentation.

$$\frac{\partial u}{\partial x} = -\left(\frac{\partial v}{\partial y} + \frac{\partial w}{\partial z}\right), \tag{5.1}$$

$$u\frac{\partial u}{\partial x} + v\frac{\partial u}{\partial y} + w\frac{\partial u}{\partial z} + \lambda_1\begin{pmatrix} u^2\frac{\partial^2 u}{\partial x^2} + 2uv\frac{\partial^2 u}{\partial x\,\partial y} + 2vw\frac{\partial^2 u}{\partial y\,\partial z} \\ +v^2\frac{\partial^2 u}{\partial y^2} + w^2\frac{\partial^2 u}{\partial z^2} + 2uw\frac{\partial^2 u}{\partial x\,\partial z}\end{pmatrix} = \nu\frac{\partial^2 u}{\partial z^2} - \nu\left(\frac{\phi_1 u}{K}\right) - Fu^2$$
$$+\frac{g}{\rho}\Big((1 - C_\infty)(T - T_\infty)\rho\beta_1 - (\rho_p - \rho)(C - C_\infty)\beta_2 - (n - n_\infty)(\rho_m - \rho)\gamma\Big), \tag{5.2}$$

$$u\frac{\partial v}{\partial x}+v\frac{\partial v}{\partial y}+w\frac{\partial v}{\partial z}+\lambda_1\begin{pmatrix}u^2\frac{\partial^2 v}{\partial x^2}+2uv\frac{\partial^2 v}{\partial x\,\partial y}+2vw\frac{\partial^2 v}{\partial y\,\partial z}\\ +v^2\frac{\partial^2 v}{\partial y^2}+w^2\frac{\partial^2 v}{\partial z^2}+2uw\frac{\partial^2 v}{\partial x\,\partial z}\end{pmatrix}=\nu\frac{\partial^2 v}{\partial z^2}-\nu\left(\frac{\phi_1}{K}\right)v-Fv^2, \tag{5.3}$$

$$u\frac{\partial T}{\partial x}+v\frac{\partial T}{\partial y}+w\frac{\partial T}{\partial z}=-\frac{1}{\rho c_p}\nabla.\boldsymbol{q}+\frac{Q_0}{\rho c_p}\left(T-T_{\infty}\right), \tag{5.4}$$

$$u\frac{\partial C}{\partial x}+v\frac{\partial C}{\partial y}++w\frac{\partial C}{\partial z}=-\nabla.\boldsymbol{J}, \tag{5.5}$$

$$u\frac{\partial n}{\partial x}+v\frac{\partial n}{\partial y}+w\frac{\partial n}{\partial z}+\frac{\tilde{b}W_c}{C_w-C_{\infty}}\left[\frac{\partial}{\partial y}\left(n\frac{\partial C}{\partial y}\right)\right]=D_m\frac{\partial^2 n}{\partial z^2}. \tag{5.6}$$

In above equation (5.4) and (5.5) the $\boldsymbol{q}$ and $\boldsymbol{J}$ represented the heat and mass flux respectively. In this chapter, we use Cattaneo-Christov diffusion model to discuss the relaxation of heat and mass fluxes. The thermal and concentration diffusion models are defined as,

$$\boldsymbol{q}+\pi_1\left[\frac{\partial \boldsymbol{q}}{\partial t}+V.\nabla\boldsymbol{q}-\boldsymbol{q}.\nabla V+(\nabla.V)\boldsymbol{q}\right]=-k\nabla T-q_r, \tag{5.7}$$

$$\boldsymbol{J}+\pi_2\left[\frac{\partial \boldsymbol{J}}{\partial t}+V.\nabla\boldsymbol{J}-\boldsymbol{J}.\nabla V+(\nabla.V)\boldsymbol{J}\right]=-D_B\nabla C-k_1^2\left(\frac{T}{T_\infty}\right)^m Exp\left(\frac{-E_a}{kT}\right)(C-C_\infty). \tag{5.8}$$

Here π_1 and π_2 are the relaxation time of heat and mass fluxes respectively.

Utilizing Rosseland approximation of radiation the radiative heat flux is defined as,

$$q_r=-\frac{4\sigma^*}{3\kappa^*}\frac{\partial T^4}{\partial z} \tag{5.9}$$

Now we expanded T^4 about T_∞ by Taylor series, we get the expression as,

$$T^4=4T^3T_\infty-3T_\infty^4 \tag{5.10}$$

Using above equations (5.7-5.10) in equations (5.4) and (5.5), we get,

$$u\frac{\partial T}{\partial x}+v\frac{\partial T}{\partial y}+w\frac{\partial T}{\partial z}+\pi_1\Phi_E=\alpha\frac{\partial^2 T}{\partial z^2}+\frac{16\sigma^*}{3\kappa^*\rho c_p}\frac{\partial}{\partial z}\left(T_\infty^3\frac{\partial T}{\partial z}\right)+\frac{Q_0}{\rho c_p}\left(T-T_{\infty}\right), \tag{5.11}$$

$$u\frac{\partial C}{\partial x}+v\frac{\partial C}{\partial y}++w\frac{\partial C}{\partial z}+\pi_2\Phi_C=D_B\frac{\partial^2 C}{\partial z^2}-k_1^2\left(\frac{T}{T_\infty}\right)^m Exp\left(\frac{-E_a}{kT}\right)\left(C-C_{\infty}\right), \tag{5.12}$$

The Φ_E and Φ_C are defined as,

$$\Phi_E = \begin{pmatrix} u^2 \frac{\partial^2 T}{\partial x^2} + 2uv \frac{\partial^2 T}{\partial x \partial y} + \left(u \frac{\partial v}{\partial x} + w \frac{\partial v}{\partial z} + v \frac{\partial v}{\partial y} \right) \frac{\partial T}{\partial y} + v^2 \frac{\partial^2 T}{\partial y^2} + w^2 \frac{\partial^2 T}{\partial z^2} + 2vw \frac{\partial^2 T}{\partial y \partial z} \\ + \left(u \frac{\partial u}{\partial x} + v \frac{\partial u}{\partial y} + w \frac{\partial u}{\partial z} \right) \frac{\partial T}{\partial x} + \left(u \frac{\partial w}{\partial x} + w \frac{\partial w}{\partial z} + v \frac{\partial w}{\partial y} \right) \frac{\partial T}{\partial z} + 2uw \frac{\partial^2 T}{\partial x \partial z} \end{pmatrix} \quad (5.13)$$

$$\Phi_C = \begin{pmatrix} u^2 \frac{\partial^2 C}{\partial x^2} + 2uv \frac{\partial^2 C}{\partial x \partial y} + \left(u \frac{\partial u}{\partial x} + w \frac{\partial u}{\partial z} + v \frac{\partial u}{\partial y} \right) \frac{\partial C}{\partial x} + v^2 \frac{\partial^2 C}{\partial y^2} + 2vw \frac{\partial^2 C}{\partial y \partial z} + w^2 \frac{\partial^2 C}{\partial z^2} \\ + \left(u \frac{\partial v}{\partial x} + v \frac{\partial v}{\partial y} + w \frac{\partial v}{\partial z} \right) \frac{\partial C}{\partial y} + 2uw \frac{\partial^2 C}{\partial x \partial z} + \left(u \frac{\partial w}{\partial x} + w \frac{\partial w}{\partial z} + v \frac{\partial w}{\partial y} \right) \frac{\partial C}{\partial z} \end{pmatrix} \quad (5.14)$$

The $F = \frac{C_b}{xK^{\frac{1}{2}}}$ is inertial coefficient. Here C_b is drag coefficient and permeability of porous medium is K.

The related boundary conditions are assumed as,

$$u = u_w \;\; v = v_w, \;\; T = T_w = T_0 + a_1 x, C = C_w = C_0 + b_1 x, n = n_w \text{ as } z = 0, \quad (5.15)$$

$$u = 0, \;\; v = 0, \;\; T \to T_\infty = T_0 + c_1 x,, C \to C_\infty = C_0 + d_1 x,, n \to n_\infty, \text{ as } z \to \infty. \quad (5.16)$$

The velocity component in $x-$, $y-$, and $z-$directions are u, v, and w respectively. The λ_1 is fluid relaxation time. The symbols ρ, ρ_p, ρ_m, γ_1, γ_2, γ_3, ϕ_1, E_a, and m are represented the density of fluid, density of particle, density of microorganism, volumetric thermal expansion, volumetric concentration expansion, average volume of a microorganism, porosity of porous medium, activation energy, and exponential index, respectively. Further, a_1, b_1, c_1, and d_1 are the positive constant.

Now we introduce the dimensionless quantities as,

$$\eta = \sqrt{\frac{a}{\nu}} z, u = axf'(\eta), v = ayg'(\eta), w = -\sqrt{a\nu}(f(\eta) + g(\eta))$$
$$T - T_\infty = (T_w - T_0)\theta(\eta), C - C_\infty = (C_w - C_0)\phi(\eta), h(\eta) = \frac{n - n_\infty}{n_w}. \quad (5.17)$$

Using Eq. (5.17), Eq. (5.1) is fulfilled automatically, whereas other Eqs. become,

$$f''' + (f+g)f'' - f'^2 + \begin{pmatrix} \beta_1(2(f+g)f'f'' - (f+g)^2 f''') \\ -\Upsilon f' - Frf'^2 + Gr(\theta - Nr\phi - Rbh) \end{pmatrix} = 0, \tag{5.18}$$

$$g''' + (f+g)g'' - g'^2 + \beta_1(2(f+g)g'g'' - (f+g)^2 g''') - \Upsilon g' - Frg'^2 = 0, \tag{5.19}$$

$$\begin{aligned} &\frac{1}{Pr}\frac{d}{d\eta}\left(\left\{1 + \frac{4}{3}Rd(1-(1-\theta_e)\theta)^3\right\}\theta'\right) - (\delta_1 f' + \theta f') + (f+g)\theta' + Q\theta \\ &-\delta_t \begin{pmatrix} (f+g)^2\theta'' + (f+g)(f'+g')\theta' - 2f'(f+g)\theta' \\ +(f'^2 - (f+g)f'')(\delta_1 + \theta) \end{pmatrix} = 0, \end{aligned} \tag{5.20}$$

$$\begin{aligned} &\frac{1}{Sc}\phi'' - (\delta_2 + \phi)f' + (f+g)\phi' - \sigma(1+\delta\theta)^m e^{-\left(\frac{E_1}{1+\delta\theta}\right)}\phi \\ &-\delta_c \begin{pmatrix} (f+g)^2\phi'' - 2f'(f+g)\phi' + (f+g)(f'+g')\phi' \\ +(f'^2 - (f+g)f'')(\delta_2 + \phi) \end{pmatrix} = 0, \end{aligned} \tag{5.21}$$

$$\frac{1}{Sb}h'' + (f+g)h' - \frac{Pe}{Sb}((h+\Gamma)\phi'' + h'\phi') = 0. \tag{5.22}$$

The concerned conditions on the boundary are,

$$\begin{aligned} &f(0) = 0, g(0) = 0, f'(0) = 1, g'(0) = \lambda, \theta(0) = 1 - \delta_1,\ \phi(0) = 1 - \delta_2,\ h(0) = 1, \\ &f'(\eta)|_{\eta\to\infty} = 0, g'(\eta)|_{\eta\to\infty} = 0 = \theta(\eta)|_{\eta\to\infty}, \phi(\eta)|_{\eta\to\infty} = 0, h(\eta)|_{\eta\to\infty} = 0. \end{aligned} \tag{5.23}$$

The parameters Υ, Nr, Fr, Gr, Rb, θ_e, Rd, δ_1, δ, and Γ are indicated the porosity parameter, buoyancy ratio parameter, Forchheimer number (permeability parameter), mixed convection parameter, Rayleigh number, temperature ratio parameter, radiation parameter, thermal stratification parameter, temperature difference parameter, and microorganism difference parameter, respectively. These parameters in dimensionless form are defined as,

$$Fr = \frac{C_b}{\sqrt{K}},\ \Upsilon = \frac{\nu\phi_1}{cK},\ \lambda = \frac{b}{a}, \beta_1 = \lambda_1 a,\ Rd = \frac{4T_\infty^3\sigma^*}{\kappa^* k},\ \delta_t = a\pi_1, \delta_c = a\pi_2, Q = \frac{Q_0}{a\rho c_p},$$

$$\delta_1 = \frac{c_1}{a_1}, \delta_2 = \frac{d_1}{b_1}, E_1 = \frac{E_a}{kT_\infty}, Sc = \frac{\nu}{D_B}, Sb = \frac{\nu}{D_m}, \mathrm{Pr} = \frac{v}{\alpha}, \delta = \frac{\Delta T}{T_\infty}, \sigma = \frac{k_1^2}{a}, \theta_e = \frac{T_w}{T_\infty}, \tag{5.24}$$

$$Pe = \frac{\tilde{b}W_c D_m}{\nu^2}, \Gamma = \frac{\Delta n}{n_\infty}, Gr = \frac{\gamma_1(1-C_\infty)\Delta T\rho_f}{a u_w}, Nr = \frac{\gamma_2(\rho_p-\rho_f)\Delta C}{\gamma_1(1-C_\infty)\Delta T\rho_f}, Rb = \frac{\gamma_3(\rho_m-\rho_f)\Delta n}{\gamma_1(1-C_\infty)\Delta T\rho_f},$$

5.1.1. Physical Quantities

The physical quantities are very substantial from engineering perspective. But in current chapter only microorganism transfer rate is encountered. Which is defined as,

$$Q_{nx} = \frac{x z_w}{D_m n_w}. \tag{5.25}$$

In above z_w is represented microorganism flux. Which is defined as,

$$z_w = -D_m \frac{\partial n}{\partial y}\bigg|_{y=0}. \tag{5.26}$$

In the dimensionless form the microorganism number becomes,

$$\left(Re_x^{-1/2} Q_{nx} = -h'(0)\right). \tag{5.27}$$

The local Reynolds number is Re_x.

5.2. Results and Discussion

In this section, we investigated graphically, the steady Darcy–Forehheimer flow of radiative Maxwell fluid influenced by Cattaneo–Christov theory and activation energy over a stretching sheet. The stratification conditions are employed on the boundary of the sheet. The graphical description is prepared for the several parameters along the velocity, temperature, concentration, and microorganism distribution. The emerging parameters are the velocity ratio parameter (λ), relaxation parameter (β_1), mixed convection parameter (Gr), porosity parameter (Υ), Forchheimer number (Fr), buoyancy ratio parameter (Nr), temperature ratio parameter (θ_e), Schmidt number (Sc), Rayleigh number (Rb), heat generation parameter (Q), radiation parameter (Rd), thermal relaxation parameter (δ_t), thermal stratification parameter (δ_1), concentration stratification parameter (δ_2), temperature difference parameter (δ), Prandtl number (Pr), reaction rate parameter (σ), concentration relaxation parameter (δ_c), activation energy parameter (E_1), bio-convection Schmidt number (Sb), microorganism difference parameter (Γ), and Peclet number parameter (Pe) respectively. Further, tabulated data is calculated for microorganism number. The specified values of parameters are defined as $\beta_1 = 0.3$, $\Upsilon = 0.4$, $Fr = 0.1$, $Gr = 0.5$, $Nr = 1.0$, $Rb = 0.8$, $\theta_e = 0.5$, $Rd = \delta = Q = 0.1 = \delta_2 = \delta_1$, $Pr = 1.5 = Sc$, $\delta_t = 0.3$, $\sigma = 0.5$, $\delta_c = 0.2$, $E_1 = 0.5$, $\Gamma = 0.1$, $Sb = 1.5 = Pe$. The numerical results of velocity gradient ($-f''(0)$ and $-g''(0)$) and temperature gradient ($-\theta'(0)$) for validation of the method is obtained in the **table (5.1)** and **table (5.2)** and compared by existing literature. It has been found good similarity with earlier published results. The impact of numerous parameters β_1, Fr, λ, σ, Γ and Pe on microorganism number is shown in **table 5.3.** It is cleared from the tabulated date that for the different values of β_1 and Fr the microorganism number shows decreasing behavior, whereas the opposite trend is seen for greater values of λ. Further, it is noted that due to enhancement of σ, Γ, and Pe, the $-h'(0)$ enhances consequently. The transportation of heat and mass rate are not observed in the current study.

Table (5.1): Assessment table of velocity gradient for various values of λ, when $\beta_1 = 0.0$.

	$-f''(0)$			$-g''(0)$		
λ	HPM result [99]	Ref. [100]	Current results	HPM result [99]	Ref. [100]	Current results
0.0	1.000	1.000	1.0004	0.00	0.00	0.00
0.1	1.02025	1.020253	1.02062	0.06684	0.066849	0.066951
0.2	1.03949	1.039498	1.03977	0.14873	0.148730	0.148771
0.3	1.05795	1.057959	1.05818	0.24335	0.243360	0.243349
0.4	1.07578	1.075789	1.07597	0.34920	0.349212	0.349333
0.5	1.09309	1.093093	1.09324	0.46520	0.465206	0.465317

Table (5.2): Comparison table of temperature gradient for Pr, when $Rd = \delta_t = \delta_1 = 0.0$.

Pr	Khan and Pop [101]	Shooting technique	Bvp4c technique
0.7	0.4539	0.45391	0.45390
2.0	0.9113	0.91125	0.91132
7.0	1.8954	1.89542	1.89544
20.0	3.3539	3.35397	3.35392

Table (5.3): The variation in $-h'(0)$ for the numerous parameters, when $Sb = 0.5, \Upsilon = 0.8$.

β_1	Fr	Γ	Pe	$-h'(0)$
0.0	0.5	0.1	0.5	1.09033
0.3	-	-	-	1.07255
0.5	-	-	0.5	1.06142
-	0.0	-	-	1.07054
-	0.5	0.1	-	1.06142
0.5	1.0		0.5	1.05300
-	-	0.1	-	1.06142

-	0.5	0.3	0.5	1.18919
0.5	-	0.5	-	1.31696
-	0.5	-	0.5	1.06142
0.5	-	-	0.7	1.35191
-	-	-	1.0	1.79209

5.2.1. Flow Analysis of Physical Parameters

The variation in the velocity field along x −axis and y −axis against the various value of Forchheimer number Fr is depicted in **Figs. 5.2 and 5.3.** It is noted that by an increment of Fr the momentum boundary layer become thicker, and fluid cannot move easily. Hence the $f'(\eta)$ and $g'(\eta)$ is diminishing for higher values of Fr. The variation in velocity field for several value of porosity parameter Υ is shown in **Figs. 5.4 and 5.5.** It is observed that both boundary layer thickness and velocity of fluid reduces for larger value of Υ. Physically, in the occurrence of porous media the resistance of fluid motion enhances, which lessening the velocity of fluid and boundary layer thickness. **Figs. 5.6 and 5.7** delineated the impact of Nr and Gr against the velocity profile. The graphical result shows that by growing the values of Nr and Gr then the rapid decay occurs in velocity of fluid. Physically, Gr is the ratio between the buoyancy force to viscous forces. When enlarges the values of Gr the buoyancy force increases, which decrease the fluid velocity. The influence of Rb and λ on the velocity curve is revealed in **Figs. 5.8** and **5.9.** It is examined in **Fig. 5.8** that, when Rb enhances then the velocity curve decline, whereas **Fig. 5.9** displays that for the higher estimation of λ, the velocity curve is boosted in the y-direction. It is also noted that due to magnifying the values of Rb, decays the velocity of fluid due to buoyance force which causes by bio–convection.

5.2.2. Thermal, Concentration, and Microorgansim Analysis of Physical Parameters

Fig. 5.10 observed that the higher values of β_1 corresponds higher temperature and related boundary layer thickness become thicker. Furthermore, opposite behavior of temperature is noted in **Fig. 5.11** for higher value of thermal stratification parameter δ_1. In fact, as δ_1 rises, then the temperature difference between heated surface and away from the surface declines. Therefore, temperature of fluid decreases for δ_1. Stronger values of δ_t reduce the temperature and boundary layer become thinner shown in **Fig. 5.12.** Physically**,** it certifies that the progressive nature of thermal relaxation time parameter needs more time to shift the heat from intensively packed fluid particles to the low energetic fluid particles. Thus, temperature is decayed. The importance of activation energy parameter E_1 on $\phi(\eta)$ curve is found in **Fig. 5.13**. It is clearly examined that by magnifying the values of E_1, accelerate the solutal boundary layer thinness, which rises the mass concentration. **Fig. 5.14** portrayed the influence of β_1 on the concentration distribution. It is found that mass concentration becomes stronger for larger estimation of β_1. **Fig. 5.15** presented that the $\phi(\eta)$ plot and related boundary condition become weaker for stronger value of mass relaxation parameter δ_c. Further, maximum concentration is obtained when $\delta_c = 0$. **Figs. 5.16 and 5.17** revealed the impact of β_1 and Γ (bio-convection parameter) on microorganism distribution. It is shown that for higher values of β_1 the microorganism density enhances, while opposite trend is noted for higher values of Γ.

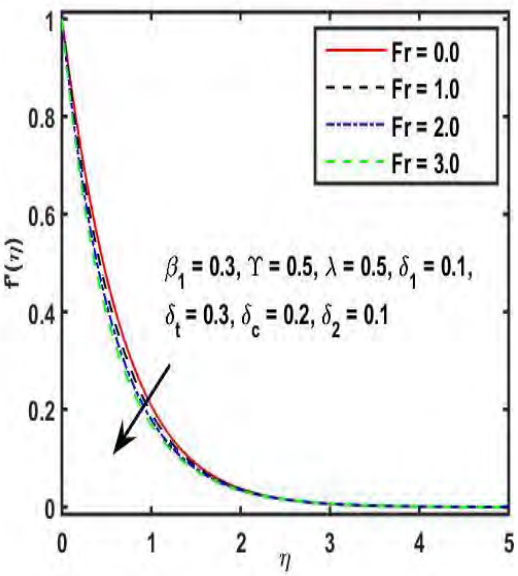

Fig. 5.2: Plot of $f'(\eta)$ for Fr.

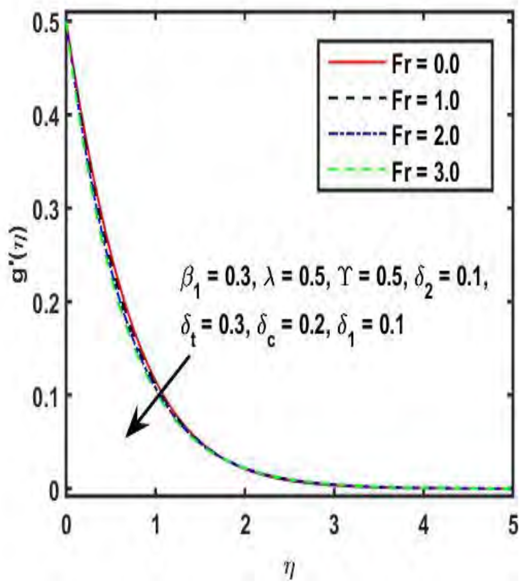

Fig. 5.3: Plot of $g'(\eta)$ for Fr.

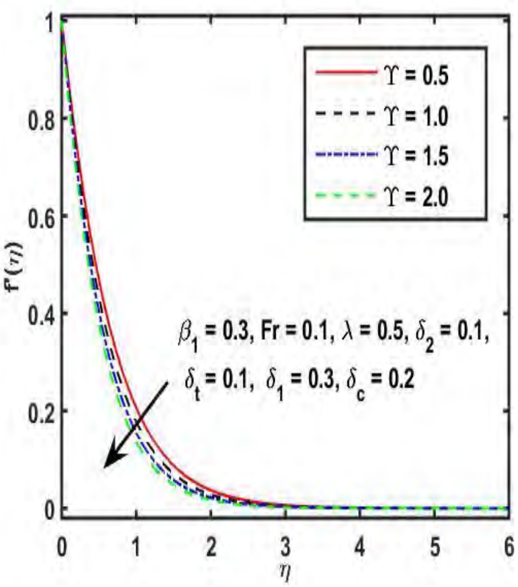

Fig. 5.4**:** Plot of $f'(\eta)$ for Υ.

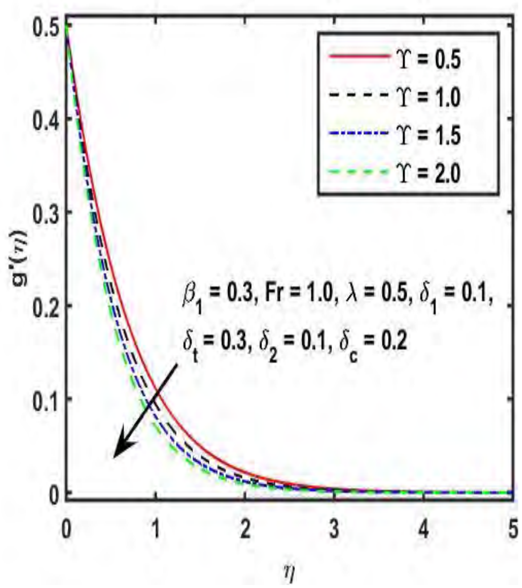

Fig. 5.5: Plot of $g'(\eta)$ for Υ.

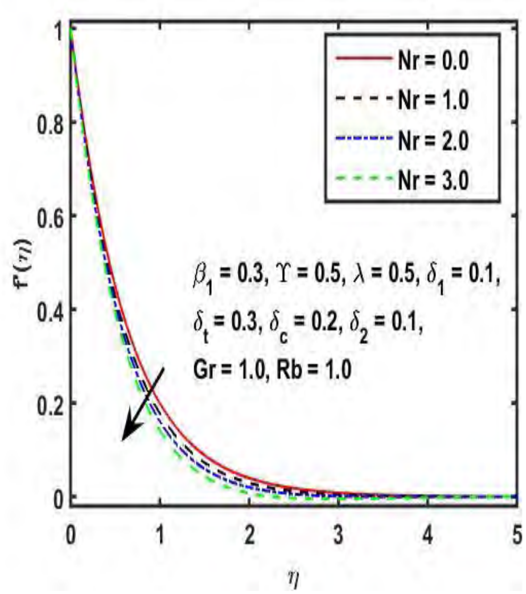

Fig. 5.6: Plot of $f'(\eta)$ for Nr.

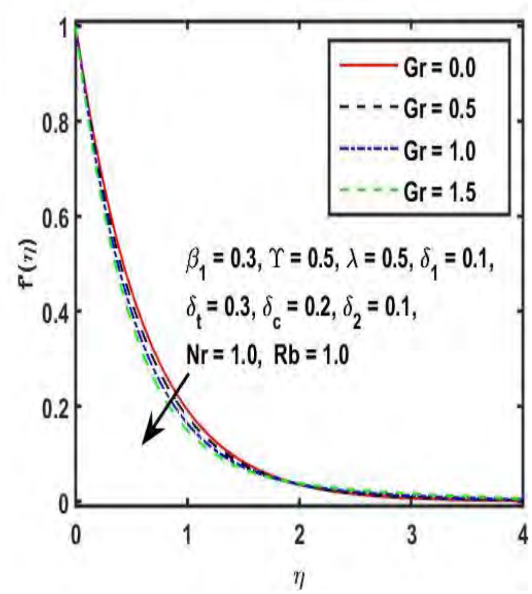

Fig. 5.7: Plot of $f'(\eta)$ for Gr.

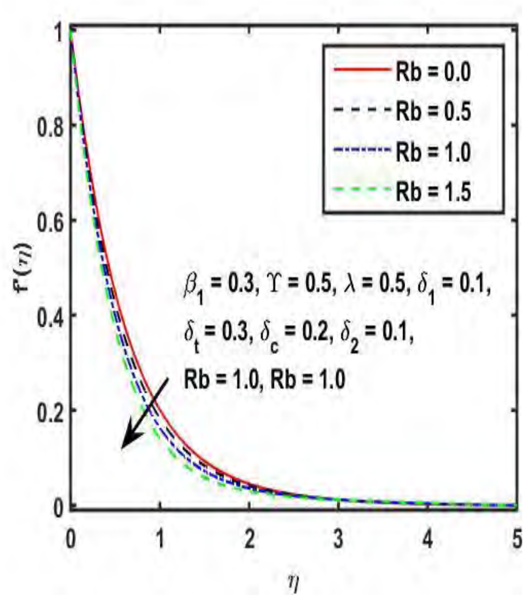

Fig. 5.8: Plot of $f'(\eta)$ for Rb.

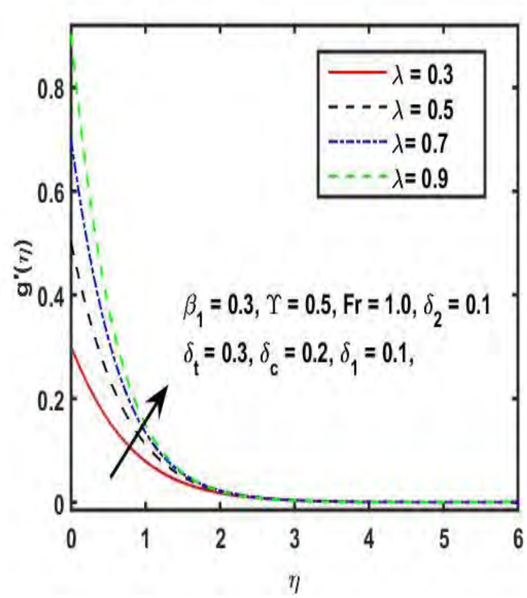

Fig. 5.9: Plot of $g'(\eta)$ for λ.

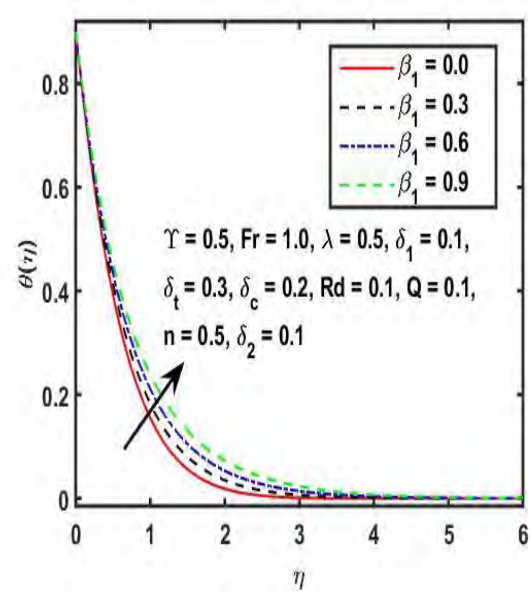

Fig. 5.10: Plot of β_1 on $\theta(\eta)$.

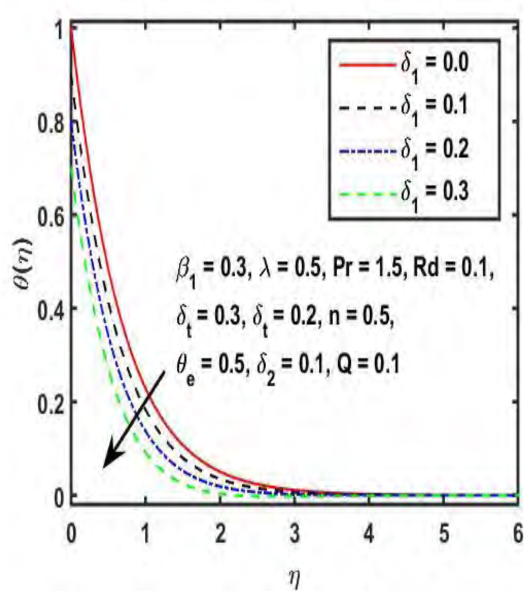

Fig. 5.11: Plot of δ_1 on $\theta(\eta)$.

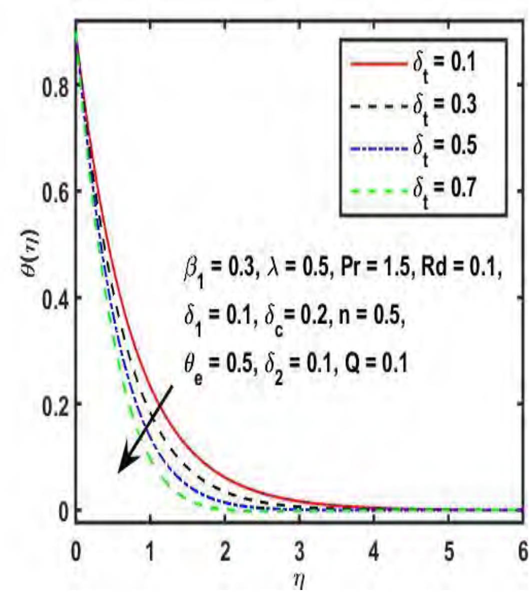

Fig. 5.12: Plot of δ_t on $\theta(\eta)$.

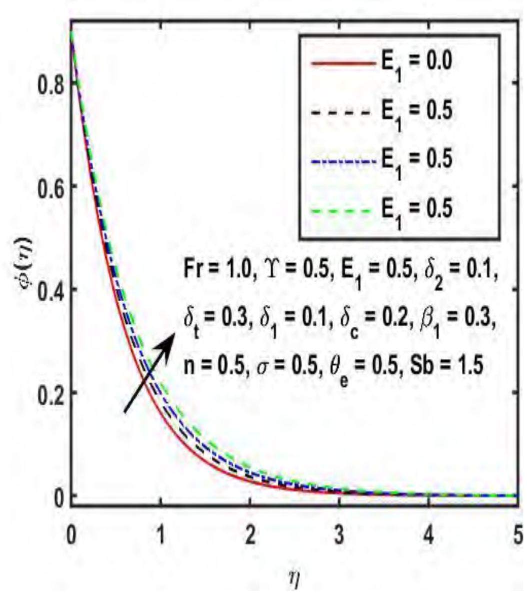

Fig. 5.13: Plot of E_1 on $\phi(\eta)$.

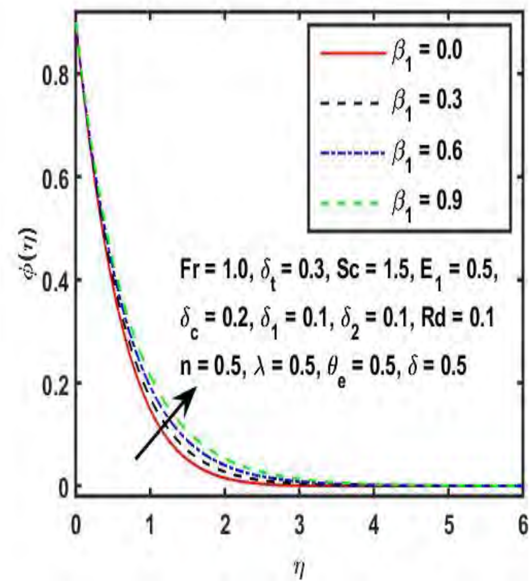

Fig. 5.14: Plot of β_1 on $\phi(\eta)$.

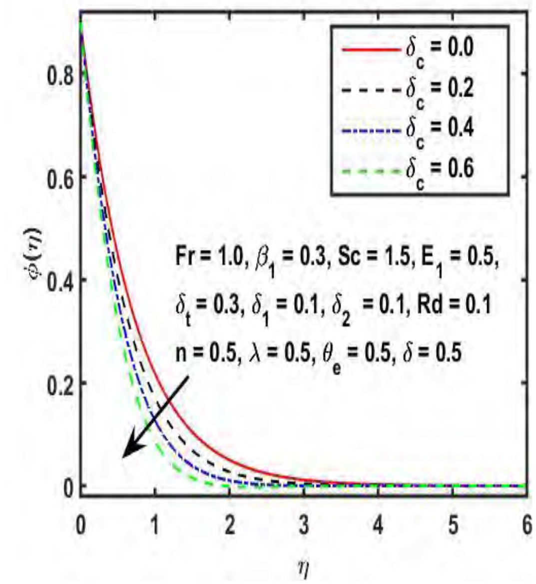

Fig. 5.15: Plot of δ_c on $\phi(\eta)$.

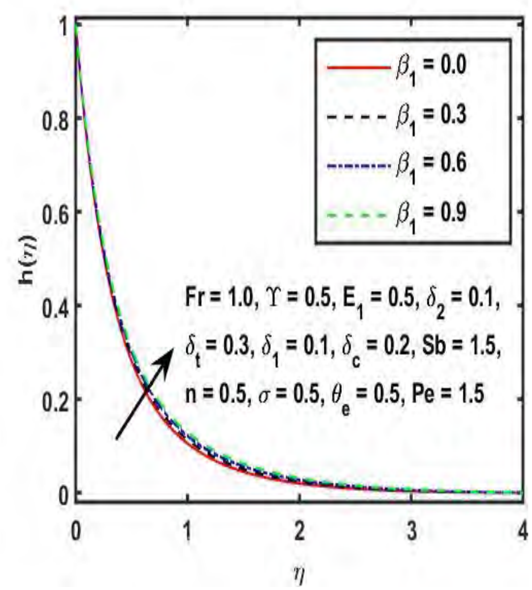

Fig. 5.16: Plot of β_1 on $h(\eta)$.

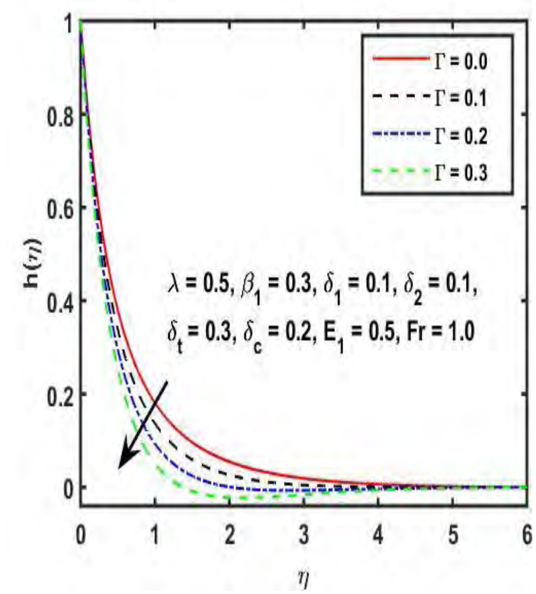

Fig. 5.17: Plot of Γ on $\phi(\eta)$.

5.3. Final Remarks

In this chapter, we studied numerically the Darcy-Forchheimer bio-convection radiative Maxwell fluid flow with double stratification through a stretching surface. Moreover, scrutiny of heat and mass is manipulated in the occurrence of Cattaneo-Christov theory and activation energy effect. The outcomes of the paper are summarized as;

- The velocity profile exhibits thinning effect for the higher values of Fr and Υ.
- The rapid decay is occurred in Gr and Rb plot of velocity by the increment of buoyancy forces.
- The temperature distribution shows the declining behavior for various estimation of δ_t.
- The concentration upsurges when raising the values of E_1.
- For higher values of β_1 the microorganism density increases, but reverse trend is noted for higher values of Γ.

Chapter 06

Implement of stratification conditions on a Casson nanofluid flow with thermophoretic and radiation effect induced by an exponentially stretching surface

In this chapter, the influence of stratification conditions on the boundary layer flow of MHD Casson nanofluid through an exponentially stretching sheet with viscous dissipation is scrutinized. To characterize the heat and solutal transfer properties in flow, we considered the thermal radiation, thermophoretic and chemical reaction effect. Additionally, microorganism theory is considered to analyze the suspended nanoparticles by the bio-convection. The flow model is nondimensionalized by using appropriate transformation and solved numerically by using bvp4c Matlab technique. The graphical and tabulated outcomes are obtained against the various parameters. It is noticed that the resistance in fluid flow increases by higher values of the Casson fluid parameter. Therefore, the axial and transverse velocities are declined. Further, it is noted from the tabulated data that growing values of Casson fluid parameter declines the skin friction and mass transfer rate but enhances the heat transfer rate.

6.1. Modelling of Problem

The consideration of the current investigation is related to incompressible, three dimensional radiative Casson nanofluid with microorganism and double stratification towards an exponentially stretching surface. Furthermore, the heat and solutal transport properties are examined with the viscous dissipation and thermophoretic effect. The fluid is conducting electrically due to the applied magnetic field. Let $u_w = aExp\left(\frac{x+y}{l}\right)$ and $v_w = bExp\left(\frac{x+y}{l}\right)$ be the fluid velocities in the $x-$ and $y-$direction along the sheet. The flow is confined to $z \geq 0,$ as shown in the **Fig. 6.1**. The sheet maintained the temperature, concentration, and microorganism with T_w, C_w, and n_w respectively, while ambient temperature T_∞, concentration C_∞, and microorganism n_∞ respectively. Mathematically, we described the equation of mass, momentum, energy, concentration, and microorganism under the boundary layer approximation as [102],

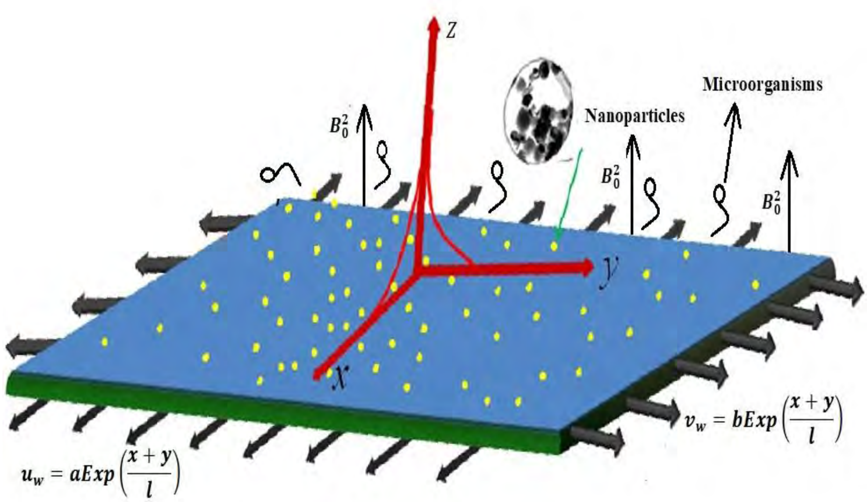

Fig. 6.1: Physical interruption of the flow.

$$\frac{\partial u}{\partial x} = -\left(\frac{\partial v}{\partial y} + \frac{\partial w}{\partial z}\right), \tag{6.1}$$

$$\rho\left(u\frac{\partial u}{\partial x} + v\frac{\partial u}{\partial y} + w\frac{\partial u}{\partial z}\right) = \mu\left(1+\frac{1}{\beta}\right)\frac{\partial^2 u}{\partial z^2} - \sigma_1 B_0^2 u, \tag{6.2}$$

$$\rho\left(u\frac{\partial v}{\partial x} + v\frac{\partial v}{\partial y} + w\frac{\partial v}{\partial z}\right) = \mu\left(1+\frac{1}{\beta}\right)\frac{\partial^2 v}{\partial z^2} - \sigma_1 B_0^2 v, \tag{6.3}$$

$$u\frac{\partial T}{\partial x}+v\frac{\partial T}{\partial y}+w\frac{\partial T}{\partial z}-\left(1+\frac{1}{\beta}\right)\frac{\mu}{\rho c_p}\left(\left(\frac{\partial u}{\partial z}\right)^2+\left(\frac{\partial v}{\partial z}\right)^2\right)=\alpha\frac{\partial^2 T}{\partial z^2}+\tau\left(\frac{D_T}{T_\infty}\left(\frac{\partial T}{\partial z}\right)^2+D_B\frac{\partial T}{\partial z}\frac{\partial C}{\partial z}\right)$$
$$-\frac{1}{\rho c_p}\frac{\partial q_r}{\partial z}, \tag{6.4}$$

$$u\frac{\partial C}{\partial x}+v\frac{\partial C}{\partial y}+w\frac{\partial C}{\partial z}+\frac{\partial}{\partial z}\left(V_T\left(C-C_\infty\right)\right)=\frac{D_T}{T_\infty}\frac{\partial^2 T}{\partial z^2}+D_B\frac{\partial^2 C}{\partial z^2}-k_1\left(C-C_\infty\right), \tag{6.5}$$

$$u\frac{\partial n}{\partial x}+v\frac{\partial n}{\partial y}+w\frac{\partial n}{\partial z}=D_m\frac{\partial^2 n}{\partial z^2}-\frac{\tilde{b}W_c}{\left(C-C_\infty\right)}\frac{\partial}{\partial z}\left(n\frac{\partial C}{\partial z}\right). \tag{6.6}$$

Where the symbols $\nu, \sigma_1, \alpha, \beta, D_T, D_B, \tau, D_m, W_c, q_r$, and $\tilde{b}$ denotes the kinematic viscosity, electrical conductivity, thermal diffusivity, Casson fluid parameter, thermal diffusivity coefficient, Brownian diffusion coefficient, ratio of heat capacity to base fluid, diffusivity of microorganism, maximum cell swimming speed, radiative heat flux, and chemotaxis constant, respectively.

The prescribed surface and free stream conditions are [103-104],

$$\begin{aligned}
&u\big|_{z=0}=u_w(x,y),\ v\big|_{z=0}=v_w(x,y),\quad w\big|_{z=0}=0,\quad T\big|_{z=0}=T_w=T_0+a_1Exp\left(\frac{x+y}{2l}\right),\\
&C\big|_{z=0}=C_w=C_0+b_1Exp\left(\frac{x+y}{2l}\right),\ n\big|_{z=0}=n_w=n_0+e_1Exp\left(\frac{x+y}{2l}\right),\\
&u\big|_{z\to\infty}\to 0, v\big|_{z\to\infty}\to 0, T\big|_{z\to\infty}\to T_\infty=T_0+c_1Exp\left(\frac{x+y}{2l}\right),\\
&C\big|_{z\to\infty}\to C_\infty=C_0+d_1Exp\left(\frac{x+y}{2l}\right), n\big|_{z\to\infty}\to n_\infty=n_0+e_2Exp\left(\frac{x+y}{2l}\right).
\end{aligned} \tag{6.7}$$

In above equation (6.7) a_1, b_1, c_1, d_1, e_1 and e_2 are the positive constant.

The radiative heat flux q_r by using Rosseland approximation is defined as,

$$q_r=\frac{-4\sigma^*}{3\kappa^*}\left(\frac{\partial T^4}{\partial z}\right) \tag{6.8}$$

In the above equation, σ^* is Stefan Boltzmann constant and the κ^* mean absorption coefficient. Further, we expand T^4 by means of Taylor series about T_∞ and neglecting the higher order terms, we get $T^4 \approx 4TT_\infty{}^3 - 3T_\infty{}^4$. Hence, equation (6.4) condenses to,

$$u\frac{\partial T}{\partial x}+v\frac{\partial T}{\partial y}+w\frac{\partial T}{\partial z}=\frac{16\sigma^*}{3\rho c_p\kappa^*}\left(T_\infty{}^3\frac{\partial^2 T}{\partial z^2}\right)+\alpha\frac{\partial^2 T}{\partial z^2}+\tau\left(\frac{D_T}{T_\infty}\left(\frac{\partial T}{\partial z}\right)^2+D_B\frac{\partial T}{\partial z}\frac{\partial C}{\partial z}\right)$$
$$+\left(1+\frac{1}{\beta}\right)\frac{\mu}{\rho c_p}\left(\left(\frac{\partial u}{\partial z}\right)^2+\left(\frac{\partial v}{\partial z}\right)^2\right), \tag{6.9}$$

The thermophoretic velocity V_T of colloidal particles is expressed as,

$$V_T=\frac{-k_t\nu}{T_r}\frac{\partial T}{\partial z}.$$

Here $k_t\nu$ is thermophoretic coefficient and T_r is reference temperature.

6.1.1. Similarity Transformation

The appropriate transformation is defined as,

$$\eta=\sqrt{\frac{a}{2l\nu}}zExp\left(\frac{x+y}{2l}\right),\ u=aExp\left(\frac{x+y}{l}\right)f'(\eta), v=aExp\left(\frac{x+y}{l}\right)g'(\eta),$$
$$w=-\sqrt{\frac{a\nu}{2l}}Exp\left(\frac{x+y}{2l}\right)\left(f+\eta f'+g+\eta g'\right),\ T=T_\infty+T_0Exp\left(\frac{x+y}{2l}\right), \tag{6.10}$$
$$C=C_\infty+C_0Exp\left(\frac{x+y}{2l}\right), n=n_\infty+n_0Exp\left(\frac{x+y}{2l}\right).$$

Here $f(\eta)$, and $g(\eta)$ are the dimensionless components of velocity in $x-$and $y-$direction. Moreover, the $\theta(\eta)$, $\phi(\eta)$, and $h(\eta)$ are the dimensionless factor for temperature, concentration, and microorganism, respectively.

Via similarity variables, the above PDEs are converted into following coupled ODEs,

$$\left(1+\frac{1}{\beta}\right)f''' + ff'' - M^2 f' + gf'' - (f'+g')f' = 0, \tag{6.11}$$

$$\left(1+\frac{1}{\beta}\right)g''' + fg'' - M^2 g' + gg'' - (f'+g')g' = 0, \tag{6.12}$$

$$\begin{aligned}&\left(1+\frac{4}{3}Rd\right)\theta'' + \Pr\left((f+g)\theta' - f'\theta - g'\theta\right) + \Pr Nb\theta'\phi' - \Pr\delta_1(f'+g')\\&+\Pr\left[Nt\theta'^2 + \left(1+\frac{1}{\beta}\right)\left(Ec_1 f''^2 + Ec_2 g''^2\right)\right] = 0,\end{aligned} \tag{6.13}$$

$$\begin{aligned}&\phi'' + Sc\left((f+g)\phi' - f'\phi - g'\phi\right) + \frac{Nt}{Nb}\theta'' - Sc\delta_2(f'+g')\\&-Sc\left[\sigma\phi + S_2(f'+g') + \tau_1\left(\theta''(\phi+\Psi) + \theta'\phi'\right)\right] = 0,\end{aligned} \tag{6.14}$$

$$h'' + Sb(f+g)h' - Sbf'h - Sb\delta_3(f'+g') - Sbg'h - Pe\left[\phi'h' + (h+\Gamma)\phi''\right] = 0, \tag{6.15}$$

The appropriate conditions are,

$$\begin{aligned}&f(0)=0,\ f'(0)=1,\ g'(0)=\lambda,\ g(0)=0,\ \theta(0)=1-\delta_1,\ \phi(0)=1-\delta_2,\ h(0)=1-\delta_3,\\&f'(\eta)=g'(\eta)=0,\ \theta(\eta)=0=\phi(\eta),\ h(\eta)=0,\ as\ \eta\to\infty.\end{aligned} \tag{6.16}$$

Here M, β, Rd, Ec_1, Ec_2, Γ, δ_1, and δ_3 are symbolized the magnetic field parameter, Casson fluid parameter, radiation parameter, Eckert number in $x-$direction, Eckert number in $y-$direction, thermal stratification parameter, microorganism stratification parameter respectively. The emerging parameters are mathematically expressed as,

$$\begin{aligned}&\Pr=\frac{\nu}{\alpha},\lambda=\frac{b}{a},Sc=\frac{\nu}{D_B},Sb=\frac{\nu}{D_m},Rd=\frac{4\sigma^*T_\infty}{k^*k},\sigma=\frac{2lk_1}{a},Pe=\frac{\tilde{b}W_c}{D_m},\Gamma=\frac{n_w-n_\infty}{n_\infty},\\&M^2=\frac{2l\sigma B_0^2}{a\rho_f},\delta_1=\frac{c_1}{a_1},\delta_2=\frac{b_1}{d_1},\delta_3=\frac{e_2}{e_1},Nt=\frac{\tau D_T(T_w-T_\infty)}{T_\infty\nu},Ec_1=\frac{u_w^2}{c_p(T_w-T_\infty)},\\&Ec_2=\frac{v_w^2}{c_p(T_w-T_\infty)},Nb=\frac{\tau D_B(C_w-C_\infty)}{\nu},\Psi=\frac{C_w-C_\infty}{C_\infty}.\end{aligned} \tag{6.17}$$

6.1.2. Physical Quantities

The flow behavior, heat transfer, and mass transfer are characterized by skin friction coefficient, Nusselt number, Sherwood number, and microorganism number respectively, which are stated as,

$$C_{fx} = \frac{\tau_{wx}}{\frac{1}{2}\rho \tilde{u}_0^2}, C_{fy} = \frac{\tau_{wy}}{\frac{1}{2}\rho \tilde{v}_0^2}, Nu_x = \frac{q_w}{\kappa\left(\tilde{T}_w - \tilde{T}_\infty\right)}, Sh_x = \frac{j_w}{D_B\left(\tilde{C}_w - \tilde{C}_\infty\right)}, \ Qn_x = \frac{z_w}{D_m\left(\tilde{N}_w - \tilde{N}_\infty\right)}. \quad (6.18)$$

The shear stresses τ_{wx} and τ_{wy} in $x-$ and $y-$direction respectively, and k is thermal conductivity. Further, q_w is heat flux, j_w is mass flux, and z_w is microorganism flux. They are defined as,

$$\begin{aligned} &\tau_{wx} = \left|\left(1+\frac{1}{\beta}\right)\frac{\partial u}{\partial z}\right|_{z=0}, \ \tau_{wy} = \left|\left(1+\frac{1}{\beta}\right)\frac{\partial v}{\partial z}\right|_{z=0}, \ q_m = \left|-k\left(1+\frac{16\sigma^* T^3}{3kk^*}\right)\frac{\partial T}{\partial z}\right|_{z=0}, \\ &j_m = -D_B\left|\frac{\partial C}{\partial z}\right|_{z=0}, z_w = \left|-D_m\frac{\partial n}{\partial z}\right|_{z=0}. \end{aligned} \quad (6.19)$$

The dimensionless form is,

$$\begin{aligned} &\mathrm{Re}_x^{1/2} C_{fx} = \left(\frac{1+\beta}{\beta}\right) f''(0), \ \mathrm{Re}_x^{1/2} C_{fy} = \left(\frac{1+\beta}{\beta}\right) g''(0), \\ &\mathrm{Re}_x^{-1/2} Nu_x = -\frac{x}{l}\left(\frac{1}{1-\delta_1}\right)\left(1+\frac{4}{3}Rd\right)\theta'(0), \\ &\mathrm{Re}_x^{-1/2} Sh_x = -\frac{x}{l}\left(\frac{1}{1-\delta_2}\right)\phi'(0), \mathrm{Re}_x^{-1/2} Qn_x = -\frac{x}{l}\left(\frac{1}{1-\delta_3}\right)h'(0). \end{aligned} \quad (6.20)$$

The Reynolds number is signified as $\mathrm{Re}_x = \frac{l u_w}{\nu}$.

6.2. Results and Discussion

The solution of the existing problem is acquired by adopting bvp4c Matlab technique. The graphical results are obtained and discussed against the various parameters. Further, physical quantities for the various parameters are discussed by tabulating data. The tabulated results of skin friction, heat, mass, and microorganism transfer rate are characterized in **table (6.1–6.4).** **Table 6.1** clearly deliberates good agreement of the present problem with earlier published data. In **table 6.1** the comparison is down of the heat transfer rate for various values of Prandtl number. It shows that due to increment in $\Pr$ the heat transfer rate increases. **Table 6.2** observed the variation of skin friction in the axial and transverse direction via different parameters, which are velocity ratio parameter (λ), Casson fluid parameter (β), and magnetic parameter (M). It is designated from the tabulated data that for larger values of $\beta, \lambda,$ and M the wall shear stresses is rises consequently in the $x-$ and $y-$direction. The behavior of heat and mass transfer rate is represented in **table 6.3**. It is worth noticing that the enhancement is occurred in the heat transfer rate via several values of β, but opposite trend is noted in the case of mass transfer rate. The enlargement in Eckert number (Ec_1) shows a diminishing trend for both Nusselt and Sherwood number, while the radiation parameter (Rd) displays the opposite tendency which is increasing for the various values of Rd. The heat transfer rate, enhancing via higher values of δ_1, while due to enhancement of δ_2 the mass transfer rate is declining. In **table 6.4,** we observed the microorganism transfer rate corresponding to the various values of $Sb, Pe, \delta_3,$ and Γ. It is scrutinized from the tabulated values that the transfer rate of microorganism enhances for various values of Sb and Γ, whereas reverse trend is noticed for the several estimation of Pe and δ_3.

Table 6.1: Comparison table of $\mathrm{Re}_x^{-1/2}\, Nu_x$ for Pr with earlier published data, when $\beta \to \infty$.

Pr	Ishak [105]	Pramanik. [106]	Present results
1.0	0.9547	0.9548	0.9550
2.0	1.4715	1.4714	1.47140
3.0	1.8691	1.8691	1.86910
5.0	2.5001	2.5001	2.5000
10	3.6603	3.6603	3.66031

Table 6.2: Table of skin friction along $x-$ and $y-$ axes for several parameters.

β	λ	M	$\left(1+\frac{1}{\beta}\right) f''(0)$	$\left(1+\frac{1}{\beta}\right) g''(0)$
1.0	0.5	1.0	2.3746	0.23746
2.0	-	-	2.0564	0.20564
3.0	-	-	1.9388	0.19388
-	0.1	1.0	2.1522	0.21522
-	0.3	-	2.2999	0.68997
1.0	0.5	-	2.4387	1.2193
-	-	0.5	2.1522	0.21522
-	-	1.0	2.3746	0.23746
1.0	0.5	1.5	2.5775	0.25775

Table 6.3: $\mathrm{Re}_x^{-1/2}\, Nu_x$ and $\mathrm{Re}_x^{-1/2}\, Sh_x$ for various parameters, when $\sigma = 1.0$ and $\tau_1 = 0.5$.

β	Ec_1	δ_1	δ_2	$\mathrm{Re}_x^{-1/2}\, Nu_x$	$\mathrm{Re}_x^{-1/2}\, Sh_x$
0.5	0.5	0.1	0.1	0.31762	2.8170
0.7	-	-	-	0.43105	2.8100
0.9	-	-	0.1	0.49971	2.8033
-	0.3	0.1	-	1.0001	2.8921
-	0.4	-	-	0.71609	2.8511

-	0.5	-	-	0.43105	2.8100
		0.1	0.1	0.43105	
		0.2	-	0.3338	
		0.3	-	0.23563	
		-	0.1		2.8100
		-	0.2		2.6551
		0.1	0.3		2.4993

Table 6.4: Table of $\mathrm{Re}_x^{-1/2} Qn_x$ for various parameters, when $Pe = 0.7$.

Sb	Pe	δ_3	Γ	$\mathrm{Re}_x^{-1/2} Qn_x$
0.5	0.5	0.3	0.1	1.4211
0.7	-	-	-	1.5869
1.0	-	-	-	1.7332
-	0.5	0.3	-	1.4211
-	0.7	-	0.1	1.6322
0.5	1.0	-	-	1.8498
-	-	0.1	-	1.7838
-	-	0.2	0.1	1.6025
0.5	0.5	0.3	-	1.4211
-	-	-	0.1	1.4211
-	-	-	0.2	1.4748
0.5	0.5	0.3	0.3	1.5286

6.2.1. Flow Analysis of Physical Parameters

The variation of axial and transverse velocity against the Casson fluid parameter (β), magnetic field parameter (M), and velocity ratio parameter (λ) is captured in **Figs. (6.2–6.4).** It is worth interesting to note in **Fig. 6.2**, that the resistance of fluid is increased by enlarging β. Higher resistance of fluid clearly declines the fluid velocity in $x-$ and $y-$ direction. Hence, both $f'(\eta)$ and $g'(\eta)$ plots are declined. The impact of M on the flow velocity $f'(\eta)$ and $g'(\eta)$ is discussed in **Fig. 6.3**. It is worth noticing that the velocity profile is diminished for larger values of M. The reduction is occurred by the enlargement of Lorentz force which yield more resistance to the fluid, due to this the fluid velocity declined. The influence of λ on the $f'(\eta)$ and $g'(\eta)$ is denoted in **Fig. 6.4**. It shows that the thickening in velocity boundary layer is occurred in $x-$ direction for larger values of λ, whereas thinning in the velocity boundary layer is occurred in $y-$ direction for various values of λ.

6.2.2. Thermal Analysis of Physical Parameters

Figs. (6.5–6.7) demonstrated the graphical variation of the thermal boundary layer thickness and temperature with respect to numerous values of Casson fluid parameter (β), magnetic field parameter (M), and Eckert number $\left(Ec_1\right)$. From **Fig. 6.5**, it is examined that plot of $\theta(\eta)$ is increased for various values of the β. Physically, β is subject to yield stress at the surface, which increase the shear stresses at the wall, therefore temperature and thermal boundary layer thickness enhances. In **Fig. 6.6**, we obviously discuss the temperature variation for various values of M. It is cleared from the figure that related boundary layer thickness and temperature increased for the higher values of M. In **Fig. 6.7**, it is designated that the temperature profile boosts in $x-$ direction for greater values of Ec_1. Physically, by the increment of Ec_1 the K.E of nanofluid augmented, which causes to improvement in the thermal boundary layer thickness and temperature distribution.

6.2.3. Concentration and Microorgansim Analysis of Physical Parameters

The influence of Casson fluid parameter (β), concentration stratification parameter (δ_2), and microorganism stratification parameter (δ_3) on $\phi(\eta)$ and $h(\eta)$ plot is presented in the **Figs. (6.8–6.11).** The $\phi(\eta)$ plot is enhanced by enlarging the values of β see in the **Fig 6.8**. As a result, the concentration field boost up for higher values of β. The variation in $\phi(\eta)$ plot against the various values of δ_2 is found in **Fig. 6.9**. It is clarified from the figure that due to higher values of δ_2 concentration of nanoparticles declines. As the results of the fact, that fluid near the plate can have a lower concentration as compared to ambient fluid. The effect of β and δ_3 on the microorganism distribution is observed in the **Figs.** (**6.10** and **6.11**). It is revealed in **Fig. 6.10** that by escalating the values of β the microorganism density rises consequently. Hence the $h(\eta)$ curve rises for several values of β. From **Fig. 6.11**, it is noted that higher values of δ_3 declines the $h(\eta)$ curve.

6.2.4. Impact of Physical Parameters on the $\mathrm{Re}_x^{-1/2}\, Nu_x$, $\mathrm{Re}_x^{-1/2}\, Sh_x$, and $\mathrm{Re}_x^{-1/2}\, Qn_x$ Sketch

Figs. (6.12–6.14) is examined the variation of Nusselt, Sherwood, and microorganism number against the different parameters. **Fig. 6.12** is plotted to analyzing the impact of Nt and δ_1 on $\mathrm{Re}_x^{-1/2}\, Nu_x$ sketch. On the analyzing it is disclosed that $\mathrm{Re}_x^{-1/2}\, Nu_x$ curve is shrinking for higher values of both Nt and δ_1. **Fig. 6.13** analyzed the influence of Nb and σ on Sherwood number. It is revealed that for stronger values of Nb and σ the $\mathrm{Re}_x^{-1/2}\, Sh_x$ curve decline for both parameters. The variation in microorganism number against the various values of δ_3 and Γ

shown in **Fig. 6.14**. From the figure, it is disclosed that $\mathrm{Re}_x^{-1/2}\,Qn_x$ curve increases for Γ and shows the opposite trend for δ_3.

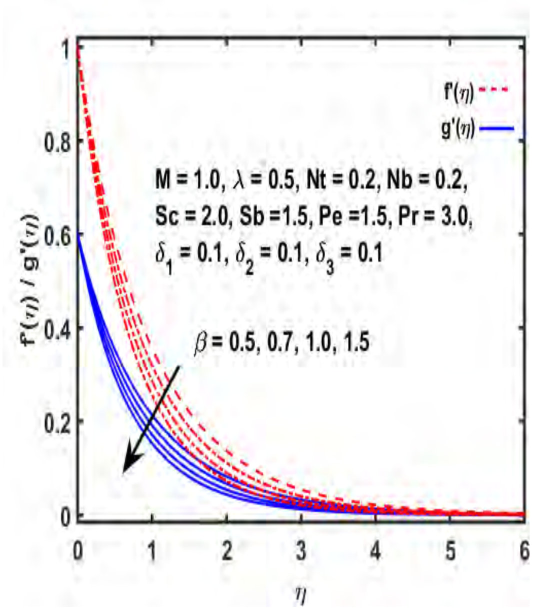

Fig. 6.2: Influence of β on $f'(\eta)$ and $g'(\eta)$.

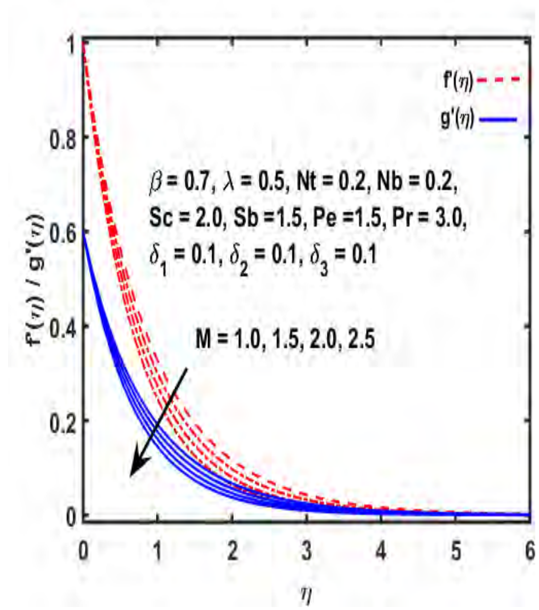

Fig. 6.3: Influence of M on $f'(\eta)$ and $g'(\eta)$.

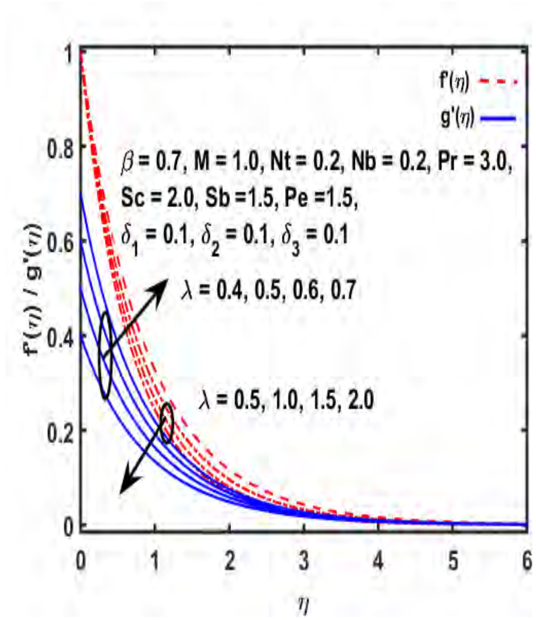

Fig. 6.4: Influence of λ on $f'(\eta)$ and $g'(\eta)$.

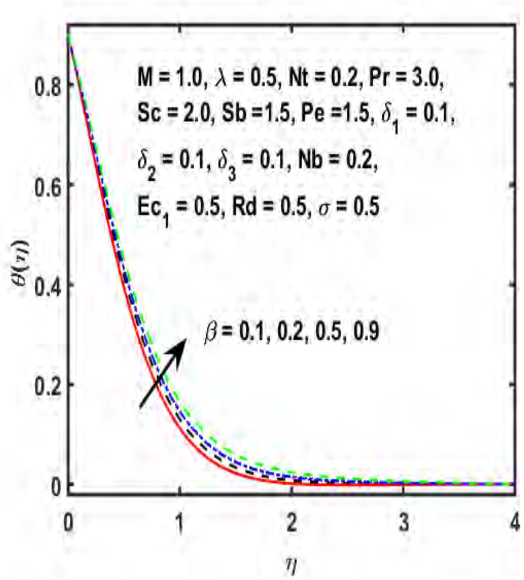

Fig. 6.5: Result of β against $\theta(\eta)$.

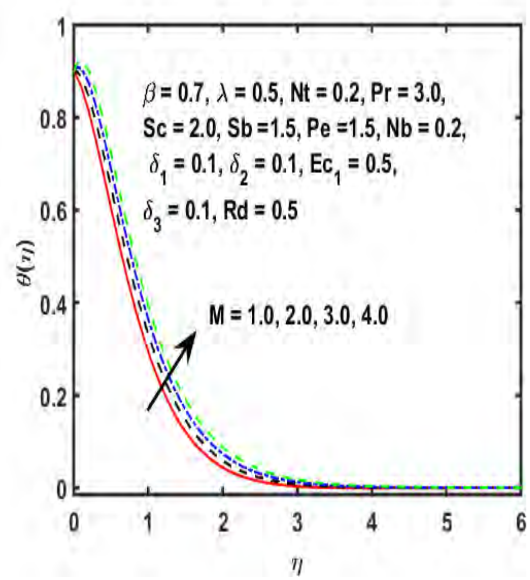

Fig. 6.6: Result of M against $\theta(\eta)$.

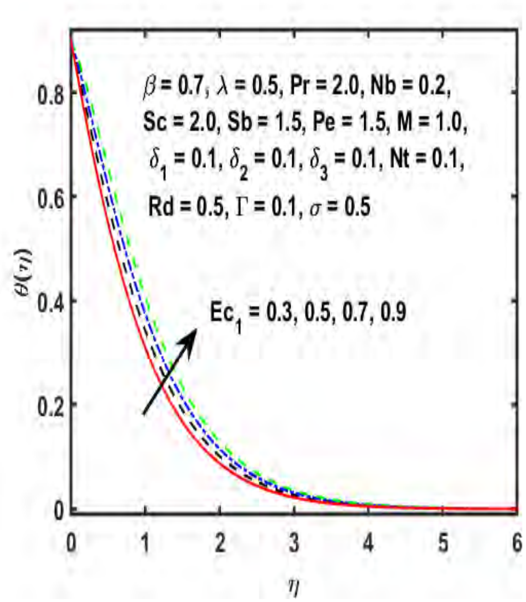

Fig. 6.7: Result of Ec_1 against $\theta(\eta)$.

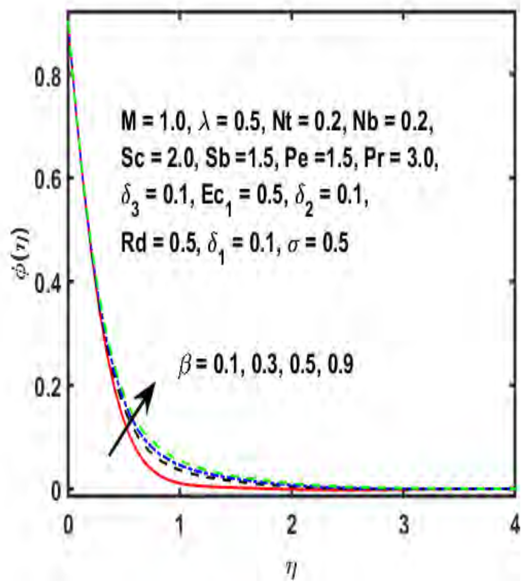

Fig. 6.8: Result of β against $\phi(\eta)$.

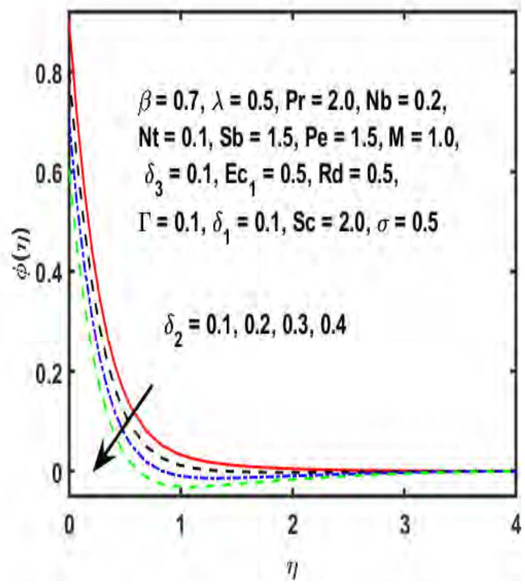

Fig. 6.9: Result of δ_2 against $\phi(\eta)$.

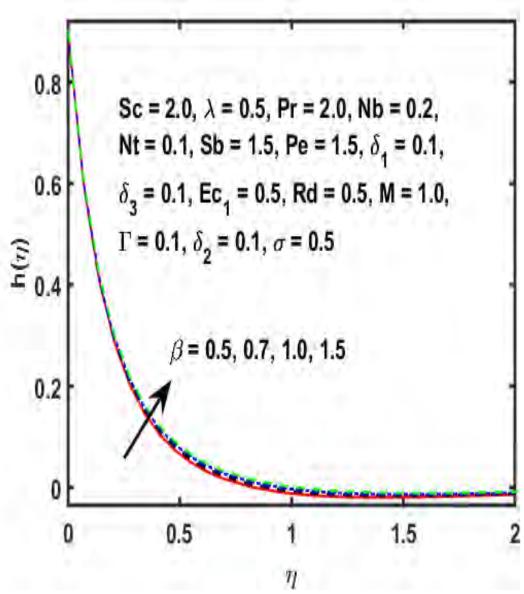

Fig. 6.10: Result of β against $h(\eta)$.

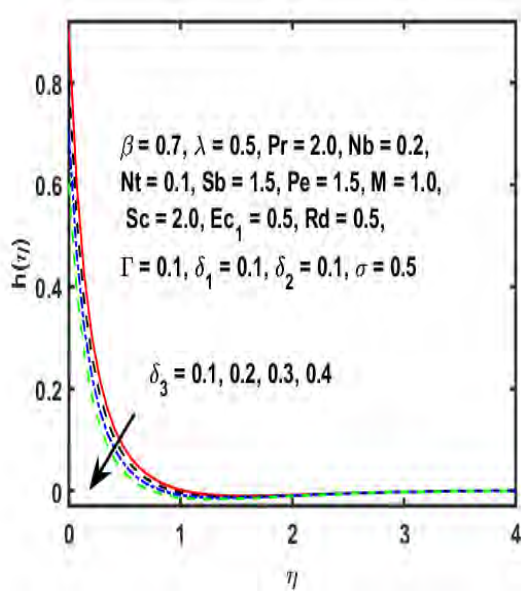

Fig. 6.11: Result of δ_3 against $h(\eta)$.

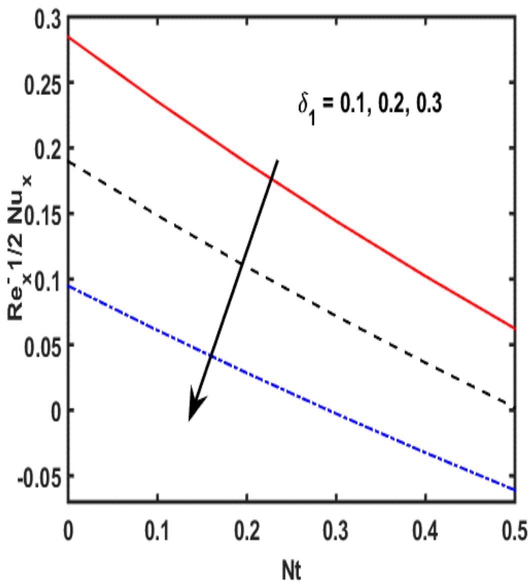

Fig. 6.12: Graph between δ_1 and Nt for $\mathrm{Re}_x^{-1/2}\, Nu_x$.

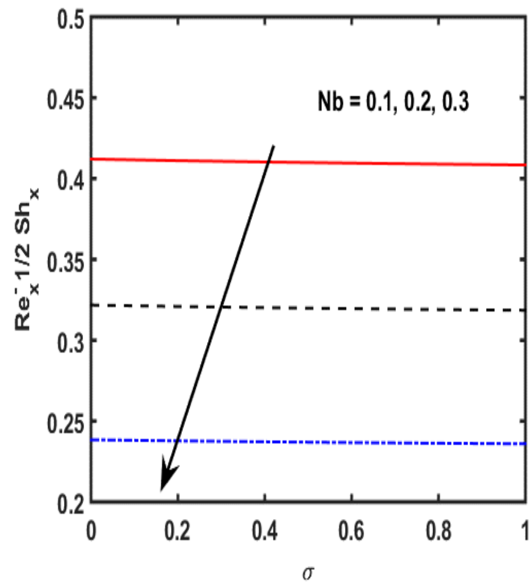

Fig. 6.13: Graph between Nb and σ for $\mathrm{Re}_x^{-1/2}\, Sh_x$.

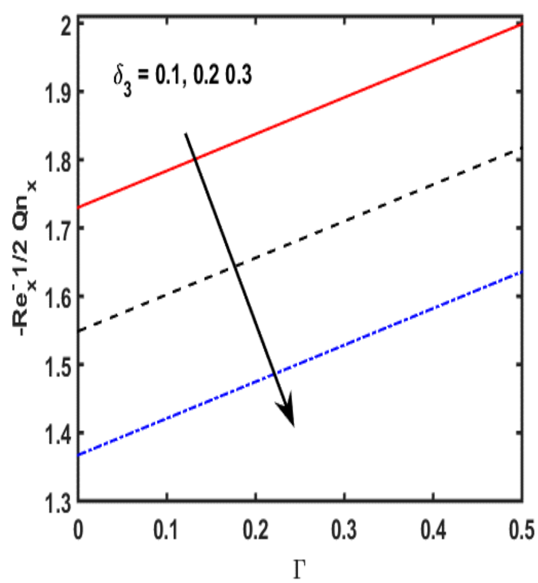

Fig. 6.14: Graph between δ_3 and Γ for $\mathrm{Re}_x^{-1/2}\, Qn_x$.

6.3. Concluding Remarks

The current chapter focuses on the flow behavior and heat transportation of MHD Casson nanoliquid flow with thermal radiation and thermophoretic effect. The mass and microorganism transfer rate are examined with the impact of chemical reaction and microorganism. The key points are given as,

- The fluid resistance enlargers for the higher values β. Hence the fluid velocity decline.
- The temperature distribution in fluid increases with the increment of Eckert number.
- The concentration of nanoparticles diminishes for higher values of δ_2, so the plot of $\phi(\eta)$ is reduced in this case.
- The skin friction is rises for the higher values of β and M.
- The heat and mass transfer rate display the opposite trend for the stronger β.

Chapter 07

Heat and mass transfer investigation of chemically reactive Burgers nanofluid with induced magnetic field by an exponentially stretching surface

In this chapter, a mathematical model is established to examine the flow of a chemically reactive Burgers nanofluid by an exponentially stretching surface along induced magnetic field. The flow investigation is discussed with the influence of thermal and concentration slip boundary conditions. Furthermore, to present the heat transfer investigation the variable thermal conductivity and heat generation / absorption effect is considered. The flow model is converted into the coupled ODEs with suitable similarity transformation. These coupled ODEs are numerically solved by the mean of BVP midrich technique. The effect of evolving parameters is observed graphically. It is noted that the velocity of fluid enhances for the numerous estimations of the relaxation parameter, while fluid velocity depicts the opposite tendency for the retardation parameter. Furthermore, it is noted that the heat and mass transfer rate boosted by the enlargement of relaxation and retardation parameter.

7.1. Mathematical Structure

Here, we examined steady, laminar, 2D incompressible stagnation point flow of Burgers nanofluid with the effect of variable thermal conductivity induced by an exponentially stretching surface. Further, the slip condition and chemical reaction are also considered and correspond to the plan $y > 0$. The induced magnetic field H_0 is applied normal to the surface. The flow configuration of the paper is illustrated in **Fig. 7.1**. The stretching velocity and free stream velocity is characterized by $u_w = aE\,\text{xp}\left(\frac{x}{l}\right)$ and $u_e = cE\,\text{xp}\left(\frac{x}{l}\right)$ respectively. The boundary temperature and concentration is T_w and C_w respectively, and away from the boundary they are T_∞ and C_∞ respectively. The influence of external forces is neglected with the occurrence of induced magnetic field. The V_w suction / injection velocity and $\mathbf{V} = (u(x,y), v(x,y), 0)$ is the velocity field. Using above assumption along with boundary layer approximation the equations of continuity, conservation magnetic field, momentum, induced magnetic field, temperature, and nanoparticle concentration is stated as,

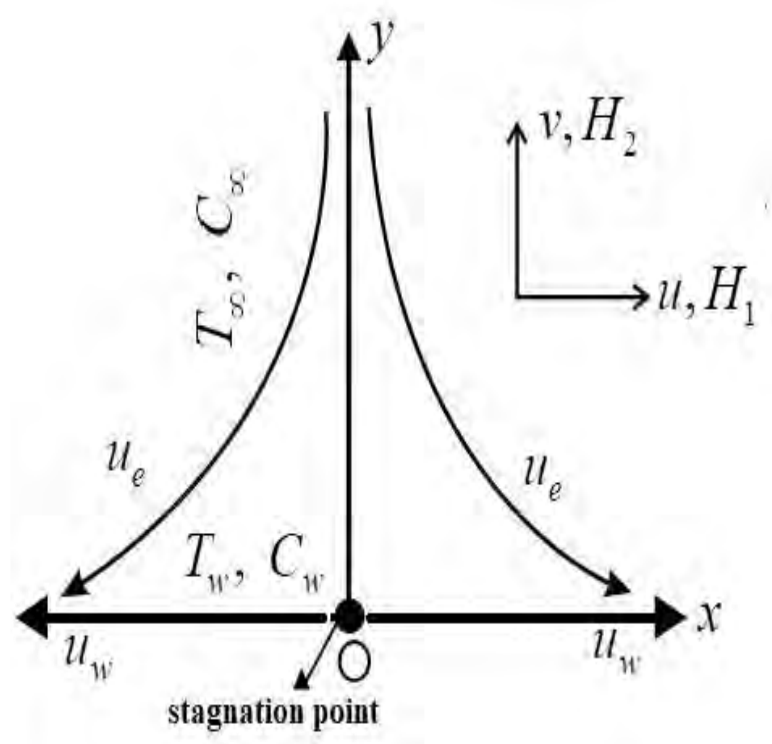

Fig. (7.1): Physical configuration of the chapter.

$$\frac{\partial u}{\partial x}=-\frac{\partial v}{\partial y}, \tag{7.1}$$

$$\frac{\partial H_1}{\partial x}=-\frac{\partial H_2}{\partial y}, \tag{7.2}$$

$$\begin{aligned}
&u\frac{\partial u}{\partial x}+v\frac{\partial u}{\partial y}+\lambda_1\begin{pmatrix} u^2\dfrac{\partial^2 u}{\partial x^2}+v^2\dfrac{\partial^2 u}{\partial y^2} \\ +2vu\dfrac{\partial^2 u}{\partial y\partial z}\end{pmatrix}+\lambda_2\begin{pmatrix} u^3\dfrac{\partial^3 u}{\partial x^3}+u^2\left\{\dfrac{\partial^2 u}{\partial x^2}\dfrac{\partial u}{\partial x}+2\dfrac{\partial v}{\partial x}\dfrac{\partial^2 u}{\partial x\partial y}-\dfrac{\partial^2 v}{\partial x^2}\dfrac{\partial u}{\partial y}\right\} \\ +3v^2\left\{\dfrac{\partial^2 u}{\partial y^2}\dfrac{\partial v}{\partial y}+\dfrac{\partial u}{\partial y}\dfrac{\partial^2 u}{\partial x\partial y}\right\}+3u^2v\dfrac{\partial^3 u}{\partial x^2\partial y} \\ +2uv\left\{\dfrac{\partial^2 u}{\partial x^2}\dfrac{\partial u}{\partial y}+\dfrac{\partial^2 u}{\partial y^2}\dfrac{\partial v}{\partial x}+\dfrac{\partial v}{\partial y}\dfrac{\partial^2 u}{\partial x\partial y}\right\} \\ -2uv\dfrac{\partial u}{\partial y}\dfrac{\partial^2 v}{\partial x\partial y}+3uv^2\dfrac{\partial^3 u}{\partial x\partial y^2}+v^3\dfrac{\partial^3 u}{\partial y^3}\end{pmatrix} \\
&=u_e\frac{\partial u_e}{\partial x}+v\begin{pmatrix}\dfrac{\partial^2 u}{\partial y^2}+\lambda_3\left\{u\dfrac{\partial^3 u}{\partial x\partial y^2}+v\dfrac{\partial^3 u}{\partial y^3}\right\} \\ -\lambda_3\left\{\dfrac{\partial u}{\partial x}\dfrac{\partial^2 u}{\partial y^2}+\dfrac{\partial u}{\partial y}\dfrac{\partial^2 v}{\partial y^2}\right\}\end{pmatrix}-\frac{\mu_0}{4\pi\rho}\left(H_e\frac{\partial H_e}{\partial x}-H_1\frac{\partial H_1}{\partial x}-H_2\frac{\partial H_1}{\partial y}\right),
\end{aligned} \tag{7.3}$$

$$u\frac{\partial H_1}{\partial x}-H_1\frac{\partial u}{\partial x}=\mu_e\frac{\partial^2 H_1}{\partial y^2}-v\frac{\partial H_1}{\partial y}+H_2\frac{\partial u}{\partial y}, \tag{7.4}$$

$$u\frac{\partial T}{\partial x}+v\frac{\partial T}{\partial y}=\frac{1}{\rho c_p}\frac{\partial}{\partial y}\left(k(T)\frac{\partial T}{\partial y}\right)-\frac{Q_0}{\rho c_p}\left(T_\infty-T\right)+\tau\left(\frac{D_T}{T_\infty}\left(\frac{\partial T}{\partial y}\right)^2+D_B\frac{\partial C}{\partial y}\frac{\partial T}{\partial y}\right), \tag{7.5}$$

$$u\frac{\partial C}{\partial x}+v\frac{\partial C}{\partial y}-k_1\left(C_\infty-C\right)=\frac{D_T}{T_\infty}\frac{\partial^2 T}{\partial y^2}+D_B\frac{\partial^2 C}{\partial y^2}. \tag{7.6}$$

The related conditions are,

$$u=u_w(x),\ v=V_w,\frac{\partial H_1}{\partial y}=H_2=0,\ T=T_w+L_2\frac{\partial T}{\partial y},\ C=C_w+L_3\frac{\partial C}{\partial y},\ \text{When }\ y\to 0 \tag{7.7}$$

$$u\to u_e,\ v\to 0,\ H_1\to H_e,\ T\to T_\infty,\ C\to C_\infty,\ \text{When }\ y\to\infty \tag{7.8}$$

In the above equation, H_e is the magnetic field at the edge of the boundary, whereas H_1 and H_2 are the component of magnetic field in $x-$direction and $y-$direction respectively. Further, the symbols $\lambda_1, \lambda_2, \lambda_3, \mu_0, \mu_e, L_2, V_w,$ and L_3 are represented the relaxation time, retardation time, material parameter of Burgers fluid, magnetic permeability, magnetic diffusivity, thermal slip factor, suction / blowing velocity, and the concentration slip factor, respectively. The $k(T)$ is a thermal conductivity in variable form, which is stated as,

$$k(T) = k_\infty\left(1+\varepsilon\left(\frac{T-T_\infty}{T_w - T_0}\right)\right). \tag{7.9}$$

In equation (7.9), and k_∞ is considered as the ambient thermal conductivity of the fluid and ε is said to be thermal conductivity parameter.

7.1.1. Similarity Variables

The appropriate similarity variables are defined as,

$$\begin{gathered}\eta = \sqrt{\frac{a}{2\nu l}} E\,\mathrm{xp}\left(\frac{x}{2l}\right) y,\ T = T_\infty + T_0 E\,\mathrm{xp}\left(\frac{x}{2l}\right)\theta(\eta), C = C_\infty + C_0 E\,\mathrm{xp}\left(\frac{x}{2l}\right)\phi(\eta),\\ u = aE\,\mathrm{xp}\left(\frac{x}{l}\right) f'(\eta), H_1 = H_0 E\,\mathrm{xp}\left(\frac{x}{l}\right) h_1'(\eta), v = -\sqrt{\frac{a\nu}{2l}} E\,\mathrm{xp}\left(\frac{x}{2l}\right)\left(\eta f'(\eta) + f(\eta)\right),\\ H_2 = -H_0\sqrt{\frac{\nu}{2al}} E\,\mathrm{xp}\left(\frac{x}{2l}\right)\left(\eta h_1'(\eta) + h_1(\eta)\right).\end{gathered} \tag{7.10}$$

In the above equation the $f(\eta)$, $h_1(\eta)$, $\theta(\eta)$, and $\phi(\eta)$ are the dimensionless variables and a, T_0, H_0, and C_0 are specified as a constant.

With the help of equation (7.10), the Eqs. (7.3-7.8) becomes,

$$\begin{gathered} f''' - 2f'^2 + ff'' - \beta_1\begin{pmatrix}\left(f^2 f''' - \eta f'^2 f'''\right)\\ +4f'^3 - 6ff'f''\end{pmatrix} + \beta_3\begin{pmatrix}3f''^2 - ff^{iv}\\ +2ff'f'''\end{pmatrix} - M\left(h'^2 + hh''\right)\\ -\beta_2\begin{pmatrix}\left(4f'^2 - 3ff''\right)^2 - f^{iv}f^3 - \left(12ff'^2 + 9\eta f'^3\right)f''\\ +\eta\left(ff'^2 f''' + 4ff'f''^2\right) + 8f^2 f'f'''\end{pmatrix} + M + \lambda^2 = 0,\end{gathered} \tag{7.11}$$

$$\Lambda h_1''' + \frac{1}{2}\left(2fh_1'' - 2h_1 f''\right) = 0, \tag{7.12}$$

$$\left(1+\varepsilon\theta\right)\theta'' + \Pr\left(f\theta' + Nb\theta'\phi' + Q\theta - f'\theta + Nt\theta'^2\right) + \varepsilon\theta'^2 = 0, \tag{7.13}$$

$$\phi'' + Sc\left(f\phi' - f'\phi - \sigma\phi\right) + \frac{Nt}{Nb}\theta'' = 0. \tag{7.14}$$

The concerned conditions are,

$$\begin{aligned} &f(0) = s,\ f'(0) = 1,\ h_1(0) = 0 = h_1''(0),\ \theta(0) = 1 + S_1\theta'(0), \phi(0) = 1 + S_2\phi'(0), \\ &f'(\eta) = \lambda,\ h_1'(\eta) = 1,\quad \theta(\eta) = 0 = \phi(\eta),\ \text{at} \quad \eta \to \infty. \end{aligned} \tag{7.15}$$

The developing parameters are represented as $\lambda, \Lambda, S_1, S_2,$ and σ which are stretching ratio parameter, magnetic Prandtl number, thermal slip parameter, concentration slip parameter, and chemical reaction parameter, respectively. Further, β_1, β_2, and β_3 are the non–Newtonian fluid parameters (Deborah numbers). The emerging parameters are mathematically defined as,

$$\begin{aligned} &\Pr = \frac{\nu}{\alpha}, \beta_1 = \frac{a\lambda_1}{2l}, \beta_2 = \frac{a^2\lambda_2}{4l^2}, \beta_3 = \frac{a\lambda_3}{2l},\ Q = \frac{Q_0}{ac_p\rho}, M = \frac{\mu}{4\pi\rho}\left(\frac{H_0}{a}\right)^2, \\ &S_1 = \gamma_1\sqrt{\frac{a}{2\nu l}}, s = V_w\sqrt{\frac{2l}{a\nu}}, Sc = \frac{\nu}{D_B}, \lambda = \frac{c}{a}, \Lambda = \frac{\mu_e}{\nu}, \sigma = \frac{2lk_1}{a}, \\ &Nb = \frac{\tau D_B C_\infty}{\nu}, Nt = \frac{\tau D_B\left(T_w - T_\infty\right)}{T_\infty \nu}, S_2 = \gamma_2\sqrt{\frac{a}{2\nu l}}. \end{aligned} \tag{7.16}$$

7.1.2. Physical Quantities

The physical quantities related to the heat and mass transfer rate are very noteworthy from an engineering perspective. These quantities are stated as,

$$\begin{aligned} &Nu_x = \frac{q_m}{k(T)(T_w - T_\infty)},\ Sh_x = \frac{j_m}{D(C_w - C_\infty)}, \\ &q_m = -k(T)\left|\frac{\partial T}{\partial z}\right|_{y=0},\ j_m = -D_B\left|\frac{\partial C}{\partial z}\right|_{y=0}. \end{aligned} \tag{7.17}$$

Here, q_m is the heat flux and j_m is the mass flux. By means of similarity transformation, the equation (7.17) gives,

$$\sqrt{\frac{2l}{x}}Nu_x = -\mathrm{Re}_x^{1/2}\,\theta'(0), \qquad (7.18)$$

$$\sqrt{\frac{2l}{x}}Sh_x = -\mathrm{Re}_x^{1/2}\,\phi'(0).$$

The local Reynold's number is $\mathrm{Re}_x = \frac{lu_w}{\nu}$.

7.2. Results and Discussion

In the current chapter, the two-dimensional Burgers nanofluid through an exponential stretching sheet with the induced magnetic field is observed. The outcomes of emerging parameters on the velocity field, induced magnetic field, temperature distribution, and concentration distribution is examined graphically. The values of emerging parameters are stated in the current chapter by $Sc = 2.0,\ \Lambda = 1.0 = Q,\ Nt = 0.1,\ \varepsilon = S_1 = 0.5 = S_2,\ Nb = 0.2,\ M = 1.5,\ \mathrm{Pr} = 2.5,$ and $\sigma = 0.1$. The **table 7.1** represented the numerical variation of the Nusselt number for several parameters. It is revealed that due to the higher values of β_1 and β_2, the enhancement occurs in the heat transfer rate, while improve the values of M causes to diminishes the heat transfer rate. Moreover, due to enlargement of S_1 and Pr, the heat transfer rate is declined for S_1, but opposite behavior is noted for Pr. The comparison of the present problem is creating with earlier published data and concluded similarity between them, which is observed in **Table 7.2**. This comparison table is enough for the justification of the current problem. **Table 7.2** is showed the variation in the heat transfer rate for the several estimations of Pr. It is seemed that the heat transfer rate boosted for greater values of $\Pr$. The numerical variation of Sherwood number against the several parameters is depicted in **table 7.3**. It is observed from the tabulated data that for the higher values of β_1 and β_2 the mass transfer rate increased consequently, while opposite behavior is examined for greater values of M. Further, higher values of S_2 and Sc cause the diversion in the concentration rate, by the fact that mass transfer rate increased for Sc, although the reverse trend is inspected for S_2

Table 7.1: Variation of Nusselt number against the several parameters, as $\beta_3 = 0.5$ and $Nb = 0.2$.

β_1	β_2	M	S_1	$\Pr$	$-\mathrm{Re}_x^{1/2}\theta'(0)$
0.0	1.0	1.5	0.5	2.5	1.2055376
0.5	-	-	-	-	1.2058175
1.0	-	-	-	-	1.20603647
0.3	0.7	1.5	-	-	1.2043141
-	1.0	-	0.5	2.5	1.20571483
-	1.5	-	-	-	1.2072341
-	-	1.0	-	-	1.2074084
-	-	1.5	-	2.5	1.2057148
0.3	-	2.0	-	-	1.2042970
-	1.0	-	0.1	-	2.03814427
-	-	1.5	0.3	-	1.53531290
-	-	-	0.5	2.5	1.20571483
0.3	-	-	-	1.0	0.7951420
-	1.0	1.5	-	2.0	1.1078357
-	-	-	0.5	3.0	1.6692830

Table 7.2: Comparison table of $-\theta'(0)$, when $\beta_1 = \beta_2 = \beta_3 = 0 = \varepsilon = S_1$.

Pr	Aman et al. [107] $(-\theta'(0))$	Zaib et al. [108] $(-\theta'(0))$	Current result $(-\theta'(0))$
0.7	0.7641	0.7641	0.76512
1.0	0.8708	0.8708	0.87181
7.0	1.7224	1.7224	1.72462

Table 7.3: Variation in mass transfer rate for the various parameters, as $\beta_3 = 0.5$ and $Nb = 0.2$.

β_1	β_2	M	S_2	Sc	$-\mathrm{Re}_x^{1/2}\,\phi'(0)$
0.0	1.0	1.5	0.5	2.0	1.255798
0.5	-	-	-	-	1.255889
1.0	-	-	-	-	1.2559568
0.3	0.7	1.5	-	-	1.255223
-	1.0	-	0.5	2.0	1.255856
-	1.5	-	-	-	1.256483
-	-	1.0	-	-	1.2565741
-	-	1.5	-	-	1.255856
0.3	-	2.0	-	-	1.255158
-	1.0	-	0.1	2.0	2.680847
-	-	1.5	0.3	-	1.710381
0.3	-	-	0.5	-	1.255856
-	1.0	-	-	1.5	1.134736
-	-	1.5	-	2.0	1.255856
-	-	-	-	2.5	1.345326

7.2.1. Flow Analysis of Physical Parameters

The variation of various parameters like relaxation parameter (β_1 and β_2) and retardation parameter (β_3) is examined in **Fig. 7.2 (a-c).** The influence of Deborah numbers (β_1 and β_2) on the plot of velocity is depicted in **Fig. 7.2 (a)** and **Fig. 7.2 (b)**. It is exposed that velocity profile is declining for the various values of both β_1 and β_2. The varying characteristics of the retardation parameter (β_3) on the velocity plot is exhibited in the **Fig. 7.2 (c).** It is scrutinized that the fluid velocity enhances against the various estimation of β_3. Physically, β_3 is the retardation time, therefore, to the enhancement of β_3, the retardation time upsurges consequently, and the fluid flow accelerated, due to this the velocity of a fluid increases.

7.2.2. Influence of Physical Parameters on Induced Magnetic Field

The variation of magnetic Prandtl number (Λ), magnetic field parameter (M), and relaxation parameters (β_1 and β_2) against $h_1'(\eta)$ plot is found in **Fig .7.3 (a-d).** It is noted that for various values of Λ the $h_1'(\eta)$ sketch and related thickness of boundary layer shows escalating behavior, which is evident in **Fig. 7.3 (a)**. The **Fig. 7.3 (b)** represented the impact of M on the induced magnetic field. It is indicated from the sketch that $h_1'(\eta)$plot and related thickness of boundary layer boosts for the several values of M. This is fact that induced magnetic field and the magnetic field are in the same direction. The effect of Deborah numbers (β_1 and β_2) on the $h_1'(\eta)$ plot is found in **Fig. 7.3 (c)** and **Fig. 7.3 (d).** It is elucidated that the $h_1'(\eta)$ sketch shows decaying behavior for the higher values of β_1 and β_2.

7.2.3. Thermal and Concentration Analysis of Physical Parameters

The influence of Deborah number (β_2) and thermal slip parameter (S_1) on the $\theta(\eta)$ distribution. is depicted in **Fig. 7.4** (**(a)** and **(b)**). **Fig. 7.4 (a)** illustrates the behavior of β_2 on the plot of

$\theta(\eta)$. It is exposed that against the several estimations of β_2, the $\theta(\eta)$ plot and related boundary layer thickness enhancing. Physically, at the higher values of Deborah number, materials behavior like a solid, therefore the fluid velocity slows down, and fluid temperature increases consequently. **Fig. 7.4 (b)** reveals the behavior of S_1 on the $\theta(\eta)$ plot. It is examined from the plot that by the stronger values of S_1 declines the temperature and related boundary layer thickness consequently. Further, no slip condition is obtained when we take $S_1 = 0$. The **Fig. 7.4** (**(c)** and **(d)**) observed the influence of Schmidt number (Sc) and concentration slip parameter (S_2) on the mass concentration distribution. **Fig. 7.4 (c)** reveals the declining behavior for the higher values of Sc on the $\phi(\eta)$ plot. Physically, Sc depends upon the molecular diffusivity. Therefore, due to the enhancement of Sc the diffusion rate slowdown, which a result, reduces the mass concentration and associated boundary layer thickness. The $\phi(\eta)$ plot reveals diminishing impact for higher values of S_2 (see in **Fig. 7.4 (d)**). Furthermore, no slip condition is achieved when we take $S_2 = 0$.

7.2.4. Effect of Physical Parameters on $\mathrm{Re}_x^{-1/2} Nu_x$ and $\mathrm{Re}_x^{-1/2} Sh_x$ Sketch

In this section, the influence of heat and mass transfer rate against the several parameters is observed graphically, which is found in **Fig. 7.5 (a** and **b)** and **Fig. 7.6 (c** and **d)**. It is noted in **Fig. 7.5 (a)** that the various values of Nt, the Nusselt number shows a diminishing effect, while the Nusselt number shows an opposite trend for several values of Pr. In **Fig. 7.5 (b)** the enhancement occurs in the Nusselt number due to higher values of ε and S_1. Further, the augmentation occurs in the Sherwood number due to higher values of σ and Sc, which is seeming in **Fig. 7.6 (c). Fig. 7.6 (d)** depicted the variation of Sherwood number due to numerous estimations of Nt and Nb. It is seemed that the higher values of Nt, the mass transfer rate is reduced, while the growing values of Nb, the mass transfer rate is boosted.

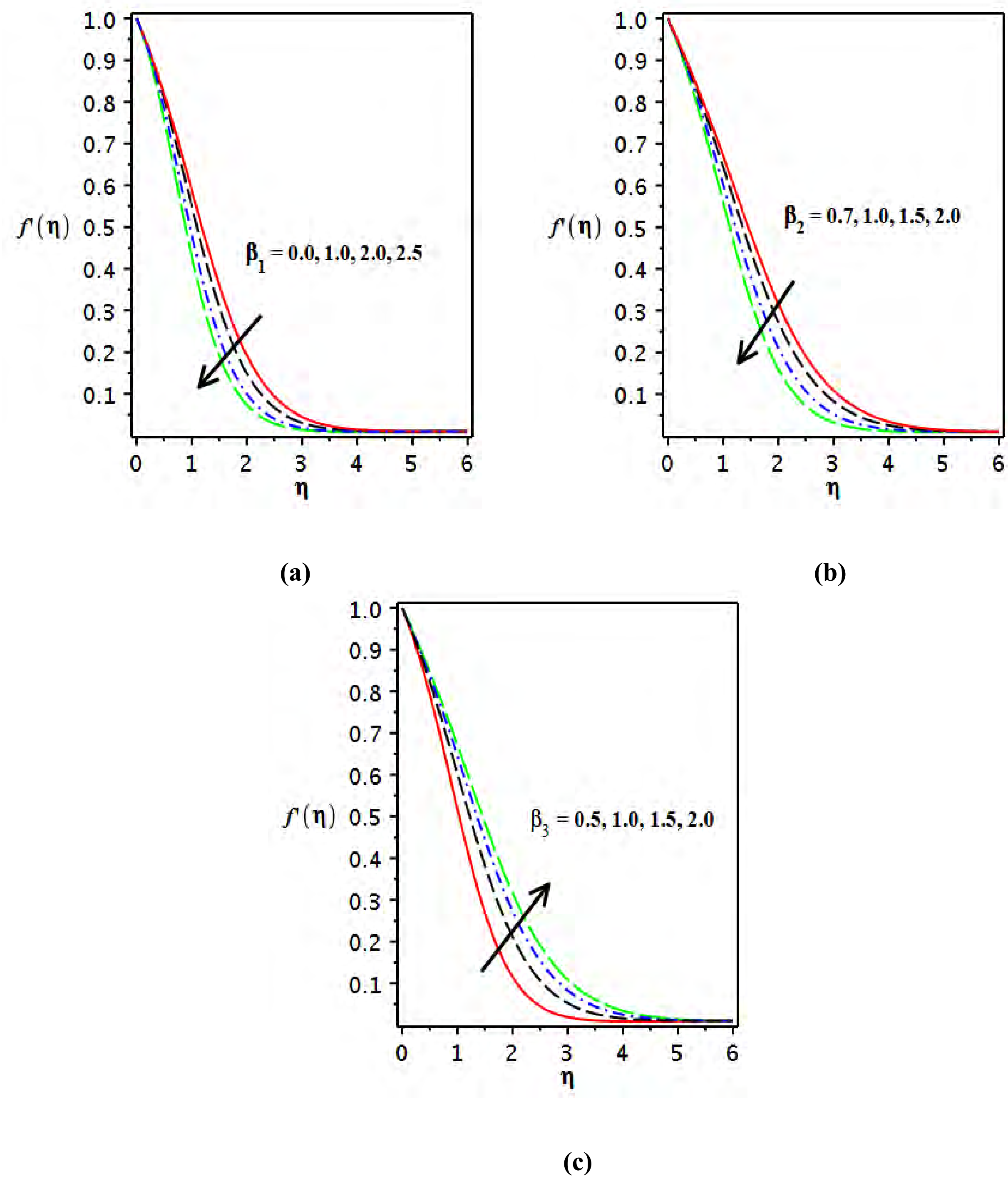

Fig. 7.2 (a-c): Variation in velocity profile due to various values of β_1, β_2 .and β_3.

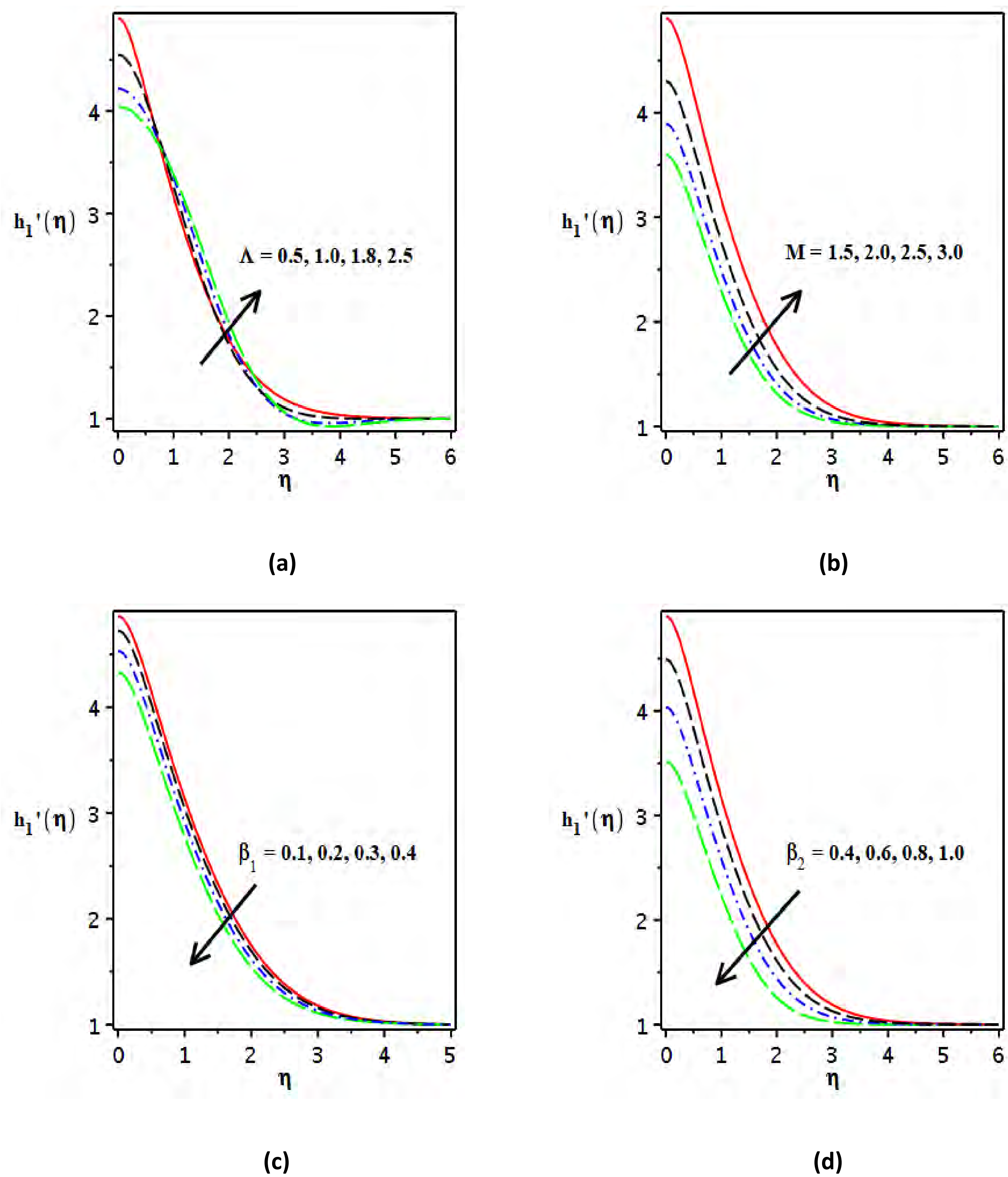

Fig. 7.3: (a-d): Variation in $h_1'(\eta)$ for the various values of Λ, M, β_1, and β_2 respectively.

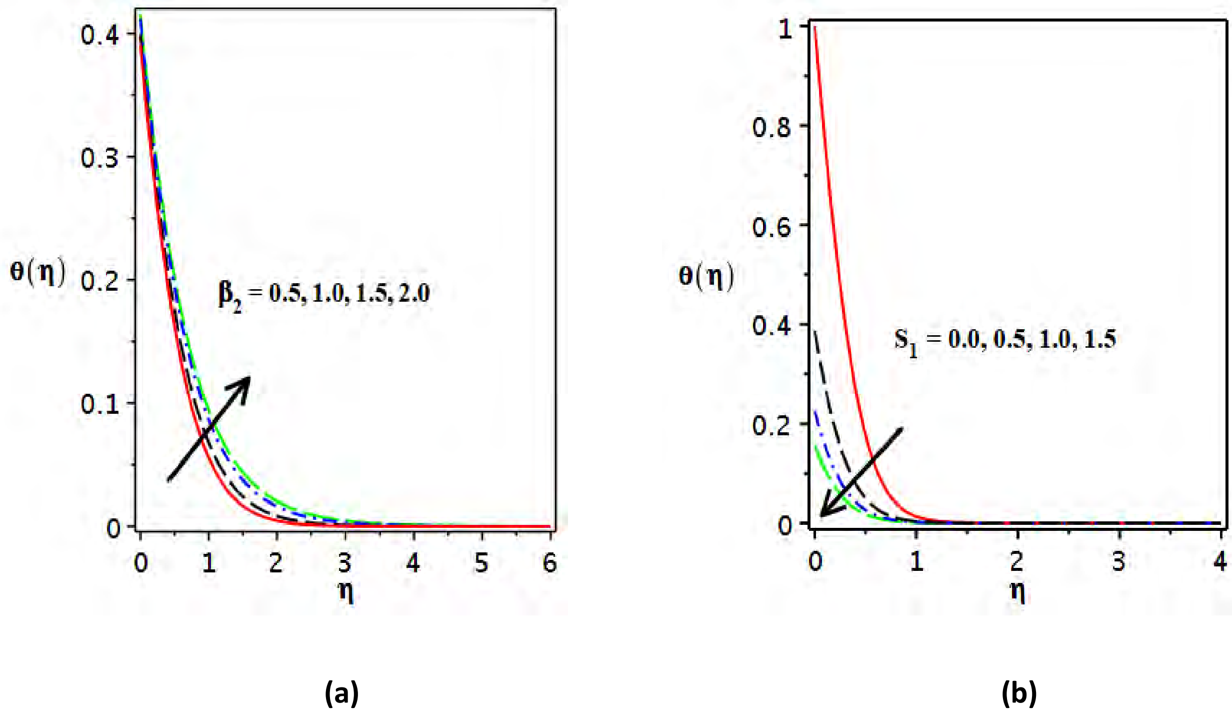

Fig.7. 4 ((a) and (b)): Variation in the $\theta(\eta)$ plot for various values of β_2 and S_1.

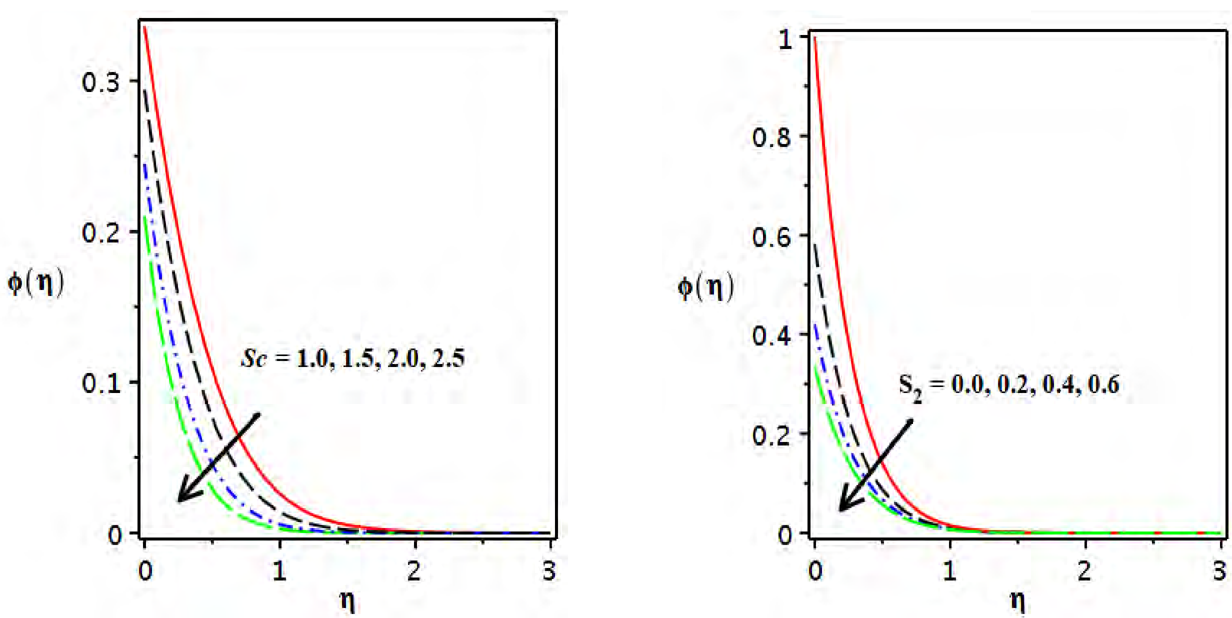

Fig. 7.4 ((c) and (d)): Variation in $\phi(\eta)$ plot for various values of Sc and S_2.

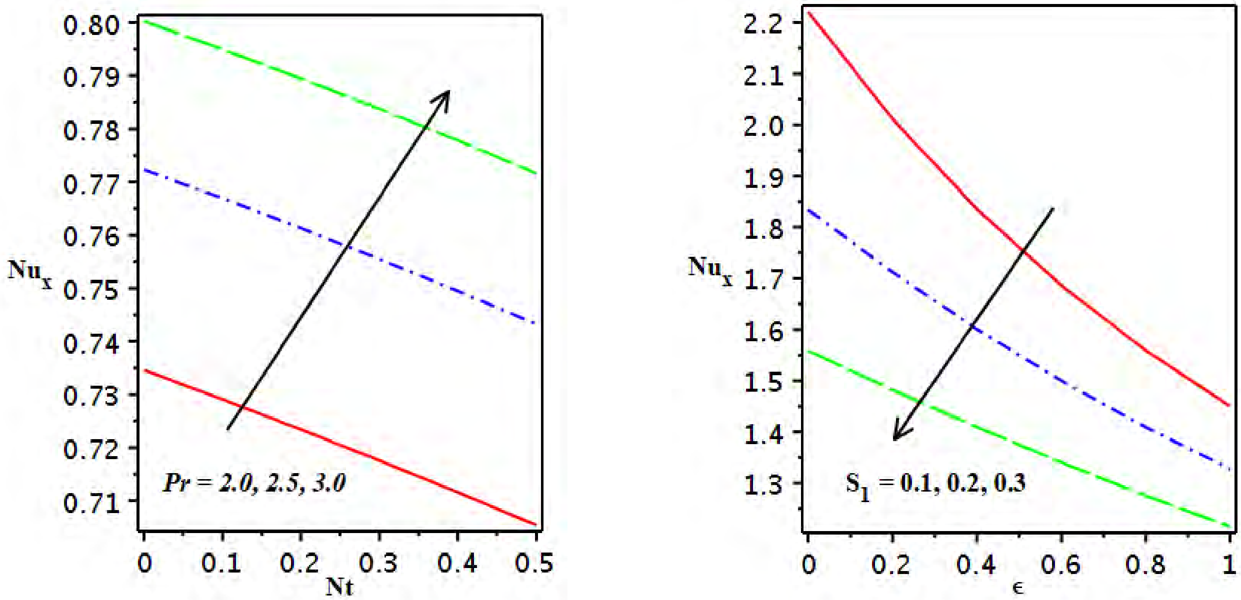

(a) (b)

Fig. 7.5 (a and **b):** Plots of Nusselt number for several values of Nt, $\Pr$, ε and S_1.

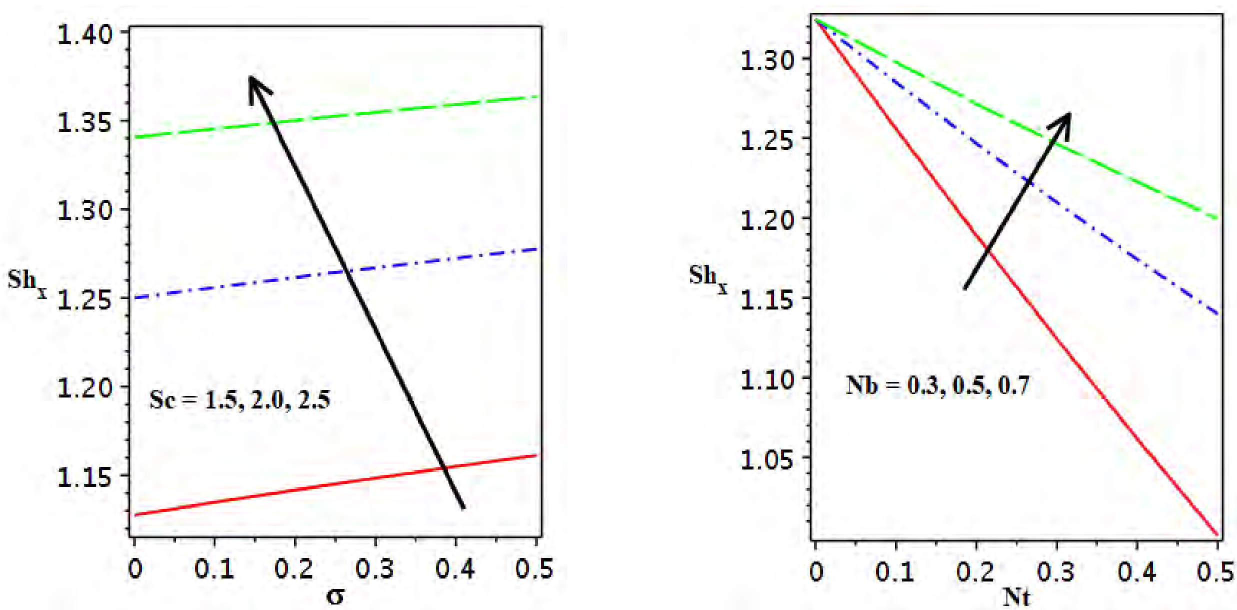

(c) (d)

Fig. 7.6 (c and **d):** Plots of Sherwood number for several values of σ, Sc, Nt and Nb.

7.3. Conclusions

In this chapter, we analyzed the various qualitative aspects relating to the solutions of Burgers nanofluid flow towards an exponentially stretching sheet with induced magnetic field. The investigation of transportation of mass and heat is presented with the influence of chemical reaction and variable thermal conductivity. Further, the thermal slip and concentration slip boundary conditions are applied to the boundary of a surface. The main results of the current chapter are,

- The velocity profile reduced for the relaxation parameter, but it reveals the opposite trend for the retardation parameter.
- The occurrence of magnetic field produces the Lorentz force, which reduce the velocity of fluid.
- The induced magnetic field and related boundary layer thickness rises for the greater values Λ and M.
- The temperature and thickness of thermal boundary layer increases by the enlargement of β_2.
- Thermal slip and concentration slip conditions vanishes for $S_1 = 0 = S_2$.
- The concentration and related boundary layer thickness reduces for the various values of S_2 and Nb.
- The heat and mass transfer rate augments due to the enhancement of β_1 and β_2.

Chapter 08

A comparative study between linear and exponential stretching sheet with double stratification of a rotating Maxwell nanofluid flow

The aim of this chapter is to explore the rotating Maxwell nanofluid flow with double stratification and activation energy. The study of mass and heat transfer is conducted with the thermophoretic and variable thermal conductivity effects. The flow study is examined across the linear / exponential stretching sheet. The similarity variable is considered to modify the flow model into the coupled ODEs. The coupled equations are computed by bvp4c Matlab technique. It is found that both rotation and stretching has a remarkable impact on the velocity profile and temperature. The heat flux condenses for higher values of rotation parameter. The reduction occurred in the rate of heat and mass transfer by enlarging value of Deborah number. The novelty of the present chapter is to analyze the Maxwell nanofluid flow in the rotating frame with activation energy and thermophoretic effect.

8.1. Mathematical Modelling

Here we analyzed the steady, 3D incompressible rotating Maxwell nanofluid flow with double stratification by considering the flow over linear and exponential stretching sheet. Additionally, we consider the activation energy and thermophoretic effect to explore the mass transfer. The flow diagram is defined in **Fig. 8.1 ((a)** and **(b))**. The flow is restricted to $z \geq 0$. The stretching velocity for linear and exponential sheet are $u_w = ax$ and $u_w = aE\,\mathrm{xp}\left(\frac{x}{l}\right)$ respectively. The fluid is rotating about the z-axis by the angular velocity (Ω). The ambient temperature and concentration is T_∞ and C_∞, while surface temperature and concentration is denoted by T_w and C_w respectively. By using above assumption and boundary layer approximation the equations of mass, momentum, temperature, and concentration are expressed as,

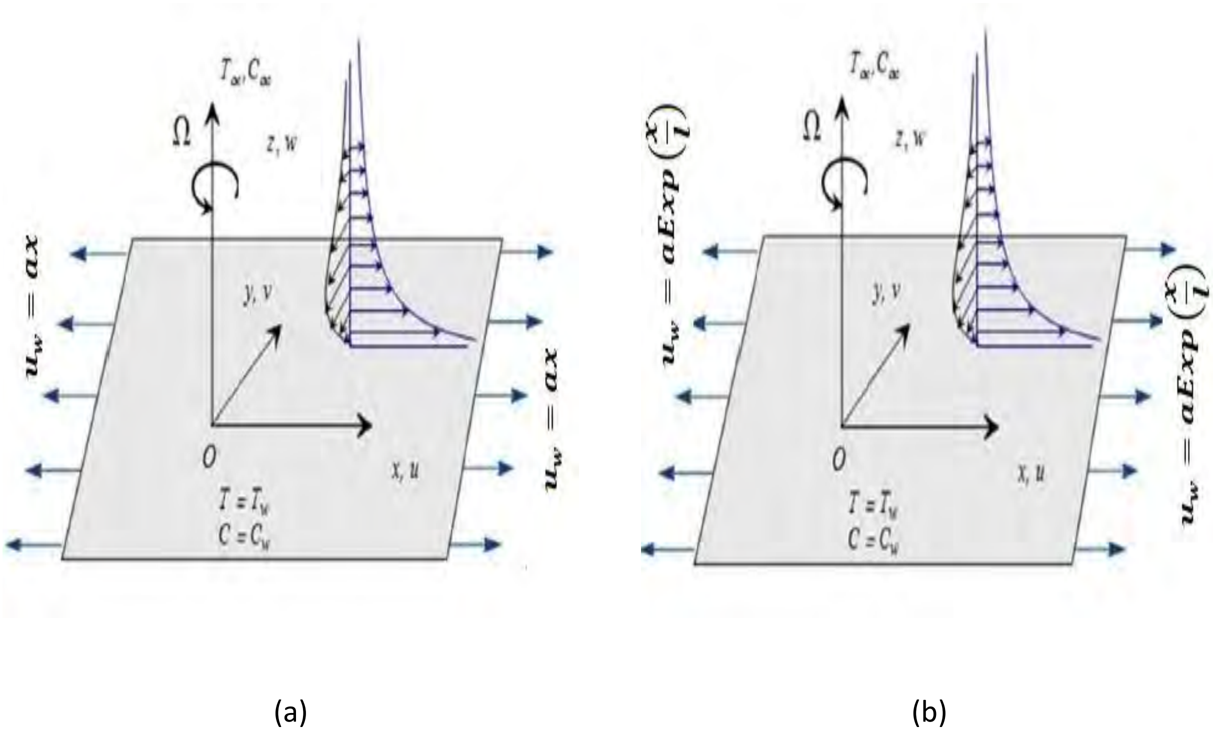

Fig. 8.1 ((a) and **(b)):** Physical interpretation of the chapter for linear and exponential sheet.

$$\frac{\partial u}{\partial x} = -\left(\frac{\partial v}{\partial y} + \frac{\partial w}{\partial z}\right) = 0, \tag{8.1}$$

$$u\frac{\partial u}{\partial x} + v\frac{\partial u}{\partial y} + w\frac{\partial u}{\partial z} + \lambda_1\begin{bmatrix} 2\left(uw\frac{\partial^2 u}{\partial x\partial z} + uv\frac{\partial^2 u}{\partial x\partial y} + vw\frac{\partial^2 u}{\partial y\partial z}\right) \\ -2\Omega\left(u\frac{\partial v}{\partial x} + w\frac{\partial v}{\partial z} + v\frac{\partial v}{\partial y}\right) + 2\Omega v\frac{\partial u}{\partial x} \\ +u^2\frac{\partial^2 u}{\partial x^2} + v^2\frac{\partial^2 u}{\partial y^2} + w^2\frac{\partial^2 u}{\partial z^2} - 2\Omega u\frac{\partial u}{\partial y} \end{bmatrix} - 2\Omega v = \nu\frac{\partial^2 u}{\partial z^2}, \tag{8.2}$$

$$u\frac{\partial v}{\partial x}+v\frac{\partial v}{\partial y}+w\frac{\partial v}{\partial z}+\lambda_1\left[\begin{array}{l}2\left(uv\frac{\partial^2 v}{\partial x\partial y}+uw\frac{\partial^2 v}{\partial x\partial z}+vw\frac{\partial^2 v}{\partial y\partial z}\right)\\+2\Omega\left(u\frac{\partial u}{\partial x}+w\frac{\partial u}{\partial z}+v\frac{\partial u}{\partial y}\right)+2\Omega v\frac{\partial v}{\partial x}\\+u^2\frac{\partial^2 v}{\partial x^2}+w^2\frac{\partial^2 v}{\partial z^2}+v^2\frac{\partial^2 v}{\partial y^2}-2\Omega u\frac{\partial v}{\partial y}\end{array}\right]+2\Omega u=\nu\frac{\partial^2 v}{\partial z^2}, \tag{8.3}$$

$$u\frac{\partial T}{\partial x}+v\frac{\partial T}{\partial y}+w\frac{\partial T}{\partial z}=\frac{1}{\rho c_p}\frac{\partial}{\partial z}\left(k(T)\frac{\partial T}{\partial z}\right)+\tau D_B\frac{\partial T}{\partial z}\frac{\partial C}{\partial z}+\tau\frac{D_T}{T_\infty}\left(\frac{\partial T}{\partial z}\right)^2, \tag{8.4}$$

$$u\frac{\partial C}{\partial x}+v\frac{\partial C}{\partial y}+w\frac{\partial C}{\partial z}+\frac{\partial}{\partial z}\left(V_T(C-C_\infty)\right)+k_1^2\left(\frac{T}{T_\infty}\right)^m Exp\left(\frac{-E_a}{kT}\right)(C-C_\infty)=D_B\frac{\partial^2 C}{\partial z^2}+\frac{D_T}{T_\infty}\frac{\partial^2 T}{\partial z^2}. \tag{8.5}$$

The suitable surface and free stream conditions for linear sheet are,

$$u=u_w(x),\ v=0=w,\ T=T_w=T_0+a_1x,\ C=C_w=C_0+b_1x,\ \text{When }z\to 0 \tag{8.6}$$

$$u\to 0, v_z\to 0, T\to T_\infty=T+c_1x_0, C\to C_\infty=C_0+d_1x.\ \text{When }z\to\infty \tag{8.7}$$

The suitable surface and free stream conditions for exponential sheet are,

$$u=u_w(x),\ v=0=w,\ T=T_w=a_1E\,\mathrm{xp}\left(\frac{x}{2l}\right)+T_0, C=C_w=b_1E\,\mathrm{xp}\left(\frac{x}{2l}\right)+C_0, \text{When }z\to 0, \tag{8.8}$$

$$u\to 0, v_z\to 0, T\to T_\infty=c_1E\,\mathrm{xp}\left(\frac{x}{2l}\right)+T_0, C\to C_\infty=d_1E\,\mathrm{xp}\left(\frac{x}{2l}\right)+C_0.\ \text{When }z\to\infty. \tag{8.9}$$

In the above equations the symbols $\rho, \nu, k, \lambda_1, E_a$, and k_1 are denoted the fluid density, kinematic viscosity, thermal conductivity, relaxation time of fluid, activation energy and chemical reaction, respectively. Further, $k(T)$ is temperature dependent thermal conductivity and V_T is thermophoretic velocity, which is defined as,

$$k(T)=k_\infty\left(1+\varepsilon\left(\frac{T-T_\infty}{T_w-T_0}\right)\right), V_T=-\nu\frac{k_t}{T_r}\frac{\partial T}{\partial z} \tag{8.10}$$

8.1.1. Similarity Transformation

The similarity transformations are stated as,

Linear sheet,

$$w=-\sqrt{a\nu}\,f(\eta),\ v=axg(\eta),u=axf'(\eta),\eta=z\sqrt{\frac{a}{\nu}},$$
$$\frac{T-T_\infty}{T_w-T_0}=\theta(\eta),\ \frac{C-C_\infty}{C_w-C_0}=\phi(\eta). \tag{8.11}$$

Exponential sheet,

$$\eta=z\sqrt{\frac{a}{2\nu l}}E\operatorname{xp}\left(\frac{x}{2l}\right),\ T-T_\infty=T_0E\operatorname{xp}\left(\frac{Nx}{2l}\right)\theta(\eta),C-C_\infty=C_0E\operatorname{xp}\left(\frac{Mx}{2l}\right)\phi(\eta),$$
$$u=aE\operatorname{xp}\left(\frac{x}{l}\right)f'(\eta),v=aE\operatorname{xp}\left(\frac{x}{l}\right)g(\eta),w=-\sqrt{\frac{a\nu}{2l}}E\operatorname{xp}\left(\frac{x}{2l}\right)\left(\eta f'(\eta)+f(\eta)\right), \tag{8.12}$$

In Eq. (8.12) T_0 and C_0 are stated as a constant. Further, N and M are the temperature and concentration exponent.

Using above transformations, the Eqs. (8.2-8.9) in dimensionless form,

Linear sheet,

$$f'''+ff''-\beta_1 fg'-\beta_1\left(f^2f'''-2ff'f''\right)+2\lambda_r g-f'^2=0, \tag{8.13}$$

$$g''-2\lambda_r f'+g'f+\beta_1\left(2ff'g'-f^2g''\right)-2\lambda_r\beta_1\left(f'^2+g^2-ff''\right)-gf'=0, \tag{8.14}$$

$$\left(1+\varepsilon\theta\right)\theta''+\Pr\left(f\theta'-f'\theta-\delta_1 f'+Nb\theta'\phi'+Nt\theta'^2\right)+\varepsilon\theta'^2=0, \tag{8.15}$$

$$\phi''+Sc\left(f\phi'-\tau_1\left(\theta'\phi'-(\phi+\Psi)\theta''\right)-f'\phi-\sigma\left(1+\delta\theta\right)^m e^{\left(\frac{-E_1}{1+\delta\theta}\right)}\phi-\delta_2 f'\right)+\frac{Nt}{Nb}\theta''=0. \tag{8.16}$$

Exponential sheet,

$$f''' + f''f + 3\beta_1 ff''f' - 2f'^2 - 2\beta_1 f'^3 + 2\lambda_r\left(4g - 2\beta_1\left(fg' + \eta f''g\right)\right) - \frac{\beta_1}{2}\left(f^2 f''' - \eta f'^2 f''\right) = 0, \tag{8.17}$$

$$\begin{aligned} & g'' + fg' + 3\beta_1 ff'g' - 2gf' - 2\beta_1 f'^2 g - \frac{\beta_1}{2}\left(f^2 g'' - \eta f'^2 g'\right) \\ & -4\lambda_r\left(f' - \beta_1\left(\frac{1}{2}ff'' - f'^2 - g^2 - \frac{\eta}{2}gg'\right)\right) = 0, \end{aligned} \tag{8.18}$$

$$(1+\varepsilon\theta)\theta'' + \Pr\left(f\theta' - Nf'\theta + Nb\theta'\phi' + Nt\theta'^2 - \delta_1 f'\right) + \varepsilon\theta'^2 = 0, \tag{8.19}$$

$$\frac{1}{Sc}\phi'' + f\phi' - Mf'\phi + \frac{Nt}{NbSc}\theta'' - \sigma(1+\delta\theta)^m e^{\left(\frac{-E_1}{1+\delta\theta}\right)}\phi - \tau_1\left(\theta'\phi' - (\phi+\Psi)\theta''\right) - \delta_2 f' = 0, \tag{8.20}$$

The associated surface and free stream conditions are,

$$\left(\begin{array}{l} f(0) = 0 = g(0),\ f'(0) = 1,\ \theta(0) = 1-\delta_1,\ \phi(0) = 1-\delta_2, \\ f'(\eta) = 0 = g'(\eta),\ \theta(\eta) = 0 = \phi(\eta),\ \text{at} \quad \eta \to \infty. \end{array}\right). \tag{8.21}$$

The evolving parameters are represented by $\beta_1, \lambda_r, \delta, E_1,$ and τ_1, which are relaxation parameter, rotation parameter, temperature ratio parameter, activation energy parameter, and thermophoretic parameter, respectively. Mathematically parameters are defined as,

$$\begin{aligned} & \Pr = \frac{\nu}{\alpha},\ \tau_1 = \frac{-k_t\left(T_w - T_\infty\right)}{T_r},\ \delta_1 = \frac{T_w - T_\infty}{T_\infty},\ \beta_1 = a\lambda_1,\ \lambda_r = \frac{\Omega}{a},\ Sc = \frac{\nu}{D_B},\ Nt = \frac{\tau D_T\left(T_w - T_\infty\right)}{\nu T_\infty}, \\ & Nb = \frac{\tau D_B\left(C_w - C_\infty\right)}{\nu},\ E_1 = \frac{E_a}{kT_\infty},\ S_1 = \frac{a_1}{b_1},\ S_2 = \frac{c_1}{d_1},\ \sigma = \frac{k_1}{a}. \end{aligned} \tag{8.22}$$

The parameters which are reformed in exponential sheet are implied as,

$$\beta_1 = \frac{a\lambda_1 e^{\frac{x}{l}}}{l}, \lambda_r = \frac{\Omega l}{e^{\frac{x}{l}}a},\ \sigma = \frac{k_1 l}{e^{\frac{x}{l}}a}. \tag{8.23}$$

8.1.2 Physical Quantities

The quantities which deal with the rate of heat and mass transfer are very vital in the engineering perspective. These physical quantities are defined as,

$$
\begin{aligned}
&Nu_x = \frac{q_m}{k(T)(T_w - T_\infty)},\ Sh_x = \frac{j_m}{D_B(C_w - C_\infty)},\\
&q_m = \left| -k(T)\frac{\partial T}{\partial z} \right|_{z=0},\ j_m = \left| -D_B \frac{\partial C}{\partial z} \right|_{z=0}.
\end{aligned} \tag{8.24}
$$

Here the heat and mass flux are q_m and j_m respectively. With the help of transformations, the Eqn. (8.24) takes the form,

$$
\begin{aligned}
&\left(1-\delta_1\right)\mathrm{Re}_x^{-\frac{1}{2}}\, Nu_x = -\theta'(0),\\
&\left(1-\delta_2\right)\mathrm{Re}_x^{-\frac{1}{2}}\, Sh_x = -\phi'(0).
\end{aligned} \tag{8.25}
$$

The local Reynold's numbers are stated for linear and exponential stretching sheet as,

$\mathrm{Re}_x = \frac{xu_w}{\nu}$ and $\mathrm{Re}_x = \frac{lu_w}{\nu}$ respectively.

8.1.3. Solution Methodology

In this chapter, we solve numerically the Eqs. (8.14–8.22) by the means of bvp4c built-in Matlab technique. We converted the Eqs. (8.14–8.22) into the system of 1st order Eqs. as,

Linear sheet,

$$\left(f = Z_1, f' = Z_2, f'' = Z_3, g = Z_4, g' = Z_5, \theta = Z_6, \theta' = Z_7, \phi = Z_6, \phi' = Z_7 \right), \tag{8.26}$$

$$ZZ_1 = \left(1 - \beta_1 Z_1^2\right)^{-1}\left(\beta_1 Z_1 Z_5 - Z_1 Z_3 + 2\beta_1 Z_1 Z_2 Z_3 - 2\lambda_r Z_4 + Z_1^2\right), \tag{8.27}$$

$$ZZ_2 = \left(1 - \beta_1 Z_1^2\right)^{-1}\left(Z_2 Z_4 - Z_1 Z_5 - 2\beta_1 Z_1 Z_2 Z_5 + 2\lambda_r \beta_1\left(Z_1^2 + Z_4^2 - Z_1 Z_3\right)\right), \tag{8.28}$$

$$ZZ_3 = \left(1+\varepsilon Z_6\right)^{-1}\left[\Pr\left(Z_2Z_6 - Z_1Z_7 + S_1Z_2 - NbZ_7Z_9 - NtZ_7^2\right) - \varepsilon Z_7^2\right], \tag{8.29}$$

$$ZZ_4 = Sc\begin{pmatrix} Z_2Z_8 - Z_1Z_9 + S_2Z_2 + \sigma\left(1+\delta Z_6\right)^m e^{\left(\frac{-E_1}{1+\delta Z_6}\right)} Z_8 \\ +\tau_1\left(Z_7Z_9 - \left(Z_8+\Psi\right)(ZZ_3)\right) \end{pmatrix} - \frac{Nt}{Nb} ZZ_3. \tag{8.30}$$

Exponential sheet,

$$ZZ_1 = \left(1 - \frac{\beta_1}{2} Z_1^2\right)^{-1} \begin{pmatrix} 2\beta_1 Z_2^3 - Z_1Z_3 - 3\beta_1 Z_1Z_2Z_3 + 2Z_1^2 - \frac{\beta_1}{2}\eta Z_2^2 Z_3 \\ -2\lambda_r\left(4Z_4 - 2\beta_1\left(Z_1Z_5 + \eta Z_3Z_4\right)\right) \end{pmatrix}, \tag{8.31}$$

$$ZZ_2 = \left(1 - \frac{\beta_1}{2} Z_1^2\right)^{-1} \begin{pmatrix} 2Z_2Z_4 + 2\beta_1 Z_2^2 Z_4 - Z_1Z_3 - 3\beta_1 Z_1Z_2Z_5 + 2Z_1^2 - \frac{\beta_1}{2}\eta Z_2^2 Z_5 \\ +4\lambda_r\left(Z_2 - \beta_1\left(\frac{1}{2}Z_1Z_3 - Z_2^2 - Z_4^2 - \frac{\eta}{2}Z_4Z_5\right)\right) \end{pmatrix}, \tag{8.32}$$

$$ZZ_3 = \left(1+\varepsilon Z_6\right)^{-1}\left[\Pr\left(NZ_2Z_6 - Z_1Z_7 + S_1Z_2 - NbZ_7Z_9 - NtZ_7^2\right) - \varepsilon Z_7^2\right], \tag{8.33}$$

$$ZZ_4 = Sc\begin{pmatrix} MZ_2Z_8 - Z_1Z_9 + S_2Z_2 + \sigma\left(1+\delta Z_6\right)^m e^{\left(\frac{-E_1}{1+\delta Z_6}\right)} Z_8 \\ +\tau_1\left(Z_7Z_9 - \left(Z_8+\Psi\right)(ZZ_3)\right) \end{pmatrix} - \frac{Nt}{Nb} ZZ_3. \tag{8.34}$$

The related boundary conditions in the first order form as,

$$\begin{pmatrix} Z_0(1) = 0 = Z_0(4), Z_0(2) = 1, Z_0(6) = 1 - S_1, Z_0(8) = 1 - S_2, \\ Z_{\inf}(2) = 0 = Z_{\inf}(5), Z_{\inf}(6) = 0,\ Z_{\inf}(5) = 0. \end{pmatrix}. \tag{8.35}$$

8.2. Results and Discussion

The current chapter observed numerically, the rotating Maxwell nanofluid flow with double stratification and activation energy past a linear and exponential stretching surface. The graphical consequence is presented for evolving parameters against the velocity, temperature, and concentration distribution. The defined values of the parameters are $\beta_1 = 0.2, \Pr = 3.5,$ $\varepsilon = Nt = Nb = 0.1 = \delta_1 = \delta_2,\ E_1 = 0.5,\ \delta = 0.3,\ \sigma = 0.5,\ Sc = 2.5,\ \lambda_r = 0.5,$ and $\tau_1 = 1.0$. The reliability of the present investigation is proved by constructing the comparison table with earlier published data and finding similarity between two, which is acknowledged in **Table 8.1**. This comparison table is sufficient for the justification of the present investigation. **Table 8.1** is the assessment of $f''(0)$ for the different values of β_1. It is found that stronger values of β_1 improve the velocity gradient. The comparison between linear and exponential stretching sheet on $-\theta'(0)$ and $-\phi'(0)$ for the several parameters is presented in **table 8.2**. It is portrayed in the **table 8.2** that the heat and mass transfer rate shows diminishing behavior for β_1 and λ_r, while growing trend is noted against the δ_2 and τ_1. Further, from the tabulated data, it is cleared that the emerging parameter against exponential sheet gives more better results as compare to the linear stretching sheet. Therefore, it is concluded that exponential stretching sheet gives more valuable results as compared to other surfaces.

Table 8.1: Assessment of $f''(0)$ with published results, when $\varepsilon = \tau_1 = 0 = \lambda_r = \delta_1 = \delta_2$.

	Sadeghy et al. [109]	Khan et al. [110]	Present results
β_1	$f''(0)$	$f''(0)$	$f''(0)$
0.0	1.00000	1.00000	1.00480
0.2	1.05490	1.051889	1.05215
0.4	1.10084	1.101903	1.10204
0.6	1.15016	1.150137	1.15022
0.8	1.19872	1.196711	1.19672

Table 8.2: Valuation of results between linear and exponential sheet for $-\theta'(0)$ and $-\phi'(0)$.

Variation of several parameters as $Nt = 0.1 = Nb, \sigma = 0.5.$				Linear sheet		Exponential sheet	
β_1	λ_r	δ_2	τ_1	$-\theta'(0)$	$-\phi'(0)$	$-\theta'(0)$	$-\phi'(0)$
0.0	0.5	0.1	1.0	1.9744	2.8991	1.286	2.6013
0.3	-	-	-	1.9119	2.6994	1.2097	2.4792
0.6	-	-	-	1.8374	2.4844	1.1319	2.3645
0.2	0.3	-	-	1.9896	2.9573	1.3421	2.7217
-	0.5	0.1	-	1.9335	2.7664	1.2351	2.5187
-	0.7		1.0	1.8719	2.5804	1.1311	2.3574
-	0.5	0.0	-		2.487		2.3626
0.2	-	0.1	-		2.7664		2.5187
-	-	0.2	-		3.1157		2.7137
-	0.5	-	0.5		2.3698		2.0349
-	-	-	1.0		2.7664		2.5187
0.2	-	0.1	1.5		3.4384		3.2121

8.2.1. Flow Analysis of Physical Parameters

The impact of the relaxation parameter (β_1) and rotation parameter (λ_r) on the velocity field $f'(\eta)$ and $g(\eta)$ for linear and exponential sheet is shown in **Figs. (8.2–8.5)**. The variation in $f'(\eta)$ and $g(\eta)$ sketch for various values of β_1 is observed in **Figs. 8.2** and **8.3**. It reveals that the velocity profile is reduced as increasing the β_1. Further, we noted that Newtonian fluid is regained for $\beta_1 = 0$. Physically, the viscous effects are dominant for smaller β_1, but elastic effects are dominate in the case of larger values of β_1. Hence, the fluid velocity reduces. The impact of λ_r on the $f'(\eta)$ and $g(\eta)$ sketch is examined in the **Figs. 8.4** and **8.5.** It is described that the different values of λ_r, reduce the plot of $f'(\eta)$ and $g(\eta)$ and associated boundary layer become thinner. Physically, the rotation parameter diminishes the fluid motion in the $x-$direction because it is the ratio between rotations to the stretching rate. The rotation effect illustrates the Coriolis force which leads to accelerate the fluid flow, hence larger λ_r provides the opposition to the fluid motion. The negative value of $g(\eta)$ plot exposes that the flow in the negative $y-$direction only due to rotation and oscillatory behaves produce. Therefore, the velocity of the fluid is declined in both directions.

8.2.2. Thermal Analysis of Physical Parameters

The impact of the relaxation parameter (β_1), rotation parameter (λ_r), variable thermal conductivity parameter (ε), thermophoresis parameter (Nt), Prandtl number ($\Pr$), and thermal stratification parameter (δ_1) on the $\theta(\eta)$ distribution is shown in **Figs. (8.6–8.11)**. It is illustrated in **Figs. 8.6** and **8.7** that the plot of $\theta(\eta)$ is improved for the higher values of β_1 and λ_r. Physically, for stronger estimation of λ_r the thermal boundary layer become thicker and more kinetic energy provides to the fluid, hence the fluid temperature and associated boundary layer thickness is boosted. The qualitatively similar effect is noted for the different values of $\Pr$ and δ_1 in **Figs. 8.8** and **8.9**. By amplifying the values of $\Pr$ and δ_1 the temperature and related thickness of boundary layer reduces. The occurrence of the thermal stratification effect, the effective temperature between the ambient fluid and sheet will be decreased, therefore the temperature distribution decays. The **Figs. 8.10** and **8.11** designates the variation in the $\theta(\eta)$ plot for several values of ε and Nt. It is depicted that both thermal boundary layer thickness and temperature enlarges by the flourishing values of ε and Nt. Physically, due to augmentation of thermophoretic parameter yields stronger thermophoretic forces in the direction of the temperature gradient, as a result the temperature of fluid enhances.

8.2.3. Concentration Analysis of Physical Parameters

The **Figs. (8.12–8.19)** portrayed the influence of relaxation parameter (β_1), chemical reaction parameter (σ), rotation parameter (λ_r), Brownian motion parameter (Nb), thermophoretic parameter (τ_1), Schmidt number (Sc), and concentration stratification parameter (δ_2), activation energy parameter (E_1), on the $\phi(\eta)$ plot. It is plotted in **Figs. 8.12** and **8.13** that for various values of β_1 and λ_r displays the growing behavior for the concentration plot. Physically, for the larger λ_r the boundary layer thickness as well as $\phi(\eta)$ distribution enhances due to increment of rotation velocity Ω. The behavior of Sc and δ_2 on the $\phi(\eta)$ plot is exhibited in **Figs. 8.14** and **8.15**. It is evinced from the **Figs. 8.14** and **8.15** that the sketched shows shrinking trend due to escalating the values of Sc and δ_2. Physically, δ_2 is the concentration difference between the ambient fluid and the sheet. Therefore, mass concentration declines for δ_2. Additionally, for $\delta_2 = 0$, the recommended surface concentration condition is recovered. The variation in $\phi(\eta)$ distribution for the several values of σ and τ_1 is designated in **Figs. 8.16** and **8.17**. It demonstrates that the mass concentration is diminished due to the higher values of σ and τ_1. Physically, by the augmentation in τ_1, the particle concentration all over the domain shrinkages, which cause the reduction in $\phi(\eta)$ plot and related boundary layer thickness. Moreover, the greater values of σ producing higher molecular motion, which increases transport phenomenon and reduces the fluid concentration. The variation in $\phi(\eta)$ curve for the various estimations of the activation energy parameter is sketched in **Fig. 8.18.** It demonstrates that the thickening of the concentration boundary layer enhances due to the higher values of E_1. This occurs, because the high activation energy and low temperature lead to slow down the reaction rate, hence mass concentration increases due to slow reaction rate. **Fig. 8.19** elucidates that the higher estimation of Nb produce lower concentration and declining the thickness of related boundary layer.

8.2.4. Influence of Physical Parameters on $\mathrm{Re}_x^{-\frac{1}{2}} Nu_x$ and $\mathrm{Re}_x^{-\frac{1}{2}} Sh_x$ Sketch

In this section, the consequence of heat and mass transfer rate on the linear and exponential stretching sheet is examined graphically. **Figs. (8.20–8.23)** established the variation in the heat and mass transfer rate for the several parameters. It is illustrated in **Fig. 8.20** that the heat transfer rate diminishes for higher values of β_1 and ε. Further, the growth in the Sherwood number is occurred due to enhancement of τ_1, while the reverse trend is found for stronger values of β_1 (see in **Fig. 8.21**). **Fig. 8.22** shows the dominate behavior for the heat transfer rate due to several values of δ_1, but opposite tendency is observed for the higher estimation of Nt. **Fig. 8.23** scrutinized that δ_2 and σ has similar results for the mass transfer rate. It is shown that as enhancing the values of δ_2 and σ, the Sherwood number is increased.

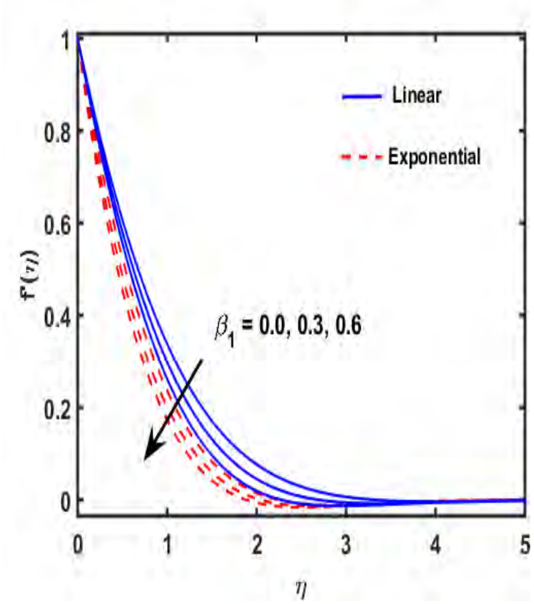

Fig. 8.2: Graph of β_1 for $f'(\eta)$.

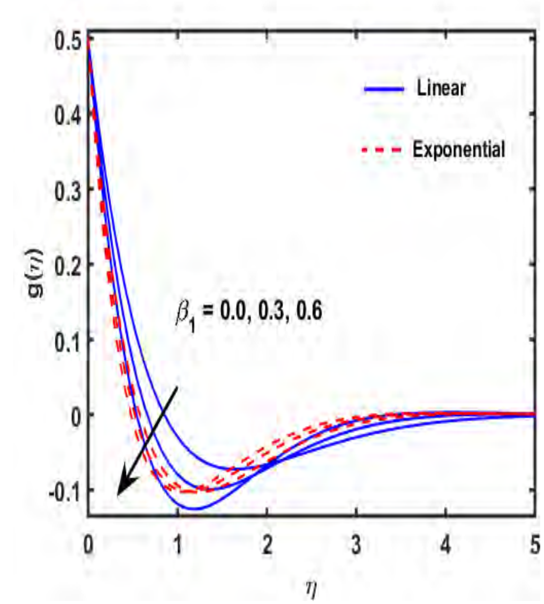

Fig. 8.3: Graph of β_1 for $g(\eta)$.

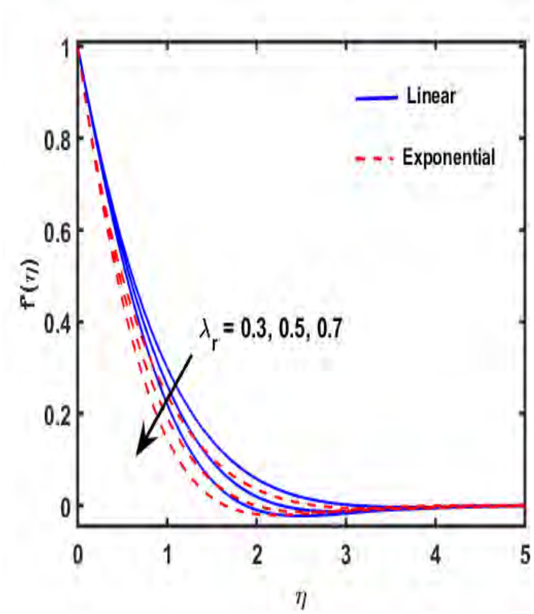

Fig. 8.4: Graph of λ_r for $f'(\eta)$.

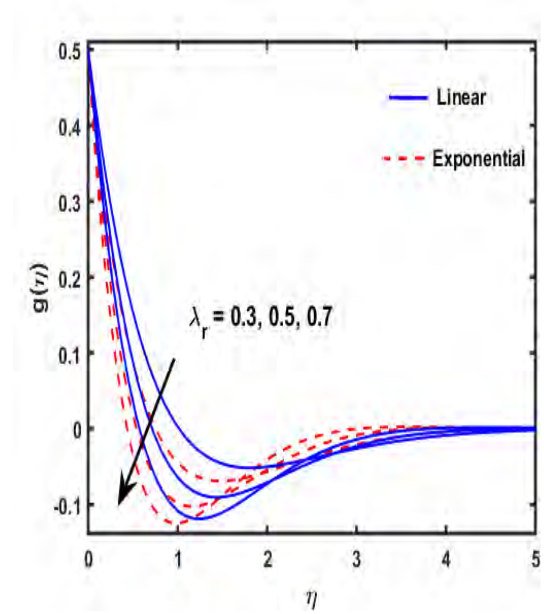

Fig. 8.5: Graph of λ_r for $g(\eta)$.

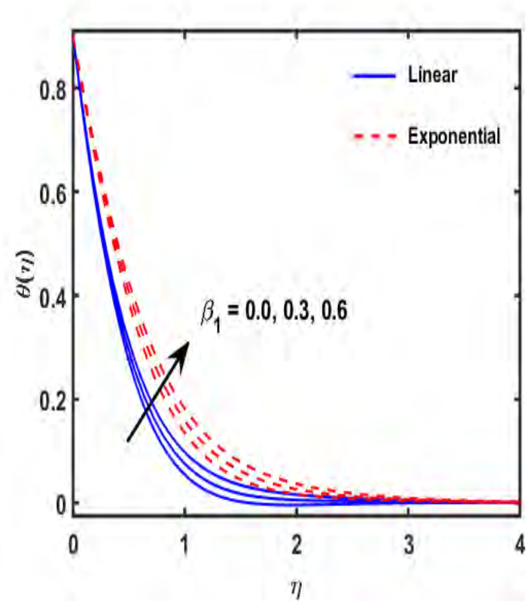

Fig. 8.6: Graph of β_1 for $\theta(\eta)$.

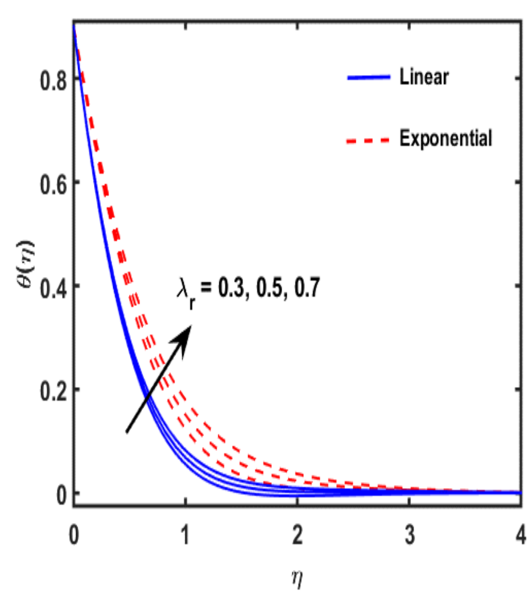

Fig. 8.7: Graph of λ_r for $\theta(\eta)$.

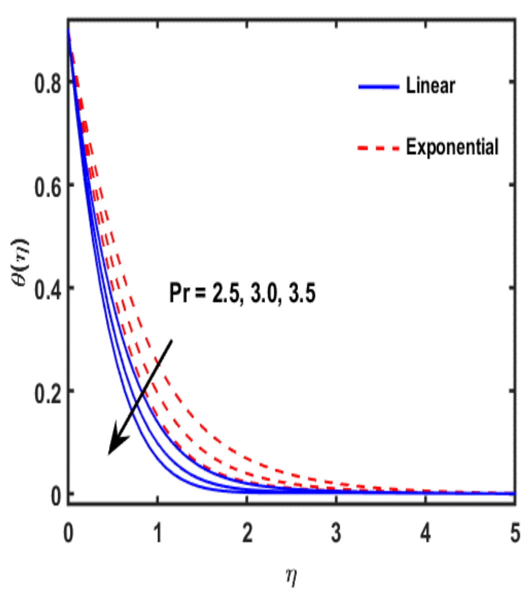

Fig. 8.8: Graph of Pr for $\theta(\eta)$.

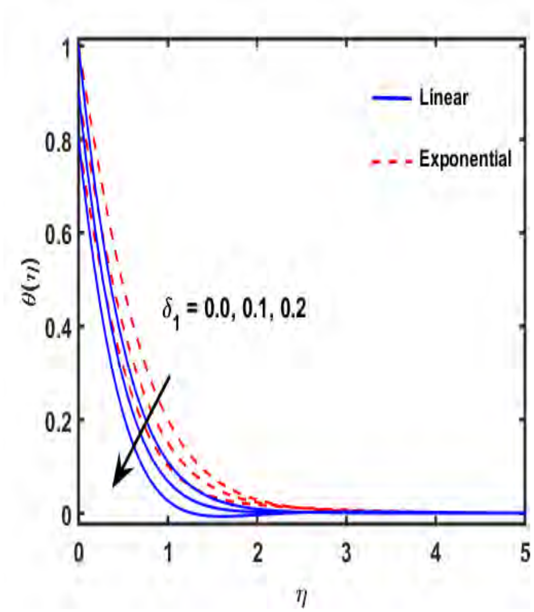

Fig. 8.9: Graph of δ_1 for $\theta(\eta)$.

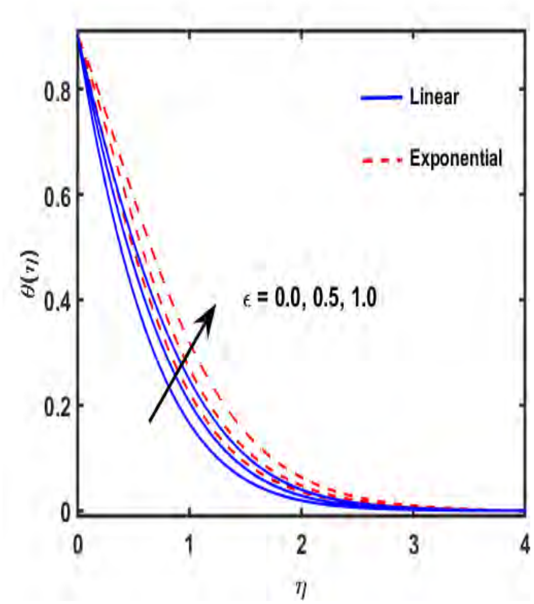

Fig. 8.10: Graph of ε for $\theta(\eta)$.

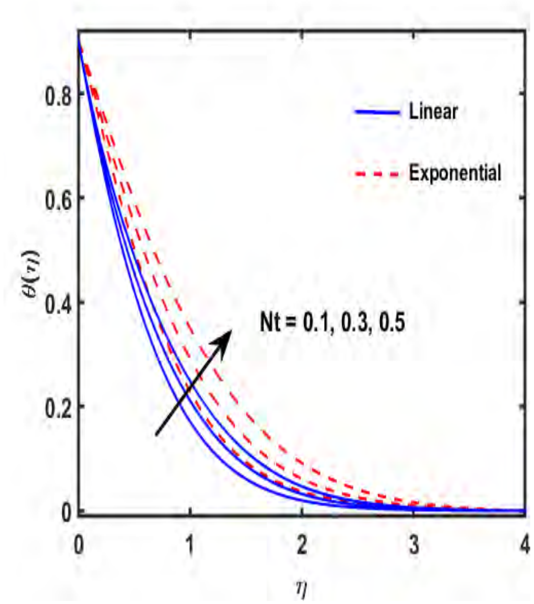

Fig. 8.11: Graph of Nt for $\theta(\eta)$.

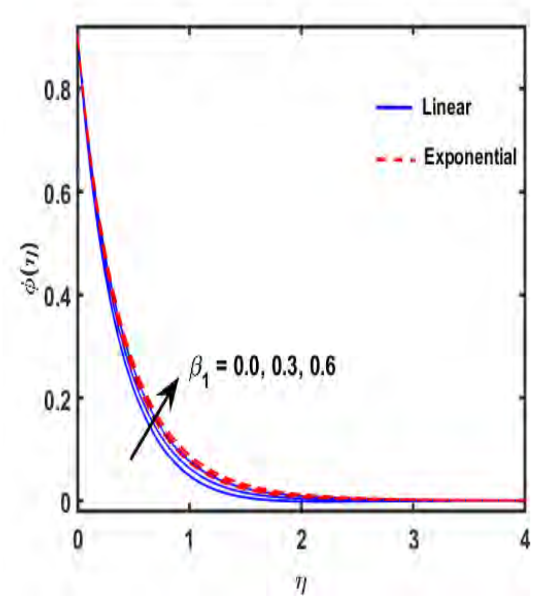

Fig. 8.12: Graph of β_1 for $\phi(\eta)$.

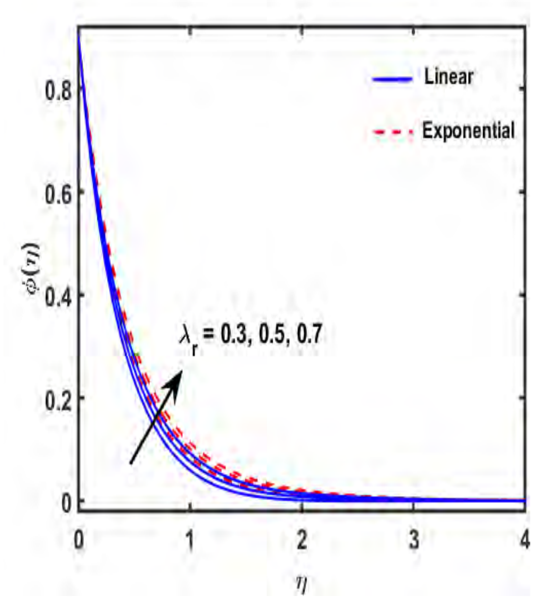

Fig. 8.13: Graph of λ_r for $\phi(\eta)$.

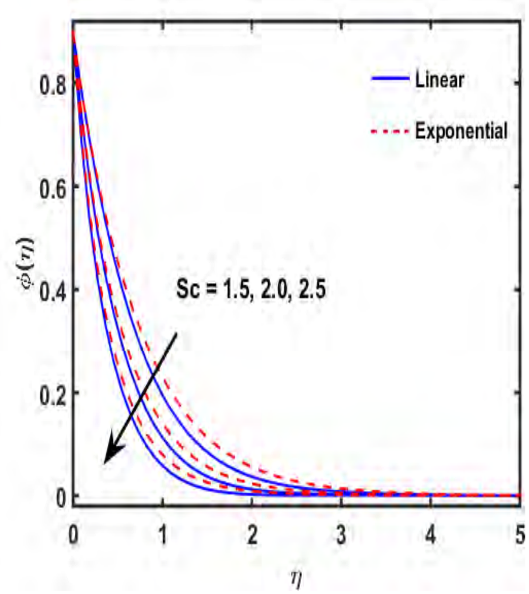

Fig. 8.14: Graph of Sc for $\phi(\eta)$.

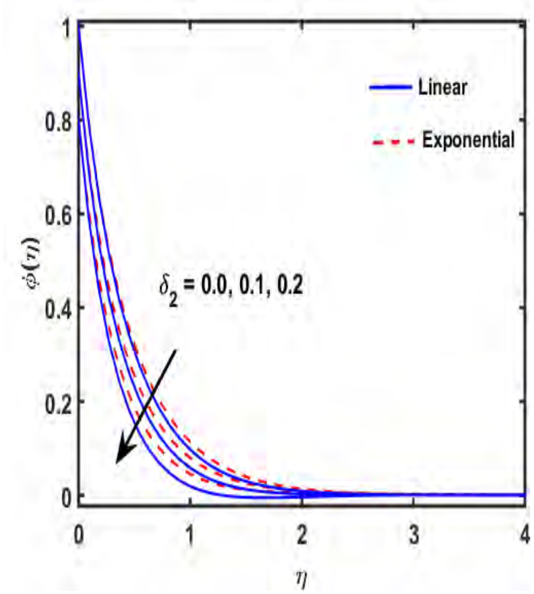

Fig. 8.15: Graph of δ_2 for $\phi(\eta)$.

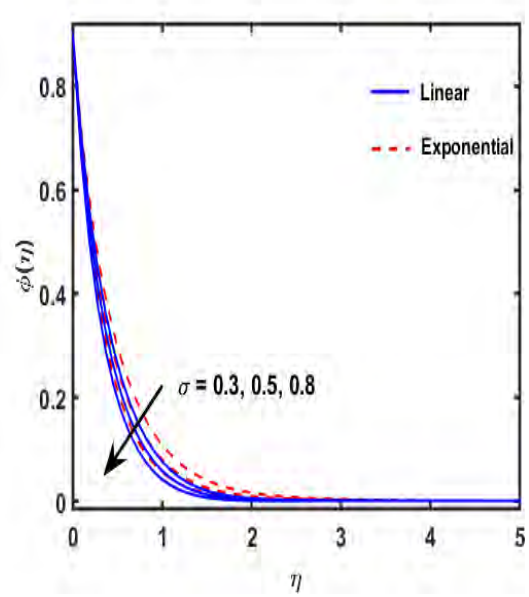

Fig. 8.16: Graph of σ for $\phi(\eta)$.

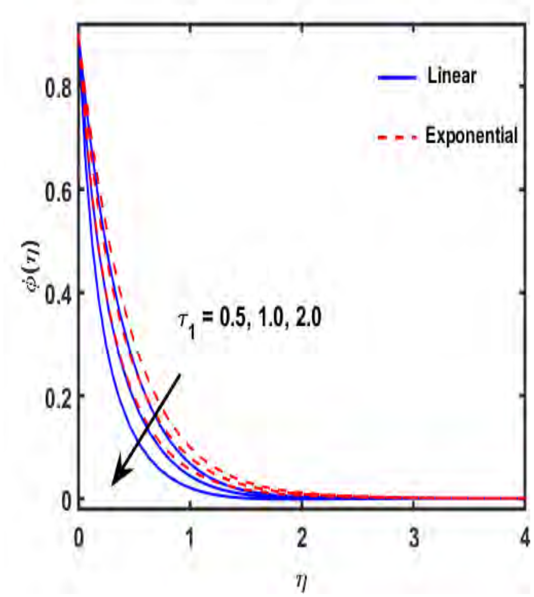

Fig. 8.17: Graph of τ_1 for $\phi(\eta)$.

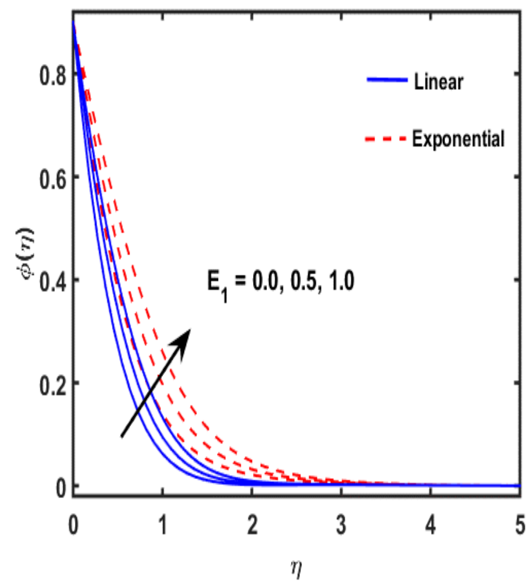

Fig. 8.18: Graph of E_1 for $\phi(\eta)$.

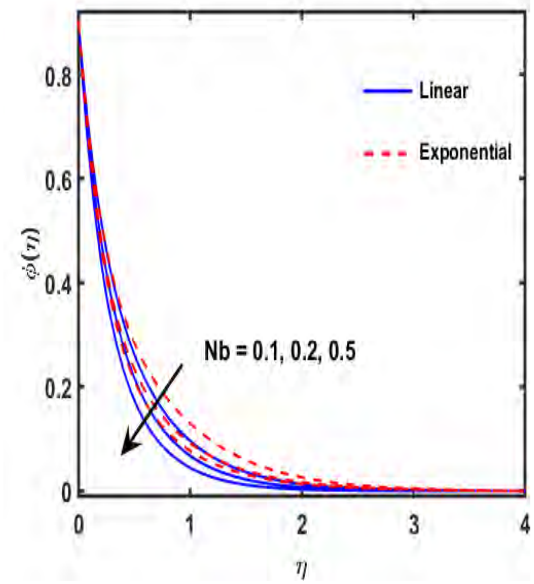

Fig. 8.19: Graph of Nb for $\phi(\eta)$.

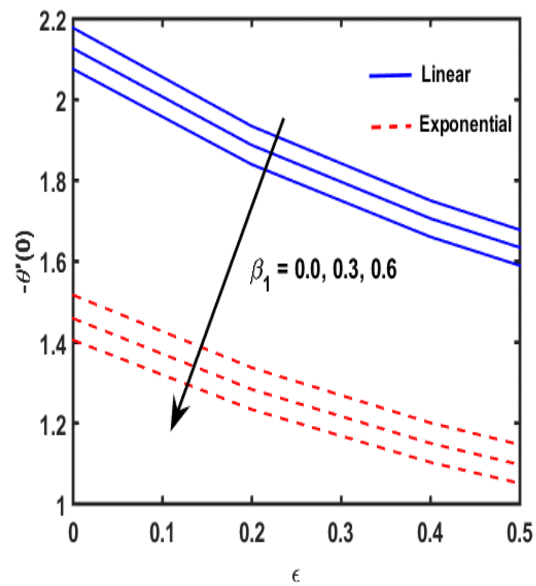

Fig. 8.20: Sketch $-\theta'(0)$ between β_1 and ε.

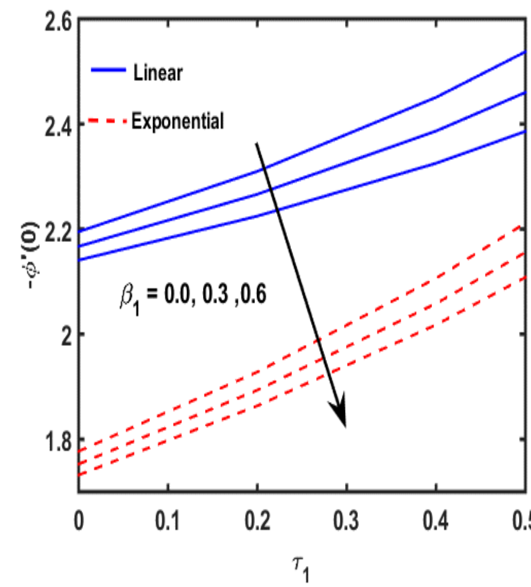

Fig. 8.21: Sketch $-\theta'(0)$ between β_1 and τ_1.

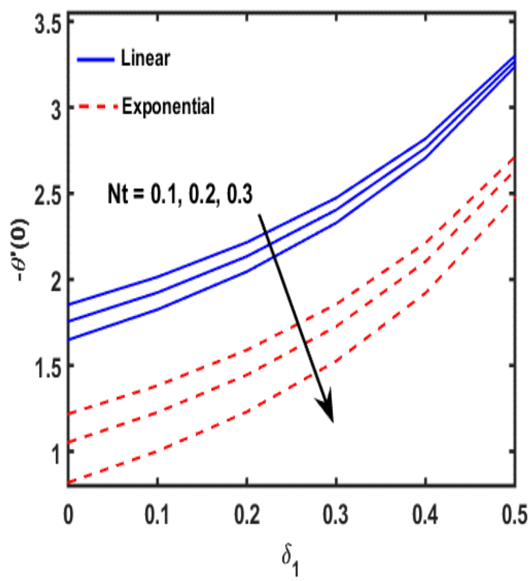

Fig. 8.22: Sketch $-\theta'(0)$ between Nt and δ_1.

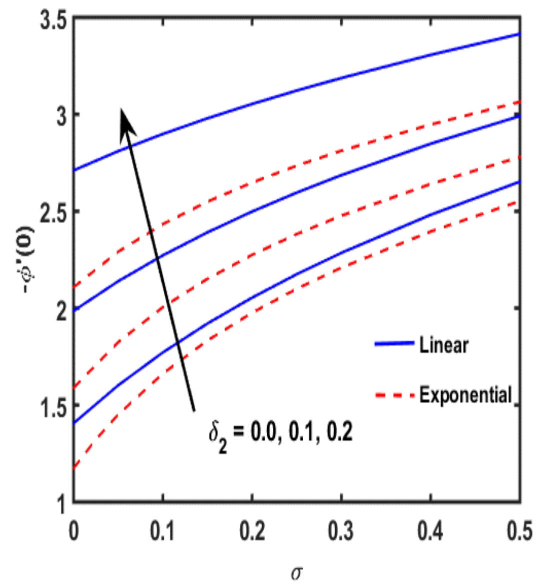

Fig. 8.23: Sketch $-\theta'(0)$ between S_2 and σ.

8.3. Concluding Remarks

Here, we described the rotating Maxwell nanofluid flow induced by an exponential and linear stretching sheet. The stratification conditions are implemented on the boundary of sheet. The non-dimensionalized mathematical model is solved by bvp4c Matlab technique. The key results of the chapter are highlighted as:

- The fluid velocity is reduced due to the enhancement of rotation and relaxation parameter.
- The temperature and related boundary layer thickness enhances by the enhancement of β_1 and λ_r.
- The boundary layer thickness and temperature is enhanced due to higher value of Nt.
- By higher values of τ_1, the concentration and related boundary layer thickness diminishes.
- Weaker concentration is noted for higher estimation of σ and δ_2.

Chapter 09

Transient flow of Maxwell Nanofluid Over a Shrinking Surface: Numerical Solutions and Stability Analysis

This chapter explored the theoretical analysis of heat and mass transfer of Maxwell nanofluid across a permeable shrinking surface with thermal radiation. The thermal and concentration configuration involves the heat absorption / generation and chemical reaction in the flow regime. This physical configuration is transformed into terms of non-dimensional differential system. A numerical investigation of the governing equations is carried out with Bvp4c Matlab technique. Further, it has been found that shrinking and suction at porous surface leads to multiple solutions of the system. The results in terms of line graphs portray that the stronger suction at shrinking surface possess higher heat and mass transfer rate at the surface. The heat transfer rate enhances by the larger values of Biot number. Further, the velocity, temperature and mass distribution indicate maximum values at stronger relaxation parameter.

9.1. Mathematical Formulation

The investigation of an unsteady, laminar, 2D, stagnation point flow of radiative Maxwell nanofluid through a shrinking sheet with chemical reaction is discussed. The convective boundary condition is also taken into the account at the sheet. Further, the analysis of heat transfer made with the effect of heat generation / absorption. **Fig. (9.1)** displays the geometry of the fluid. The stretching and free stream velocities are $u_w = \frac{ax}{(1-\alpha_0 t)}$ and $u_e = \frac{cx}{(1-\alpha_0 t)}$ respectively. The fluid concentration and temperature are taken C and T respectively, but the wall concentration and temperature are C_w and T_w respectively and away from the wall it denotes by C_∞ and T_∞ respectively. By using the velocity field $\mathbf{V} = [u(x,y,t), v(x,y,t), 0]$ and above supposition the governing equations of mass, momentum, energy, and concentration follows as,

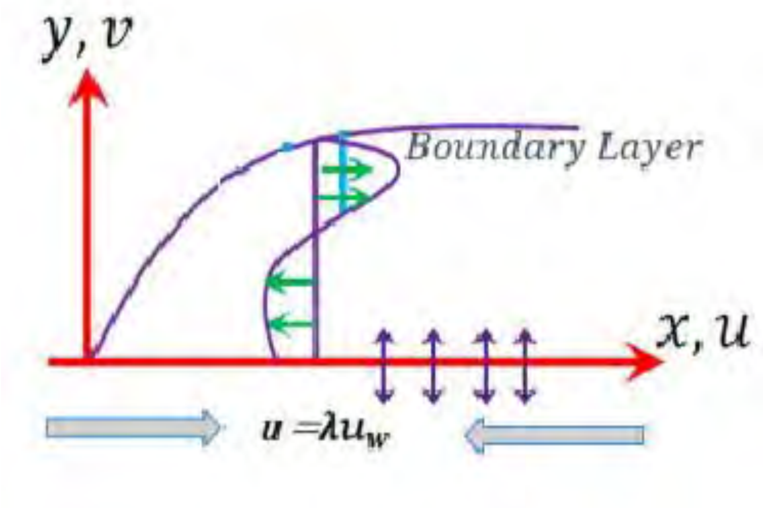

Fig. 9.1: Flow geometry of the problem.

$$\frac{\partial u}{\partial x} + \frac{\partial v}{\partial y} = 0, \tag{9.1}$$

$$\frac{\partial u}{\partial t} + u\frac{\partial u}{\partial x} + v\frac{\partial u}{\partial y} + \lambda_1\begin{pmatrix} u^2\frac{\partial^2 u}{\partial x^2} + v^2\frac{\partial^2 u}{\partial y^2} + 2uv\frac{\partial^2 u}{\partial x\,\partial y} \\ +\frac{\partial^2 u}{\partial t^2} + 2u\frac{\partial^2 u}{\partial x\,\partial t} + 2v\frac{\partial u}{\partial y\,\partial t} \end{pmatrix} = \nu\frac{\partial^2 u}{\partial y^2} + u_e\frac{\partial u_e}{\partial x} + \frac{\partial u_e}{\partial t}, \tag{9.2}$$

$$\frac{\partial T}{\partial t} + u\frac{\partial T}{\partial x} + v\frac{\partial T}{\partial y} = \alpha\frac{\partial^2 T}{\partial y^2} + \tau\left(\frac{D_T}{T_\infty}\left(\frac{\partial T}{\partial y}\right)^2 + D_B\frac{\partial T}{\partial y}\frac{\partial C}{\partial y}\right) - \frac{1}{\rho c_p}\frac{\partial q_r}{\partial y} + \frac{Q_0}{\rho c_p}(T - T_\infty), \tag{9.3}$$

$$\frac{\partial C}{\partial t} + u\frac{\partial C}{\partial x} + v\frac{\partial C}{\partial y} + D_B\frac{\partial^2 C}{\partial y^2} + \frac{D_T}{T_\infty}\frac{\partial^2 T}{\partial y^2} - k_1(C - C_\infty), \tag{9.4}$$

By Rosseland approximation [111], the radiative heat flux is stated as,

$$q_r = \frac{4\sigma^*}{3\kappa^*}\frac{\partial T^4}{\partial y}. \tag{9.5}$$

In above equation the Stefan–Boltzmann constant is σ^*. We expand T^4 by using Taylor's series around T_∞ and ignoring higher order terms as,

$$T^4 \approx 4T_\infty^3 T - 3T_\infty^4. \tag{9.6}$$

Hence, we get,

$$\frac{\partial q_r}{\partial y} = -\frac{16\sigma^*}{3\kappa^*}\frac{\partial T^2}{\partial y^2}. \tag{9.7}$$

So, the above equation (9.3) is written as,

$$\frac{\partial T}{\partial t} + u\frac{\partial T}{\partial x} + v\frac{\partial T}{\partial y} = \alpha\left(1 + \frac{16\sigma^*}{3kk^*}T_\infty^3\right)\frac{\partial^2 T}{\partial y^2} + \tau\left(\frac{D_T}{T_\infty}\left(\frac{\partial T}{\partial y}\right)^2 + D_B\frac{\partial T}{\partial y}\frac{\partial C}{\partial y}\right) + \frac{Q_0}{\rho c_p}\left(T - T_\infty\right), \tag{9.8}$$

The related boundary conditions are,

$$\begin{gathered} u = \lambda u_w,\ v = \frac{-v_0}{(1-\alpha_0 t)},\ h_w(T - T_w) = k\left(\frac{\partial T}{\partial y}\right),\ C = C_w, \text{ as } y \to 0, \\ u = u_e, T \to T_\infty, C \to C_\infty, \text{ as } y \to \infty. \end{gathered} \tag{9.9}$$

In the above equations the velocity components are u and v in $x-$ and $y-$directions, respectively. The wall velocity is $\left(u_w = \frac{ax}{(1-\alpha_0 t)}\right)$, wall temperature is $\left(T_w = T_\infty + \frac{T_0 x^2}{(1-\alpha_0 t)^2}\right)$, and wall concentration is $\left(C_w = C_\infty + \frac{C_0 x^2}{(1-\alpha_0 t)^2}\right)$.

The similarity transformation is defined as,

$$\psi = \sqrt{\frac{\nu c}{(1-\alpha_0 t)}}\, x f(\eta),\ \ \eta = y\sqrt{\frac{c}{\nu(1-\alpha_0 t)}},$$
$$T = T_\infty + \frac{T_0 x^2}{(1-\alpha_0 t)^2}\theta(\eta),\ \ C = C_\infty + \frac{C_0 x^2}{(1-\alpha_0 t)^2}\phi(\eta). \tag{9.10}$$

Equation of continuity is satisfied automatically by using (9.10), while other equations becomes,

$$f''' - \begin{pmatrix} f'^2 - ff'' \\ +A\left(\frac{\eta}{2}f'' + f'\right) \end{pmatrix} - \beta_1 \begin{pmatrix} A^2\left(2f' + \frac{7\eta}{2}f'' + \frac{\eta^2}{4}f'''\right) \\ +A(f'^2 - 3ff'') - 2ff'f'' \\ +A\eta(f'f'' - ff''') + f^2 f''' \end{pmatrix} + 1 + A = 0, \tag{9.11}$$

$$(1 + Rd)\theta'' + Pr\left[(f\theta' - 2f'\theta) - A\left(2\theta + \frac{\eta}{2}\theta'\right) + (Nb\theta'\phi' + Nt\theta'^2) + Q\theta\right] = 0, \tag{9.12}$$

$$\phi'' + Sc(f\phi' - 2f'\phi) - ScA(2\phi + \frac{\eta}{2}\phi') + Sc\sigma\phi + \frac{Nt}{Nb}\theta'' = 0, \tag{9.13}$$

The concerned boundary conditions take the form,

$$f'(\eta) = \lambda,\ f(\eta) = s,\ \theta'(\eta) = \gamma^*(\theta(\eta) - 1), \phi(\eta) = 1, \text{ as } \eta \to 0,$$
$$f'(\eta) \to 1,\ \theta(\eta) = 0 = \ \phi(\eta), \text{ as } \eta \to \infty. \tag{9.14}$$

Here prime indicates the derivative with respect to η. Whereas the symbols λ,, A, β_1, Rd, s, and σ represents the shrinking parameter, unsteadiness parameter, relaxation parameter, radiation parameter, suction ($s > 0$) / injection ($s < 0$) parameter, and chemical reaction parameter respectively. Further, Sc, Pr and γ^*, characterizes the Schmidt number, Prandtl number and Biot number, respectively.

These parameters are defined mathematically as,

$$A=\frac{\alpha_0}{a},\beta=\lambda_0 c,Nb=\frac{\tau D_B\Delta C}{\nu},Nt=\frac{\tau D_T\Delta T}{\nu T_\infty},Sc=\frac{\nu}{D_B},\Pr=\frac{\upsilon}{\alpha},$$
$$\sigma=\frac{k_0}{a},\ Rd=\frac{16k\kappa^*}{4\sigma^* T_\infty^3},s=\frac{\upsilon_0}{\sqrt{\upsilon c}},\gamma^*=\frac{h_w^*}{k}\sqrt{\frac{\nu}{a}},Q=\frac{Q_1}{\rho c_p c}. \tag{9.15}$$

Additionally, we have taken $\lambda_1=\lambda_0(1-\alpha_0 t)$, $k_1=\frac{k_0}{(1-\alpha_0 t)}$, $Q_0=\frac{Q_1}{(1-\alpha_0 t)}$, and $h_w=h_w^*\sqrt{(1-\alpha_0 t)}$ as an initial relaxation time, reaction rate constant, heat generation or absorption and heat transfer coefficient.

9.1.1. Physical Quantities

The Nusselt and Sherwood numbers are substantial physical quantities from engineering sight. They exposed the rate of heat and mass transfer. These are stated as,

$$Nu_x=\frac{xq_m}{k(T_w-T_\infty)},Sh_x=\frac{xj_m}{D_B(C_w-C_\infty)}. \tag{9.16}$$

In above k is thermal conductivity. Also q_m and j_m are the heat flux and mass flux respectively. They are specified by,

$$q_m=\left|-k\frac{\partial T}{\partial y}-\frac{4\sigma_1^*}{3\kappa^*}\frac{\partial T^4}{\partial y}\right|_{y=0},\ j_m=-D_B\frac{\partial C}{\partial y}\bigg|_{y=0}. \tag{9.17}$$

The dimensionless form is,

$$\begin{pmatrix} Re_x^{-\frac{1}{2}}Nu_x=-(1+Rd)\theta'(0), \\ Re_x^{-\frac{1}{2}}Sh_x=-\phi'(0). \end{pmatrix}. \tag{9.18}$$

Here Re_x is the local Reynolds number.

9.1.2. Stability Analysis

From the numerical outcomes, we examined that for a various value of penetrating parameters, there exists a dual solution. In order to assess that when these two solutions are physically reliable, we test the stability analysis of the above equations (9.11-9.13). We introduced new dimensionless variable $\tau^* = \alpha_0 t$. The use of τ^* allied to the initial value problem and dependable of the question that which solution will be physically reliable. To do this we introduced following similarity variable,

$$\psi = \sqrt{\frac{\nu a}{(1-\tau)}}\, x f(\eta,\tau^*),\ \ \eta = y\sqrt{\frac{a}{\nu(1-\tau)}}\,,\ \tau^* = \alpha_0 t,$$
$$T = T_\infty + \frac{T_0 x^2}{(1-\tau^*)^2}\theta(\eta,\tau^*), \qquad C = C_\infty + \frac{C_0 x^2}{(1-\tau^*)^2}\phi(\eta,\tau^*). \tag{9.19}$$

Using equation (9.19), the Eqs. (9.11-9.13) with boundary condition can be written as,

$$\frac{\partial^3 f}{\partial \eta^3} + \begin{pmatrix} f\frac{\partial^2 f}{\partial \eta^2} - \left(\frac{\partial f}{\partial \eta}\right)^2 + A + 1 \\ -A\left(\frac{\partial f}{\partial \eta} + (1-\tau^*)\frac{\partial^2 f}{\partial \eta\, \partial \tau^*}\right) \end{pmatrix} = \beta_1 \begin{pmatrix} A^2\left(2\frac{\partial f}{\partial \eta} + 2(1-\tau^*)\frac{\partial^2 f}{\partial \eta\, \partial \tau^*} + (1-\tau^*)^2\frac{\partial^3 f}{\partial \eta\, \partial \tau^{*2}}\right) \\ +A\left(\left(\frac{\partial f}{\partial \eta}\right)^2 - (1-\tau^*)\frac{\partial f}{\partial \eta}\frac{\partial^2 f}{\partial \eta\, \partial \tau^*} - (1-\tau^*)\frac{\partial^3 f}{\partial \eta^2\, \partial \tau^*}\right) \\ -Af\frac{\partial^2 f}{\partial \eta^2} + f^2\frac{\partial^3 f}{\partial \eta^3} - 2f\frac{\partial f}{\partial \eta}\frac{\partial^2 f}{\partial \eta^2} \end{pmatrix}, \tag{9.20}$$

$$\frac{1}{Pr}(1+Rd)\frac{\partial^2 \theta}{\partial \eta^2} - 2\theta\frac{\partial f}{\partial \eta} + f\frac{\partial \theta}{\partial \eta} + Q\theta = A\left(2\theta - (1-\tau^*)\frac{\partial \theta}{\partial \tau^*}\right) + Nb\frac{\partial \theta}{\partial \eta}\frac{\partial \phi}{\partial \eta} + Nt\left(\frac{\partial \theta}{\partial \eta}\right)^2, \tag{9.21}$$

$$\frac{1}{Sc}\frac{\partial^2 \phi}{\partial \eta^2} - 2\phi\frac{\partial f}{\partial \eta} + f\frac{\partial \phi}{\partial \eta} + \sigma\phi = A\left(2\phi - (1-\tau^*)\frac{\partial \phi}{\partial \tau^*}\right) + \frac{Nt}{NbSc}\frac{\partial^2 \theta}{\partial \eta^2}. \tag{9.22}$$

With concerned boundary condition

$$f(\eta,\tau^*) = 0, \frac{\partial f}{\partial \eta}(\eta,\tau^*) = \lambda, \frac{\partial \theta}{\partial \eta}(\eta,\ \tau^*) = -\gamma^*\big(1-\theta(\eta,\tau^*)\big),\ \phi(\eta,\tau^*) = 1, \text{ as } \eta \to 0,$$
$$\frac{\partial f}{\partial \eta}(\eta,\tau^*) \to 1, \theta(\eta,\tau^*) \to 0, \phi(\eta,\tau^*) \to 0. \text{ as } \eta \to \infty. \tag{9.23}$$

The stability test for the steady flow of the solution in the form $f(\eta) = f_0(\eta), \theta(\eta) = \theta_0(\eta)$, and $\phi(\eta) = \phi_0(\eta)$, we have written [112] as,

$$f(\eta,\tau^*) = f_0(\eta) + F(\eta,\tau^*)Exp(-\gamma\tau^*),$$

$$\theta(\eta,\tau^*) = \theta_0(\eta) + G(\eta,\tau^*)Exp(-\gamma\tau^*), \tag{9.24}$$

$$\phi(\eta,\tau^*) = \phi_0(\eta) + H(\eta,\tau^*).Exp(-\gamma\tau^*)$$

Here γ is the rate of growth or decay of disturbance. As compared to steady state solution the $f_0(\eta)$, $\theta_0(\eta)$, and $\phi_0(\eta)$ are assumed to be small with respect to $F(\eta,\tau^*)$, $G(\eta,\tau^*)$, and $H(\eta,\tau^*)$ respectively. To study the linear stability of the flow problem such assumptions are made.

Hence, by linearizing, we get,

$$\frac{\partial^3 F}{\partial\eta^3} + \begin{pmatrix} f_0\frac{\partial^2 F}{\partial\eta^2} - 2f_0{}'\frac{\partial F}{\partial\eta} - f_0''F \\ -A\left(\frac{\partial F}{\partial\eta} + (1-\tau^*)\left\{\frac{\partial^2 F}{\partial\eta\,\partial\tau^*} - \gamma\frac{\partial F}{\partial\eta}\right\}\right) \end{pmatrix}$$

$$-\beta_1\left(\begin{array}{c} A^2\begin{pmatrix} 2\frac{\partial F}{\partial\eta} + (1-\tau^*)^2\left\{\frac{\partial^3 F}{\partial\eta\,\partial\tau^{*2}} - 2\gamma\frac{\partial^2 F}{\partial\eta\,\partial\tau^*} - \gamma\frac{\partial F}{\partial\eta} + \gamma^2\frac{\partial^2 F}{\partial\eta\,\partial\tau^*}\right\} \\ +2(1-\tau^*)\left\{\frac{\partial^2 F}{\partial\eta\,\partial\tau^*} - \gamma\frac{\partial F}{\partial\eta}\right\} \end{pmatrix} \\ +A\begin{pmatrix} 2f_0'\frac{\partial F}{\partial\eta} - (1-\tau^*)\left\{f_0\frac{\partial^2 F}{\partial\eta\,\partial\tau^*} - \gamma f_0\frac{\partial F}{\partial\eta}\right\} - (1-\tau^*)\left\{f_0\frac{\partial^3 F}{\partial\eta^2\,\partial\tau^*} - \gamma f_0\frac{\partial^2 F}{\partial\eta^2}\right\} \\ -f_0\frac{\partial^2 F}{\partial\eta^2} - f_0''F \end{pmatrix} \\ +f_0^2\frac{\partial^3 F}{\partial\eta^3} - 2f_0f_0'\frac{\partial^2 F}{\partial\eta^2} - 2f_0f_0''\frac{\partial F}{\partial\eta} + 2(f_0f_0''' - f_0f_0'')F \end{array}\right), \tag{9.25}$$

$$\frac{1}{Pr}(1+Rd)\frac{\partial^2 G}{\partial\eta^2} + \begin{pmatrix} 2Nt\theta_0'\frac{\partial G}{\partial\eta} - 2f_0'G - 2\theta_0\frac{\partial F}{\partial\eta} \\ +f_0\frac{\partial G}{\partial\eta} + F\theta_0' + \delta G \end{pmatrix} - A\left(2G - (1-\tau^*)\left\{\frac{\partial G}{\partial\tau^*} - \gamma G\right\}\right)$$
$$+Nb\left\{\theta_0'\frac{\partial H}{\partial\eta} + \theta_0'\frac{\partial G}{\partial\eta}\right\}, \tag{9.26}$$

$$\frac{1}{Sc}\frac{\partial^2 H}{\partial\eta^2} + \begin{pmatrix} \frac{Nt}{NbSc}\frac{\partial^2 G}{\partial\eta^2} - 2f_0'H - 2\phi_0\frac{\partial F}{\partial\eta} \\ +f_0\frac{\partial H}{\partial\eta} + F\phi_0' + \sigma H \end{pmatrix} - A\left(2H - (1-\tau^*)\left\{\frac{\partial H}{\partial\tau^*} - \gamma H\right\}\right). \tag{9.27}$$

We want to explore the stability analysis of the steady state solution by putting $\tau^* = 0$. Hence, $F(\eta) = F_0(\eta), G(\eta) = G_0(\eta)$, and $H(\eta) = H_0(\eta)$ in the above equations classify the initial growth or decay of the solution, in this respect we have to solve the linear eigenvalue of the problem,

$$\begin{pmatrix} (1-\beta_1 f_0'^2)F_0''' + \{f_0 + \beta_1 A f_0(1-\gamma) + 2\beta_1 f_0 f_0'\}F_0'' \\ +\left(2\beta_1 f_0 f_0'' - \beta_1 A^2 f_0(1-\gamma)\right)F_0' - \left(2f_0' + A(1-\gamma) + \beta_1 A(2f_0' - \gamma f_0)\right)F_0' \\ +(f_0'' + \beta_1 A f_0'' + 2\beta A f_0' f_0'' - 2\beta A f_0 f_0''')F_0 \end{pmatrix} = 0, \tag{9.28}$$

$$\begin{pmatrix} \frac{1}{Pr}(1+Rd)G_0'' + (f_0 + Nb\phi_0' + 2Nt\theta_0')G_0' + (Q - A(2-\gamma) - 2f_0')G_0 \\ -2F_0'\theta_0 + F_0\theta_0' + Nb\phi_0' H_0' \end{pmatrix} = 0, \tag{9.29}$$

$$\frac{1}{Sc}H_0'' + f_0 H_0' + (\sigma - A(2-\gamma) - f_0)H_0 - 2F_0'\phi_0 + F_0\phi_0' + \frac{Nt}{Nb}G_0'' = 0. \tag{9.30}$$

The concerned boundary conditions are,

$$\begin{gathered} F_0(\eta) = 0, F_0'(\eta) = 0, G_0'(\eta) = \gamma^* G_0(\eta), H_0(\eta) = 0 \text{ as } \eta \to 0, \\ F_0'(\eta) = 0 = G_0(\eta), H_0(\eta) = 0 \text{ as } \eta \to \infty, \end{gathered} \tag{9.31}$$

It should be noted in the above homogenous equations with the homogeneous boundary conditions found an eigenvalue γ. The solution of above equations gives infinite eigenvalues such that $(\gamma_1 < \gamma_2 < \gamma_3 \ldots \ldots.)$. If the lowest eigenvalue is positive, the disturbance is decaying and the solution becomes stable, but when the lowest value is negative, then the disturbance is growing, and the solution is unstable.

9.1.3. Numerical Method

The solution of Eqs. (9.11-9.13) with Eq. (9.14) is constructed via bvp4c Matlab technique. The Bvp4c function solves the first order system of differential equations. For this purpose, we must transform Eqs. (9.11-9.14) into the system of 1^{st} order differential equations. The interval of convergence takes between 0 to 6, with $\eta_\infty = 6$.

$$\begin{pmatrix} f = y(1), f' = y(2), f'' = y(3), \theta = y(4), \\ \theta' = y(5), \phi = y(6), \phi' = y(7). \end{pmatrix}, \tag{9.32}$$

$$yy_1 = \left(\frac{1}{1-\beta_1 A^2\frac{\eta^2}{4}+\beta_1 A\eta y(1)-\beta_1 y(1)^2}\right)\begin{pmatrix} y(2)^2 - y(1)y(3) + A\left(y(2)+\frac{\eta}{2}y(3)\right) - A \\ +\beta_1 A^2\left(2y(2)+\frac{7\eta}{4}y(3)\right) - 2\beta_1 y(1)y(2)y(3) \\ +\beta_1 A\left(2y(2)^2 - 3y(1)y(3) + \eta y(2)y(3)\right) - 1 \end{pmatrix}, \tag{9.33}$$

$$yy_2 = \frac{Pr}{1+Rd}\begin{pmatrix} A\left\{2y(4)+\frac{\eta}{2}y(5)\right\} + 2y(2)y(4) - y(1)y(5) \\ -Nby(5)y(7) - Nty(5)^2 - Qy(4) \end{pmatrix}, \tag{9.34}$$

$$yy_3 = Sc\left(A\left\{2y(6)+\frac{\eta}{2}y(7)\right\} + y(2)y(6) - y(1)y(7) + \sigma y(6)\right) - \frac{Nt}{Nb}yy_2, \tag{9.35}$$

The suitable boundary conditions in 1^{st} order are,

$$\begin{pmatrix} y_0(1) = \mathrm{S}, y_0(2) = \lambda, y_0(5) + \gamma^*\left(1 - y_0(5)\right) = 0, \;\; y_0(6) = 1, \\ y_{\mathrm{Inf}}(2) = 1, y_{\mathrm{Inf}}(4) = 0 = y_{\mathrm{Inf}}(6). \end{pmatrix}. \tag{9.36}$$

9.2. Results and Discussion

In this section, we analyzed the multiple solutions of an unsteady two-dimensional radiative Maxwell nanofluid through a shrinking sheet with the convective boundary condition. The physical model in terms of differential system is solved numerically by using bvp4c function in Matlab. Physical behavior of the controlling parameters such as unsteadiness (A), relaxation (β_1), suction / injection (s), thermophoresis (Nt), Brownian motion (Nb), heat generation / absorption (Q), radiation (Rd), chemical reaction (σ), shrinking (λ), Schmidt number (Sc), Biot number (γ^*), and Prandtl number (Pr) across the velocity, temperature, and concentration distribution is presented. Moreover, the heat and mass transfer rate are also presented in the **Figs. (9.2-9.7)**. We have to observe the dual nature solution for shrinking case of the system of equations (9.11-9.13) with boundary condition (9.14). From the figures, it is cleared that the far field boundary conditions are satisfied asymptotically. In view of this, the applied numerical technique is valid and ensure that the existence of dual solutions given in **Figs (9.2-9.7)**. Form stability analysis and physical argumentation of the involved parameters we expect that the first solutions are reliable. Although, the second solution is physically unstable, but it cannot be neglected. It is noted that both the solution come to an end at certain values of shrinking parameter (λ), which is known as critical value ($\lambda_c = \lambda < 0$). From **Figs (9.2-9.7)**, it is noticed that there are two solutions when ($\lambda_c < \lambda$) and no solution for ($\lambda < \lambda_c$).

The diversion in Nusselt number and Sherwood number against different physical parameter are analyzed in the **Figs**. **(9.2)** and **(9.3)**. The impact of β_1 on Nu_x and Sh_x is illustrated in **Figs. 9.2(a** and **b). Fig. 9.2(a)** depicts that up to critical values ($\lambda_c = -1.610, -1.610, -1.62$), there are two solutions of the heat transfer rate, and both the solutions diminishes for increasing β_1. Similarly, for the mass transfer rate two solutions are found when $\lambda > \lambda_c (= -1.5454, -1.5433, -1.5412)$ in **Fig. 9.2(b)**. It is observed that rising the values of β_1, Sh_x revealed opposite behavior for both solutions, i.e., the upper branch solution enhances and lower branch solution declines. **Figs. 9.2(c** and **d)** deliberates the variation of Nu_x and Sh_x for several values of A. It is noticed that as we increase A, the upper branch solution for both Nusselt and Sherwood number possess rising behavior, while the lower branch solutions of Nu_x and Sh_x depicts lower trend for increasing A. Further mentioning that beyond the critical values $\lambda_c (= -1.596, -1.623)$ there is no solution for Nusselt number. Similarly, up to critical values $\lambda_c (= -1.5413, -1.5566, -1.572)$ two solution exists for Sherwood number. The solutions are unique when $\lambda = \lambda_c$. The variation of Nusselt and Sherwood number is considered in **Figs. 9.3(a and b)** for various values of s against λ. There are two solutions exist within the range $\lambda > \lambda_c$, one solution exists when $\lambda = \lambda_c$, and no solution exists when $\lambda < \lambda_c$ for both Nu_x and Sh_x. **Fig. 9.3(a)** shows that $\lambda_c (= -1.757, -1.614, -1.485)$ are the critical values up to which the solutions of Nu_x exist. Whereas **Fig. 9.3(b)** depicts the existence of solutions for Sh_x with critical values are found as $\lambda_c(= -1.5413, -1.5566, -1.5720)$. It is important to note that suction parameter maintains steady boundary layer near the surface, thus, stronger suction effect possesses maximum heat and mass transfer. This effect is true for both Nu_x and Sh_x in the upper branch solution, whereas inverse trends is observed in the second solution of both Nu_x and Sh_x. The variations in the Nu_x and Sh_x. against λ and various of Q and σ is illustrated in **Figs. 9.3(c** and **d)**. It is verified in **Fig. 9.3(c)** that for the several values of Q, the Nu_x plot showing a decaying trend for the lower branch solution, whereas the upper branch solution is enhanced. Further, the increment occurs in an upper solution branch of Sh_x for various values of σ, whereas it declines in lower solution branch as shown in **Fig. 9.3(d)**. **Fig. 9.3(e)** displays the variation in Nu_x plot for distinct values of γ^* with the critical values ($\lambda_c = -1.5415, -1.5415, -1.5414$). It is mentioned that for the greater values of the γ^*, the Nu_x plot boost up for both upper and lower branch solutions. The influence of β_1 on the velocity distribution is exposed in **Fig. 9.4(a).** There are two solutions of $f'(\eta)$ for the shrinking case for various values of β_1. It is cleared from the fig that velocity curve shows increment for the first solution and lowering behavior for the second solution. From Physical point of view, momentum boundary layer thickness reduces for greater values of β_1. Moreover, β_1 resist the fluid motion, hence the velocity profile decline. Here the first solution is considered as a physically reliable. The velocity variation for several estimation of A are shown in **Fig. 9.4(b)**. It is exhibited that the magnitude of the velocity is enhancing for the first solution, but it is declining for the second solution by increasing A, which defend that the first solution is physically reliable as compared to the second solution. Further, the second solution having a thicker boundary layer associated to the first solution. **Fig. 9.4(c)** depicts the dual solutions of $f'(\eta)$ for various estimations of s. It is observed that for larger s the velocity profile gives maximum values for the upper solution branch and lower values for the second solution. Physically, it is examined that, with the higher estimation of s the velocity dispersion in the fluid become shorter for the first solution, whereas the velocity penetrates deeper for the second solution. The influence of Q and γ^* on the thermal distribution is illustrated in **Figs. 9.5(a** and **b).** We have obtained two solutions of temperature distribution for the shrinking case. The $\theta(\eta)$ plot gives lower values against various values of Q for both upper and lower solution branches, which is shown in **Fig. 9.5(a).** The increasing nature of thermal distribution for higher values of γ^* is illustrated in **Fig. 9.5(b)**. It portrays that sketch of $\theta(\eta)$ has maximum values for the upper and lower branch solution. Physically, γ^* is directly proportional to the heat transport coefficient and inversely proportional to the thermal resistance. Thus, its increment leads to an enhancement in thermal distribution, which is evident in **Fig.9.5(b)**. The influence of β_1 on the $\theta(\eta)$ and $\phi(\eta)$ plots is demonstrated in the **Figs. 9.6(a-d)**. It is observed that higher relaxation parameter possesses stronger thermal boundary layer thickness. Thus, thermal distribution enhances for various values of β_1. Further, both the solutions of $\theta(\eta)$ gives higher values for maximum β_1, which is depicted in **Fig. 9.6(a).** The mass concentration gradient also depicts the increasing behavior against β_1 shown in **Fig. 9.6(b)**. It is noted that first solution of $\phi(\eta)$ reduces for different values of β_1, whereas second solution depicts opposite behavior. **Figs. 9.6 (c** and **d)** portrays the line graphs of $\theta(\eta)$ and $\phi(\eta)$ for the several values of the A. The thermal distribution gives two solutions, the first solution is an increasing nature for various values of A, whereas the second solution is a decreasing function of unsteadiness parameter as revealed in **Fig. 9.6(c)**. **Fig. 9.6(d)** portrays the dual nature solution of $\phi(\eta)$ plot for several values of A. It is examined that the upper solution branch of $\phi(\eta)$ declines at maximum A, while the lower solution branch gives slightly growing behavior for the higher values of A. **Figs. 9.7(a-f)** exhibits the variation in the plot of $\theta(\eta)$ and $\phi(\eta)$ against several parameters. It is observed that the thermal distribution possesses decreasing nature in both solution branches for stronger suction effect. While for the mass concentration this effect reports lower values for first solution and higher values for the second solution, which is illustrated in **Figs. 9.7(a** and **b).** The influence of chemical reaction effect on $\theta(\eta)$ and $\phi(\eta)$ plot is considered in **Figs. 9.7(c** and **d).** We have examined two solutions in each case, and it signifies the enhancement in temperature distribution occurs, whereas mass distribution tends to decrease as chemical reaction effect gets stronger. The **Fig. 9.7(e)** inspects the variation in $\theta(\eta)$ distribution in-terms of two solutions upper and lower branch against different values of Rd. It is noticed that both solutions possess maximum $\theta(\eta)$, as stronger radiation implies a thicker thermal boundary layer and higher temperature of fluid. The impact of Sc on the $\phi(\eta)$ plot is considered in **Fig. 9.7(f)**. It is noted that both the solutions decrease for higher values of Sc. Physically, Sc is the ratio between thermal to mass diffusivity. Therefore, concentration distribution and related boundary layer thickness reduce.

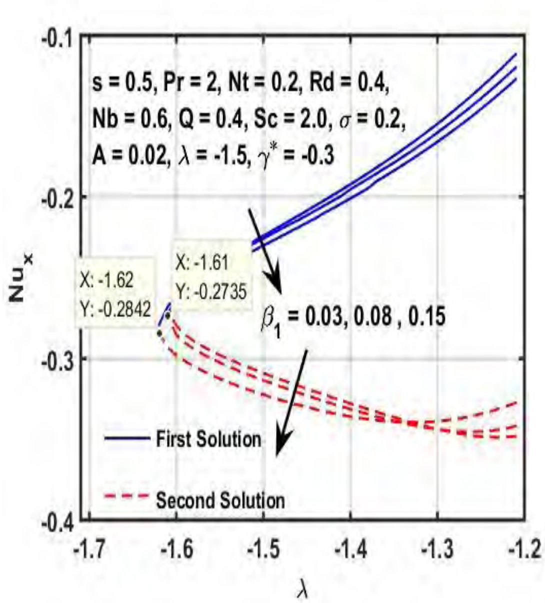

Fig. 9.2 (a): Graph of Nu_x for β_1 versus λ

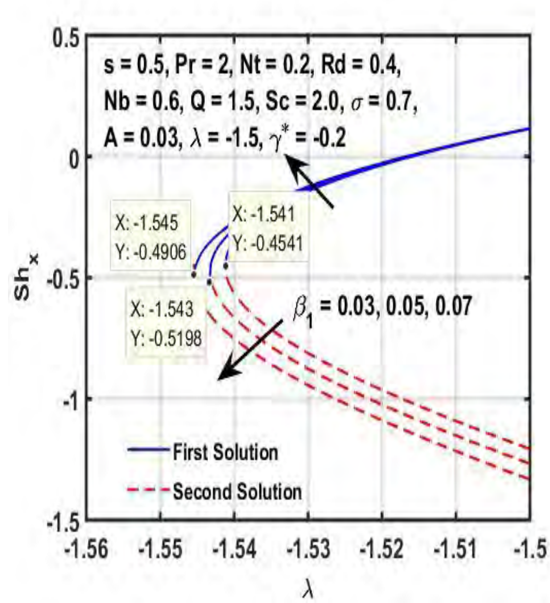

Fig. 9.2 (b): Graph of Sh_x for β_1.

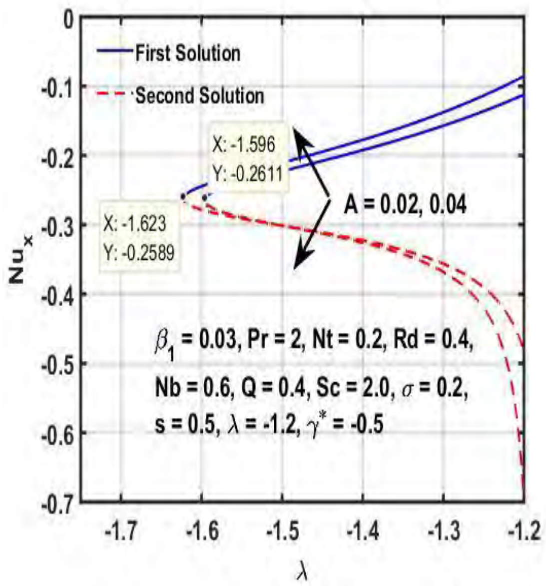

Fig. 9.2 (c): Graph of Nu_x for A.

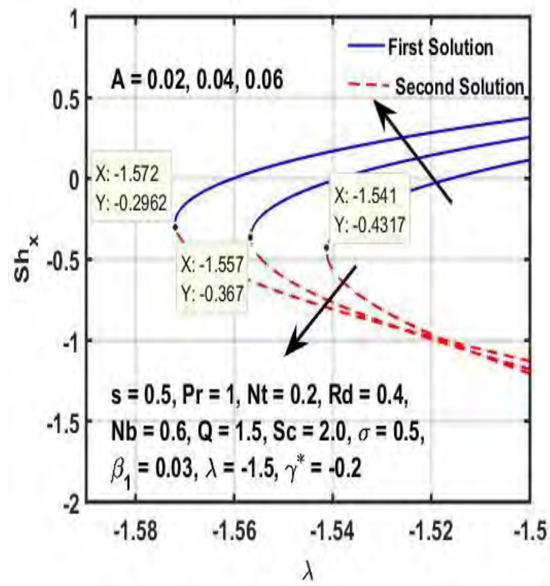

Fig. 9.2 (d): Graph of Sh_x for A.

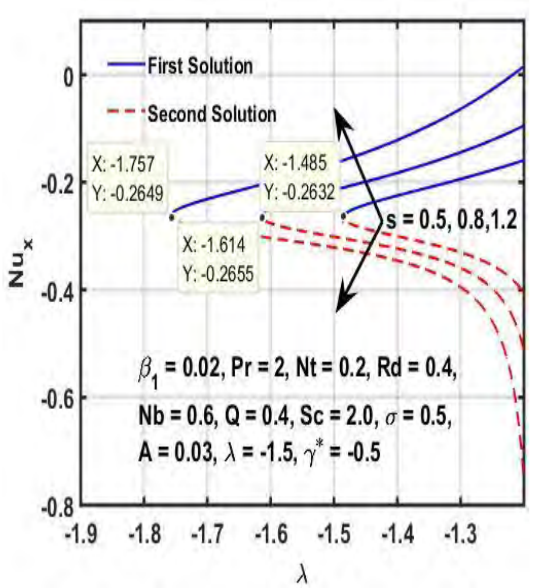

Fig. 9.3 (a): Graph of Nu_x for s.

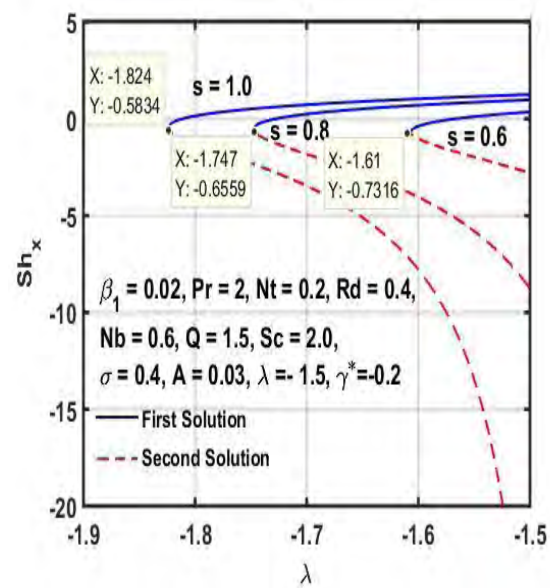

Fig. 9.3 (b): Graph of Sh_x for s.

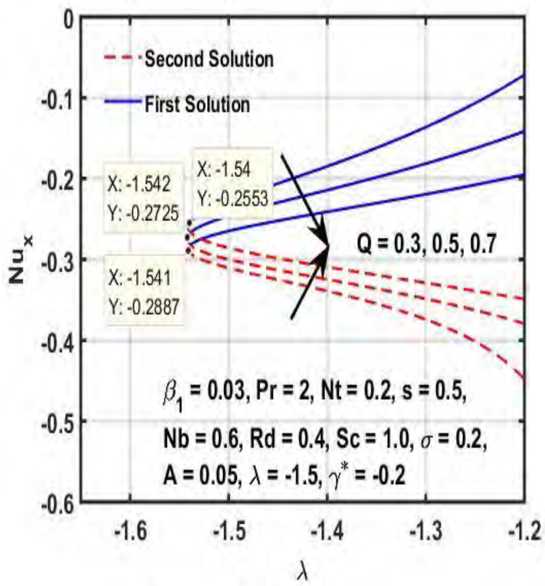

Fig. 9.3 (c): Graph of Nu_x for Q.

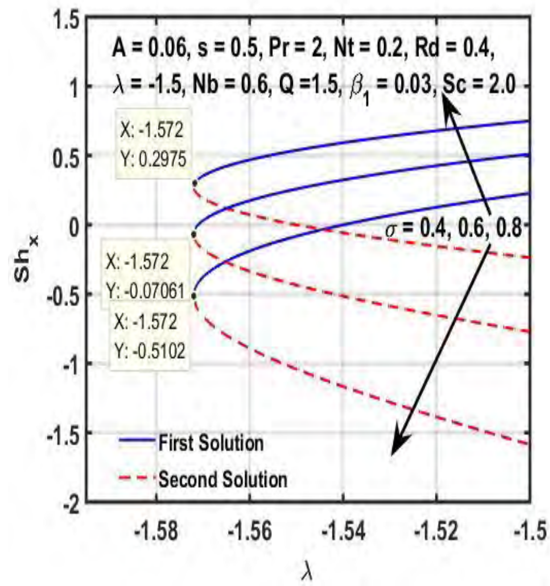

Fig. 9.3 (d): Graph of Sh_x for σ.

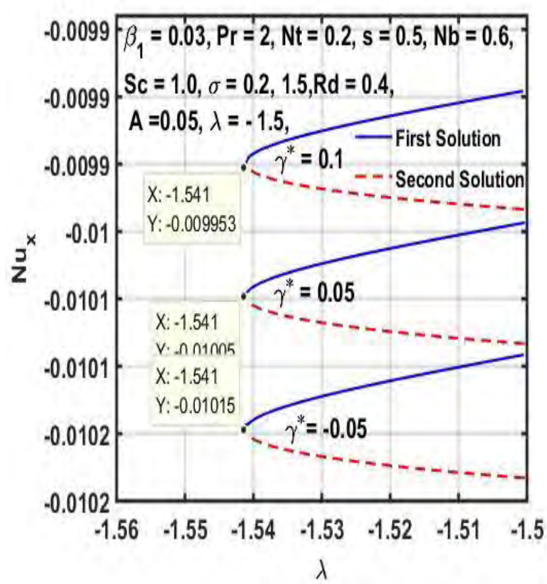

Fig. 9.3 (e): Graph of Nu_x for γ^*.

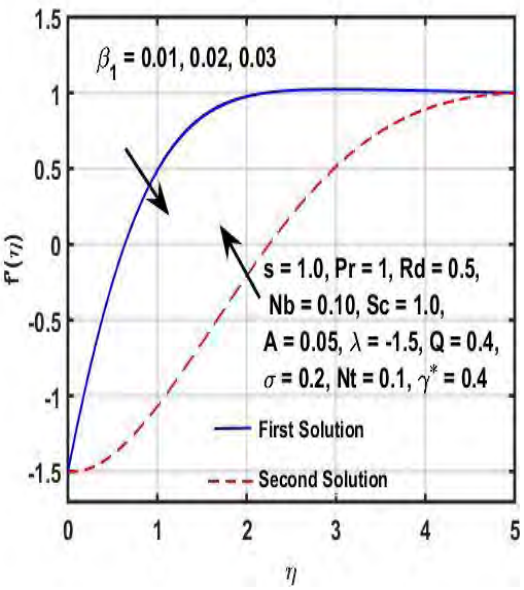

Fig. 9.4 (a): Plot of velocity for β_1.

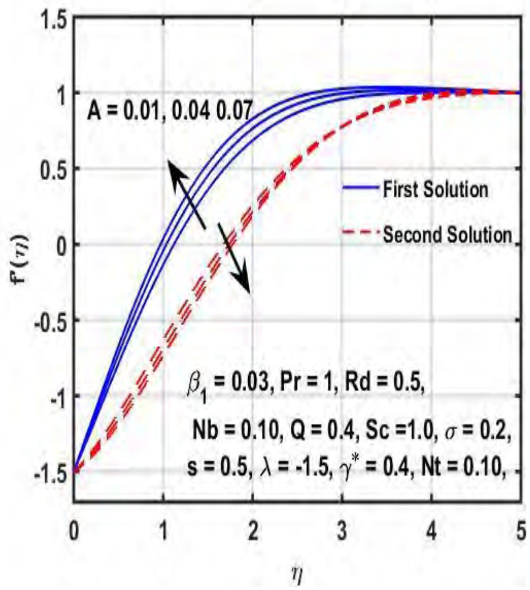

Fig. 9.4 (b): Plot of velocity for A.

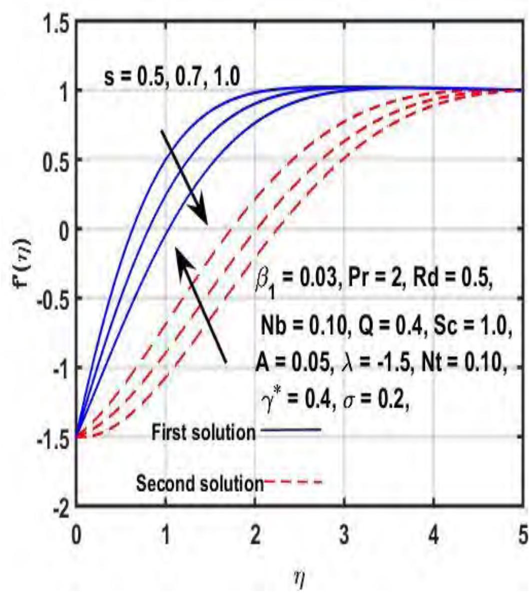

Fig. 9.4 (c): Plot of velocity for s.

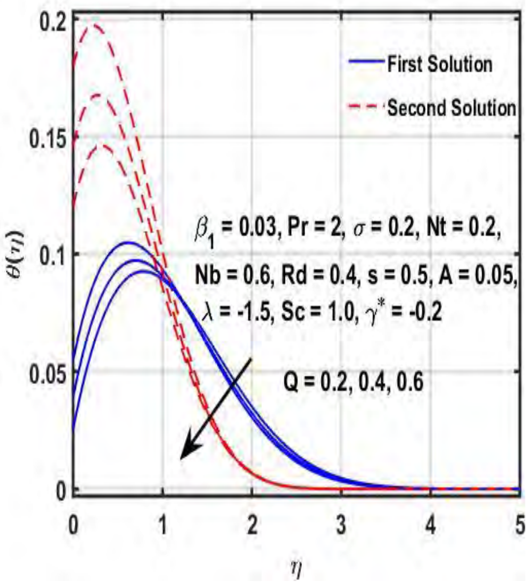

Fig. 9.5 (a): Plot of $\theta(\eta)$ for Q.

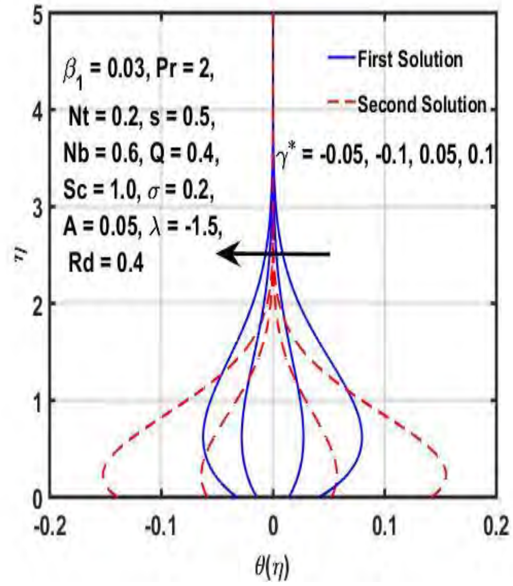

Fig. 9.5 (b): Plot of $\theta(\eta)$ for γ^*.

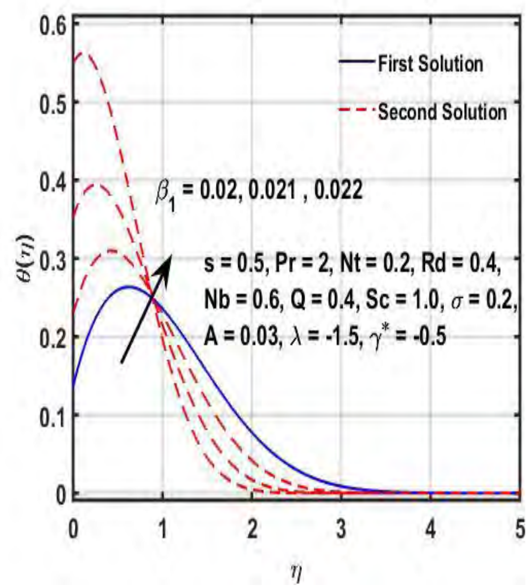

Fig. 9.6 (a): Plot of $\theta(\eta)$ for β_1.

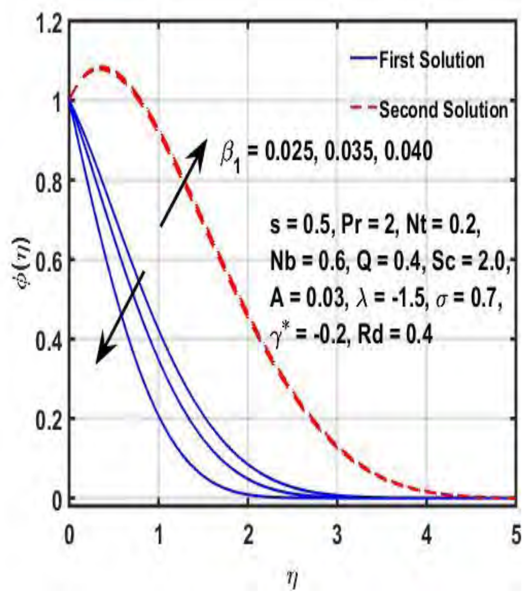

Fig. 9.6 (b): Plot of $\phi(\eta)$ for β_1.

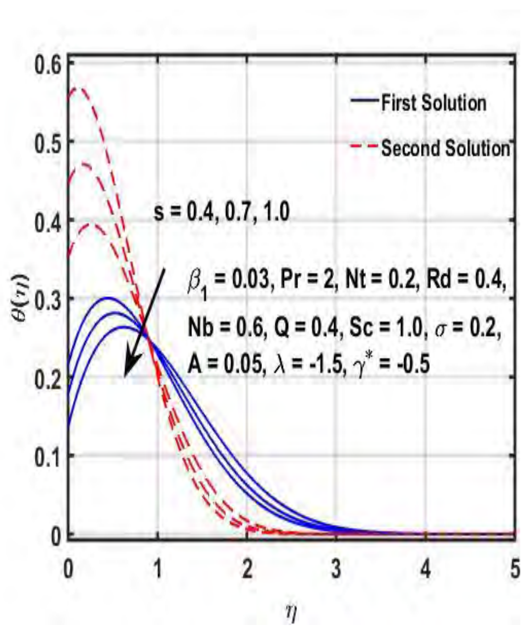

Fig. 9.7 (a): Plot of $\theta(\eta)$ for s.

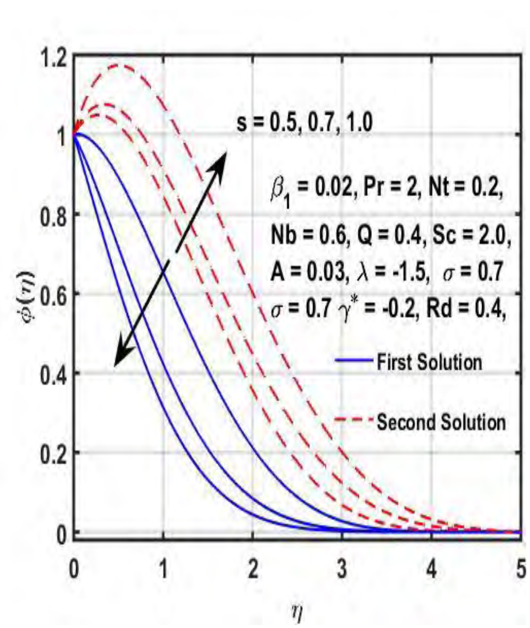

Fig. 9.7 (b): Plot of $\phi(\eta)$ for s.

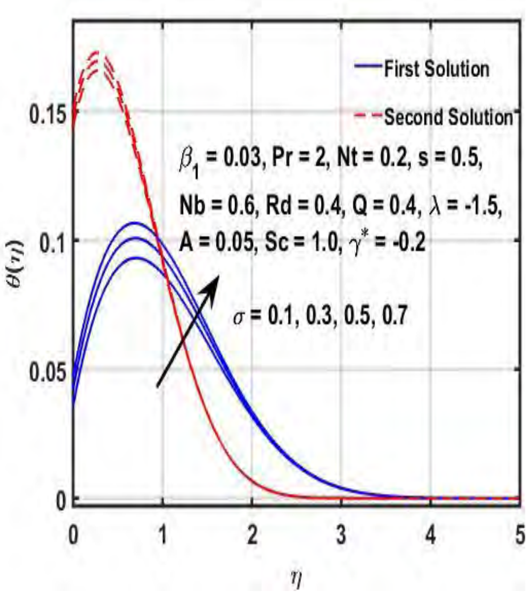

Fig. 9.7 (c): Plot of $\theta(\eta)$ for σ.

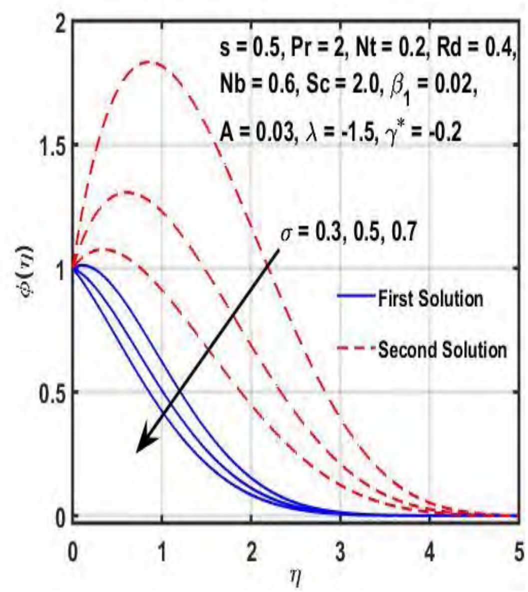

Fig. 9.7 (d): Plot of $\phi(\eta)$ for σ.

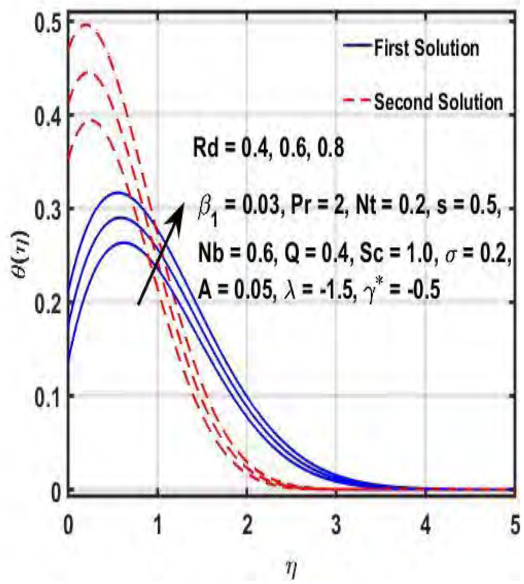

Fig. 9.7 (e): Plot of $\theta(\eta)$ for Rd.

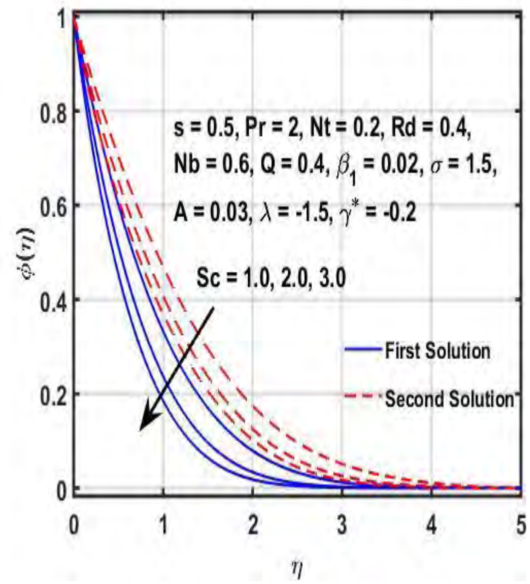

Fig. 9.7 (f): Plot of $\phi(\eta)$ for Sc.

9.3. Final Remarks

In this chapter, we presented the unsteady boundary layer flow of Maxwell nanofluid with thermal radiation. In addition, a shrinking surface is used as a source of fluid motion and consider the convective boundary condition at the sheet. The numerical computation of the present problem is done by bvp4c Matlab technique. The important results are highlighted below,

- The special feature of this study is to existence of the dual solution for shrinking parameter.
- The momentum boundary layer and fluid velocity enhance for the lower branch solution and decline for the upper branch solution with the enhancement of β_1.
- The effect of s on the velocity field for both solutions is opposite, i.e., the first solution increases but the second one reduces.
- Larger values of A lead to increases the temperature for the first solution and exhibit opposite

trend for the second solution.

- The temperature and concentration scattering shows reverse trend for higher values of σ.
- The heat transfer rate is declined for both solutions with enlarging β_1.
- The mass transfer rate shows opposite results for the first and the second solution with the increment of β_1.
- The Nusselt and Sherwood number showing similar effects for various estimation of A. It is seen that the first solution increases and second solution diminishes.
- The Newtonian fluid is obtained by taking the values of $\beta_1 = 0$.

References

1. J. C. Maxwell. "IV. On the dynamical theory of gases." ***Philosophical transactions of the Royal Society of London 157 (1867): 49-88.***
2. J. M. Burgers. "Mechanical considerations-model systems-phenomenological theories of relaxation and of viscosity." ***First report on viscosity and plasticity 1 (1935).***
3. Casson, N. "A flow equation for pigment-oil suspensions of the printing ink type." ***Rheology of disperse systems (1959).***
4. N. T. M. Eldabe, G. Saddeck, and A. F. El-Sayed. "Heat transfer of MHD non-Newtonian Casson fluid flow between two rotating cylinders." ***Mechanics and Mechanical Engineering 5, no. 2 (2001): 237-251.***
5. D. Vieru, C. Fetecau, and C. Fetecau. "Flow of a generalized Oldroyd-B fluid due to a constantly accelerating plate." ***Applied Mathematics and Computation 201, no. 1-2 (2008): 834-842***.
6. C. Fetecau, M. Nazar, and C. Fetecau. "Unsteady flow of an Oldroyd-B fluid generated by a constantly accelerating plate between two side walls perpendicular to the plate." ***International Journal of Non-linear Mechanics 44, no. 10 (2009): 1039-1047.***
7. L. Zheng, F. Zhao, and X. Zhang. "Exact solutions for generalized Maxwell fluid flow due to oscillatory and constantly accelerating plate." ***Nonlinear Analysis: Real World Applications 11, no. 5 (2010): 3744-3751***.
8. S. Nadeem, R. U. Haq, and C. Lee. "MHD flow of a Casson fluid over an exponentially shrinking sheet." ***Scientia Iranica 19, no. 6 (2012): 1550-1553.***

9. S. Nadeem, R. U. Haq, N. S. Akbar, C. Lee, and Z. H. Khan. "Numerical study of boundary layer flow and heat transfer of Oldroyd-B nanofluid towards a stretching sheet." ***PloS one 8, no. 8 (2013): e69811***.

10. G. K. Ramesh, and B. J. Gireesha. "Influence of heat source/sink on a Maxwell fluid over a stretching surface with convective boundary condition in the presence of nanoparticles." ***Ain Shams Engineering Journal 5, no. 3 (2014): 991-998.***

11. S. Mukhopadhyay, and R. S. R. Gorla. "Diffusion of chemically reactive species of a Casson fluid flow over an exponentially stretching surface." ***Ther. Ener. Pow. Engg 3 (2014): 216-221.***

12. M. Ramzan, M. Farooq, M. S. Alhothuali, H. M. Malaikah, W. Cui, and T. Hayat. "Three dimensional flow of an Oldroyd-B fluid with Newtonian heating." ***International Journal of Numerical Methods for Heat & Fluid Flow (2015).***

13. N. A. Khan, S. Khan, and S. Ullah. "MHD flow of Burger's fluid over an off-centered rotating disk in a porous medium." ***AIP Advances 5, no. 8 (2015): 087179.***

14. M. Khan, and W. A. Khan. "Steady flow of Burgers' nanofluid over a stretching surface with heat generation/absorption." ***Journal of the Brazilian Society of Mechanical Sciences and Engineering 38, no. 8 (2016): 2359-2367.***

15. N. Sandeep, and C. Sulochana. "Momentum and heat transfer behaviour of Jeffrey, Maxwell and Oldroyd-B nanofluids past a stretching surface with non-uniform heat source/sink." ***Ain Shams Engineering Journal 9, no. 4 (2018): 517-524.***

16. G. K. Ramesh, B. C. Prasannakumara, B. J. Gireesha, S. A. Shehzad, and F. M. Abbasi. "Three-dimensional flow of Maxwell fluid with suspended nanoparticles past a bidirectional

porous stretching surface with thermal radiation." ***Thermal Science and Engineering Progress 1 (2017): 6-14.***

17. M. I. Khan, M. Waqas, T. Hayat, and A. Alsaedi. "A comparative study of Casson fluid with homogeneous-heterogeneous reactions." ***Journal of colloid and interface science 498 (2017): 85-90.***
18. R. Safdar, M. Imran, and C. M. Khalique. "Time-dependent flow model of a generalized Burgers' fluid with fractional derivatives through a cylindrical domain: An exact and numerical approach." ***Results in Physics 9 (2018): 237-245.***
19. M. Waqas, M. I. Khan, T. Hayat, and A. Alsaedi. "A generalized Fourier and Fick's perspective for stretching flow of burgers fluid with temperature-dependent thermal conductivity." ***Thermal Science 23, no. 6 Part A (2019): 3425-3432.***
20. U. Farooq, D. Lu, S. Munir, M. Ramzan, M. Suleman, and S. Hussain. "MHD flow of Maxwell fluid with nanomaterials due to an exponentially stretching surface." ***Scientific reports 9, no. 1 (2019): 1-11.***
21. J. Ahmed, M. Khan, and L. Ahmad. "Stagnation point flow of Maxwell nanofluid over a permeable rotating disk with heat source/sink." ***Journal of Molecular Liquids 287 (2019): 110853.***
22. M. H. Tiwana, A. B. Mann, M. Rizwan, K. Maqbool, S. Javeed, S. Raza, and M. S. Khan. "Unsteady magnetohydrodynamic convective fluid flow of Oldroyd-B model considering ramped wall temperature and ramped wall velocity." ***Mathematics 7, no. 8 (2019): 676.***
23. M. Irfan, M. Khan, and W. A. Khan. "Impact of homogeneous–heterogeneous reactions and non-Fourier heat flux theory in Oldroyd-B fluid with variable conductivity." ***Journal of the Brazilian Society of Mechanical Sciences and Engineering 41, no. 3 (2019): 1-9.***

24. P. H. Nirmala, and A. S. Kumari. "Convection unsteady MHD of chemical reaction Burgers fluid flow over a stretching sheet in presence of radiation and heat source with surface boundary condition." ***In AIP Conference Proceedings, vol. 2246, no. 1, p. 020087. AIP Publishing LLC, 2020.***
25. K. A. Kumar, V. Sugunamma, and N. Sandeep. "Effect of thermal radiation on MHD Casson fluid flow over an exponentially stretching curved sheet." ***Journal of Thermal Analysis and Calorimetry 140, no. 5 (2020): 2377-2385.***
26. D. G. Shankar, C. S. K. Raju, M. S. J. Kumar, and O. D. Makinde. "Cattaneo-Christov Heat Flux on an MHD 3D Free Convection Casson Fluid Flow Over a Stretching Sheet." ***Engineering Transactions 68, no. 3 (2020): 223-238***.
27. J. B. J. Fourier. "Théorie analytique de la chaleur, Paris. "***Académie des Sciences*** **(1822): 3.**
28. A. Fick. "Poggendorff's Flannel. "***Physik*** **94, no. 59 (1855): 297**.
29. C. Cattaneo. "Sulla conduzione del calore. "***Atti Sem. Mat. Fis. Univ. Modena*** **3 (1948): 83-101.**
30. C. I. Christov. "On frame indifferent formulation of the Maxwell–Cattaneo model of finite-speed heat conduction. "***Mechanics Research Communications*** **36, no. 4 (2009): 481-486**.
31. S. Han, L. Zheng, C. Li, and X. Zhang. "Coupled flow and heat transfer in viscoelastic fluid with Cattaneo–Christov heat flux model." ***Applied Mathematics Letters 38 (2014): 87-93***.
32. N. Sandeep, B. R. Kumar, and M. S. J. Kumar. "A comparative study of convective heat and mass transfer in non-Newtonian nanofluid flow past a permeable stretching sheet." ***Journal of Molecular Liquids 212 (2015): 585-591***.

33. M. Khan, "A revised model to analyze the heat and mass transfer mechanisms in the flow of Carreau nanofluids." ***International Journal of Heat and Mass Transfer 103 (2016): 291-297.***

34. J. Sui, L. Zheng, and X. Zhang. "Boundary layer heat and mass transfer with Cattaneo–Christov double-diffusion in upper-convected Maxwell nanofluid past a stretching sheet with slip velocity." ***International Journal of Thermal Sciences 104 (2016): 461-468.***

35. S. Nadeem, S. Ahmad, N. Muhammad, and M. T. Mustafa. "Chemically reactive species in the flow of a Maxwell fluid." ***Results in physics 7 (2017): 2607-2613.***

36. K. L. Hsiao. "Combined electrical MHD heat transfer thermal extrusion system using Maxwell fluid with radiative and viscous dissipation effects." ***Applied Thermal Engineering 112 (2017): 1281-1288.***

37. Y. Zhang, B. Yuan, Y. Bai, Y. Cao, and Y. Shen. "Unsteady Cattaneo-Christov double diffusion of Oldroyd-B fluid thin film with relaxation-retardation viscous dissipation and relaxation chemical reaction." ***Powder Technology 338 (2018): 975-982.***

38. M. Khan, M. Y. Malik, T. Salahuddin, and F. Khan. "Generalized diffusion effects on Maxwell nanofluid stagnation point flow over a stretchable sheet with slip conditions and chemical reaction." ***Journal of the Brazilian Society of Mechanical Sciences and Engineering 41, no. 3 (2019): 1-9.***

39. T. Sajid, M. Sagheer, and S. Hussain. "Impact of temperature-dependent heat source/sink and variable species diffusivity on radiative Reiner–Philippoff fluid." ***Mathematical Problems in Engineering 2020 (2020).***

40. M. I. Khan, F. Alzahrani, and A. Hobiny. "Heat transport and nonlinear mixed convective nanomaterial slip flow of Walter-B fluid containing gyrotactic microorganisms." ***Alexandria Engineering Journal 59, no. 3 (2020): 1761-1769***.

41. S. U. S. Choi, and J. A. Eastman. *Enhancing thermal conductivity of fluids with nanoparticles*. ***No. ANL/MSD/CP-84938; CONF-951135-29. Argonne National Lab., IL (United States), 1995.***

42. J. Buongiorno. "Convective transport in nanofluids." ***Journal of heat transfer 128, no. 3 (2006): 240-250***.

43. K. Khanafer, and K. Vafai. "A critical synthesis of thermophysical characteristics of nanofluids." ***International journal of heat and mass transfer 54, no. 19-20 (2011): 4410-4428.***

44. M. J. Uddin, W. A. Khan, and A. I. Ismail. "MHD free convective boundary layer flow of a nanofluid past a flat vertical plate with Newtonian heating boundary condition." ***Plos one 7, no. 11 (2012): e49499.***

45. M. M. Rahman, A. V. Roşca, and I. Pop. "Boundary layer flow of a nanofluid past a permeable exponentially shrinking/stretching surface with second order slip using Buongiorno's model." ***International Journal of Heat and Mass Transfer 77 (2014): 1133-1143***.

46. T. Hayat, T. Muhammad, S. A. Shehzad, and A. Alsaedi. "Three dimensional rotating flow of Maxwell nanofluid." ***Journal of Molecular Liquids 229 (2017): 495-500***.

47. Z. Shah, P. Kumam, and W. Deebani. "Radiative MHD Casson Nanofluid Flow with Activation energy and chemical reaction over past nonlinearly stretching surface through Entropy generation." ***Scientific reports 10, no. 1 (2020): 1-14.***

48. S. Nadeem, M. N. Khan, and N. Abbas. "Transportation of slip effects on nanomaterial micropolar fluid flow over exponentially stretching." ***Alexandria Engineering Journal 59, no. 5 (2020): 3443-3450.***

49. A. M. Al-Hanaya, F. Sajid, N. Abbas, and S. Nadeem. "Effect of SWCNT and MWCNT on the flow of micropolar hybrid nanofluid over a curved stretching surface with induced magnetic field." ***Scientific Reports 10, no. 1 (2020): 1-18.***

50. L. A. Lund, Z. Omar, J. Raza, and I. Khan. "Magnetohydrodynamic flow of Cu–Fe 3 O 4/H 2 O hybrid nanofluid with effect of viscous dissipation: Dual similarity solutions." ***Journal of Thermal Analysis and Calorimetry 143, no. 2 (2021): 915-927.***

51. T. Sarpkaya. "Flow of non- Newtonian fluids in a magnetic field." ***AIChE Journal 7, no. 2 (1961): 324-328***.

52. D. S. Djukic. "On the use of Crocco's equation for the flow of power- law fluids in a transverse magnetic field." ***AIChE Journal 19, no. 6 (1973): 1159-1163.***

53. R. Dhanai, P. Rana, and L. Kumar. "Multiple solutions in MHD flow and heat transfer of Sisko fluid containing nanoparticles migration with a convective boundary condition: Critical points." ***The European Physical Journal Plus 131, no. 5 (2016): 1-14.***

54. R. Ellahi, M. M. Bhatti, and I. Pop. "Effects of hall and ion slip on MHD peristaltic flow of Jeffrey fluid in a non-uniform rectangular duct." ***International journal of numerical methods for heat & fluid flow (2016).***

55. P. Besthapu, R. U. Haq, S. Bandari, and Q. M. Al-Mdallal. "Thermal radiation and slip effects on MHD stagnation point flow of non-Newtonian nanofluid over a convective stretching surface." ***Neural Computing and Applications 31, no. 1 (2019): 207-217.***

56. A. Ahmed, M. Khan, M. Irfan, and J. Ahmed. "Transient MHD flow of Maxwell nanofluid

subject to non-linear thermal radiation and convective heat transport." ***Applied Nanoscience 10, no. 12 (2020): 5361-5373***.

57. L. J. Crane. "Flow past a stretching plate." ***Zeitschrift für angewandte Mathematik und Physik ZAMP 21, no. 4 (1970): 645-647.***
58. P. S. Gupta, and A. S. Gupta. "Heat and mass transfer on a stretching sheet with suction or blowing." ***The Canadian Journal of Chemical Engineering 55, no. 6 (1977): 744-746.***
59. A. Chakrabarti, and A. S. Gupta. "Hydromagnetic flow and heat transfer over a stretching sheet." ***Quarterly of Applied Mathematics*** **37, no. 1 (1979): 73-78.**
60. E. Magyari, and B. Keller. "Heat and mass transfer in the boundary layers on an exponentially stretching continuous surface." ***Journal of Physics D: Applied Physics 32, no. 5 (1999): 577.***
61. J. Paullet, and P. Weidman. "Analysis of stagnation point flow toward a stretching sheet." ***International Journal of Non-Linear Mechanics 42, no. 9 (2007): 1084-1091.***
62. C. Y. Wang. "Analysis of viscous flow due to a stretching sheet with surface slip and suction." ***Nonlinear Analysis: Real World Applications 10, no. 1 (2009): 375-380.***
63. N. C. Roşca, and I. Pop. "Unsteady boundary layer flow over a permeable curved stretching/shrinking surface." ***European Journal of Mechanics-B/Fluids 51 (2015): 61-67.***
64. S. Mondal, S. K. Nandy, and P. Sibanda. "MHD flow and heat transfer of maxwell nanofluid over an unsteady permeable shrinking sheet with convective boundary conditions." ***Journal of Nanofluids 7, no. 5 (2018): 995-1003***.
65. B. Ali, Y. Nie, S. Hussain, A. Manan, and M. T. Sadiq. "Unsteady magneto-hydrodynamic transport of rotating Maxwell nanofluid flow on a stretching sheet with Cattaneo–Christov

double diffusion and activation energy." ***Thermal Science and Engineering Progress* 20 (2020): 100720.**

66. B. Ali, R. A. Naqvi, A. Mariam, L. Ali, and O. M. Aldossary. "Finite element study for magnetohydrodynamic (MHD) tangent hyperbolic nanofluid flow over a faster/slower stretching wedge with activation energy." ***Mathematics* 9, no. 1 (2021): 25**.
67. C. C. Chen, and R. Eichhorn. "Natural convection from a vertical surface to a thermally stratified fluid." **(1976): 446-451**.
68. K. Yoon, and Z. Warhaft. "The evolution of grid-generated turbulence under conditions of stable thermal stratification." ***Journal of Fluid Mechanics* 215 (1990): 601-638.**
69. D. Angirasa, and J. Srinivasan. "Natural convection heat transfer from an isothermal vertical surface to a stable thermally stratified fluid." **(1992): 917-923.**
70. M. Moorthy, and K. Senthilvadivu. "Effect of variable viscosity on free flow of non-Newtonian power-law fluids along a vertical surface with thermal stratification." ***Archives of Thermodynamics* 33, no. 4 (2012): 109-121.**
71. A. B. Rosmila, R. Kandasamy, and I. Muhaimin. "Lie symmetry group transformation for MHD natural convection flow of nanofluid over linearly porous stretching sheet in presence of thermal stratification." ***Applied Mathematics and Mechanics* 33, no. 5 (2012): 593-604.**
72. W. Ibrahim, and O. D. Makinde. "The effect of double stratification on boundary-layer flow and heat transfer of nanofluid over a vertical plate." ***Computers & Fluids* 86 (2013): 433-441.**
73. N. Muhammad, S. Nadeem, and R. U. Haq. "Heat transport phenomenon in the ferromagnetic fluid over a stretching sheet with thermal stratification." ***Results in Physics* 7 (2017): 854-861.**

74. N. Sandeep, and M. G. Reddy. "MHD Oldroyd-B fluid flow across a melting surface with cross diffusion and double stratification." ***The European Physical Journal Plus 132, no. 3 (2017): 1-18.***

75. K. S. Lakshmi, G. Sarojamma, and O. D. Makinde. "Dual stratification on the Darcy-Forchheimer flow of a Maxwell nanofluid over a stretching surface." ***In Defect and Diffusion Forum, vol. 387, pp. 207-217. Trans Tech Publications Ltd, 2018.***

76. I. Tlili, S. Naseer, M. Ramzan, S. Kadry, and Y. Nam. "Effects of chemical species and nonlinear thermal radiation with 3D Maxwell nanofluid flow with double stratification—an analytical solution." ***Entropy 22, no. 4 (2020): 453.***

77. J. O. Kessler. "Hydrodynamic focusing of motile algal cells." ***Nature 313, no. 5999 (1985): 218-220.***

78. J. O. Kessler. "Individual and collective fluid dynamics of swimming cells." ***Journal of Fluid Mechanics 173 (1986): 191-205.***

79. A. V. Kuznetsov. "Thermo-bioconvection in a suspension of oxytactic bacteria." ***International Communications in Heat and Mass Transfer 32, no. 8 (2005): 991-999.***

80. A. V. Kuznetsov. "Investigation of the onset of thermo-bioconvection in a suspension of oxytactic microorganisms in a shallow fluid layer heated from below." ***Theoretical and Computational Fluid Dynamics 19, no. 4 (2005): 287-299.***

81. P. Geng. and A. V. Kuznetsov. "Settling of bidispersed small solid particles in a dilute suspension containing gyrotactic micro-organisms." ***International Journal of Engineering Science 43, no. 11-12 (2005): 992-1010.***

82. P. Geng, and A. V. Kuznetsov. "Introducing the concept of effective diffusivity to evaluate the effect of bioconvection on small solid particles." ***International Journal of Transport Phenomena 7, no. 4 (2005): 321-338.***

83. S. Nadeem, M. N. Khan, N. Muhammad, and S. Ahmad. "Mathematical analysis of bio-convective micropolar nanofluid." ***Journal of Computational Design and Engineering 6, no. 3 (2019): 233-242.***

84. A. M. Rashad, and H. A. Nabwey. "Gyrotactic mixed bioconvection flow of a nanofluid past a circular cylinder with convective boundary condition." ***Journal of the Taiwan Institute of Chemical Engineers 99 (2019): 9-17.***

85. M. I. Khan, F. Alzahrani, and A. Hobiny. "Heat transport and nonlinear mixed convective nanomaterial slip flow of Walter-B fluid containing gyrotactic microorganisms." ***Alexandria Engineering Journal 59, no. 3 (2020): 1761-1769.***

86. M. Mustafa, J. A. Khan, T. Hayat, and A. Alsaedi. "Simulations for Maxwell fluid flow past a convectively heated exponentially stretching sheet with nanoparticles." ***AIP Advances 5, no. 3 (2015): 037133.***

87. M. Khan, and A. Hafeez. "A review on slip-flow and heat transfer performance of nanofluids from a permeable shrinking surface with thermal radiation: dual solutions." ***Chemical Engineering Science 173 (2017): 1-11***.

88. T. Chakraborty, K. Das, and P. K. Kundu. "Framing the impact of external magnetic field on bioconvection of a nanofluid flow containing gyrotactic microorganisms with convective boundary conditions." ***Alexandria engineering journal 57, no. 1 (2018): 61-71.***

89. S. K. Nandy, and I. Pop. "Effects of magnetic field and thermal radiation on stagnation flow and heat transfer of nanofluid over a shrinking surface." ***International Communications in Heat and Mass Transfer 53 (2014): 50-55.***

90. M. J. Uddin, M. N. Kabir, and O. A. Bég. "Computational investigation of Stefan blowing and multiple-slip effects on buoyancy-driven bioconvection nanofluid flow with microorganisms." ***International Journal of Heat and Mass Transfer 95 (2016): 116-130.***

91. S. Nadeem, and C. Lee. "Boundary layer flow of nanofluid over an exponentially stretching surface." ***Nanoscale Research Letters 7, no. 1 (2012): 1-6.***

92. N. Sandeep, and C. Sulochana. "Momentum and heat transfer behaviour of Jeffrey, Maxwell and Oldroyd-B nanofluids past a stretching surface with non-uniform heat source/sink." ***Ain Shams Engineering Journal 9, no. 4 (2018): 517-524***.

93. A. A. Afify, M. J. Uddin, and M. Ferdows. "Scaling group transformation for MHD boundary layer flow over permeable stretching sheet in presence of slip flow with Newtonian heating effects." ***Applied Mathematics and Mechanics 35, no. 11 (2014): 1375-1386.***

94. M. Ramzan, A. Liaquet, S. Kadry, S. Yu, Y. Nam, and D. Lu. "Impact of second-order slip and double stratification coatings on 3D MHD Williamson nanofluid flow with Cattaneo–Christov heat flux." ***Coatings 9, no. 12 (2019): 849.***

95. S. Mukhopadhyay. "Heat transfer analysis of the unsteady flow of a Maxwell fluid over a stretching surface in the presence of a heat source/sink." ***Chinese Physics Letters 29, no. 5 (2012): 054703.***

96. M. I. Khan, M. Waqas, T. Hayat, M. I. Khan, and A. Alsaedi. "Behavior of stratification phenomenon in flow of Maxwell nanomaterial with motile gyrotactic microorganisms in the

presence of magnetic field." ***International Journal of Mechanical Sciences 131 (2017): 426-434.***

97. T. Muhammad, A. Alsaedi, S. A. Shehzad, and T. Hayat. "A revised model for Darcy-Forchheimer flow of Maxwell nanofluid subject to convective boundary condition." ***Chinese Journal of Physics 55, no. 3 (2017): 963-976.***
98. S. Nadeem, S. Ahmad, and N. Muhammad. "Computational study of Falkner-Skan problem for a static and moving wedge." ***Sensors and Actuators B: Chemical 263 (2018): 69-76.***
99. S. A. Shehzad, A. Alsaedi, T. Hayat, and M. S. Alhuthali. "Three-dimensional flow of an Oldroyd-B fluid with variable thermal conductivity and heat generation/absorption." ***Plos One 8, no. 11 (2013): e78240***.
100. M. Sulaiman, A. Ali, and S. Islam. "Heat and mass transfer in three-dimensional flow of an Oldroyd-B nanofluid with gyrotactic micro-organisms." ***Mathematical Problems in Engineering 2018 (2018).***
101. W. A. Khan, and I. Pop. "Boundary-layer flow of a nanofluid past a stretching sheet." ***International journal of heat and mass transfer 53, no. 11-12 (2010): 2477-2483.***
102. C. S. K. Raju, and N. Sandeep. "Unsteady three-dimensional flow of Casson–Carreau fluids past a stretching surface." ***Alexandria Engineering Journal 55, no. 2 (2016): 1115-1126.***
103. M. Mustafa, A. Mushtaq, T. Hayat, and A. Alsaedi. "Radiation effects in three-dimensional flow over a bi-directional exponentially stretching sheet." ***Journal of the Taiwan Institute of Chemical Engineers 47 (2015): 43-49.***

104. T. Hayat, I. Ullah, T. Muhammad, and A. Alsaedi. "Thermal and solutal stratification in mixed convection three-dimensional flow of an Oldroyd-B nanofluid." ***Results in physics 7 (2017): 3797-3805.***

105. A. Ishak. "MHD boundary layer flow due to an exponentially stretching sheet with radiation effect." ***Sains Malaysiana 40, no. 4 (2011): 391-395.***

106. S. Pramanik. "Casson fluid flow and heat transfer past an exponentially porous stretching surface in presence of thermal radiation." ***Ain Shams Engineering Journal 5, no. 1 (2014): 205-212***.

107. F. Aman, A. Ishak, and I. Pop. "Mixed convection boundary layer flow near stagnation-point on vertical surface with slip." ***Applied Mathematics and Mechanics 32, no. 12 (2011): 1599-1606***.

108. A. Zaib, U. Khan, I. Khan, A. H. Seikh, and E. S. M. Sherif. "Entropy generation and dual solutions in mixed convection stagnation point flow of micropolar Ti6Al4V nanoparticle along a riga surface." ***Processes 8, no. 1 (2020): 14.***

109. K. Sadeghy, H. Hajibeygi, and S. M. Taghavi. "Stagnation-point flow of upper-convected Maxwell fluids." ***International Journal of Non-Linear Mechanics 41, no. 10 (2006): 1242-1247***.

110. W. A. Khan, M. Irfan, and M. Khan. "An improved heat conduction and mass diffusion models for rotating flow of an Oldroyd-B fluid." ***Results in physics 7 (2017): 3583-3589.***

111. K. Das, P. R. Duari, and P. K. Kundu. "Nanofluid flow over an unsteady stretching surface in presence of thermal radiation." ***Alexandria engineering journal 53, no. 3 (2014): 737-745.***

112. P. D. Weidman, D. G. Kubitschek, and A. M. J. Davis. "The effect of transpiration on self-similar boundary layer flow over moving surfaces." ***International journal of engineering science 44, no. 11-12 (2006): 730-737.***